CHAPTER 1: Prologue

1.1 Introduction

Cardiogenesis is a dynamic process directed by numerous feedback loops. The primary function of the adult heart is pumping blood through the circulatory system. In relation to other organs, the heart is unique because it can perform its function throughout development (i.e., the primitive heart tube, despite its rudimentary shape, can drive circulation as well). One reason this is possible may be that the output of cardiac function, blood flow, is also an input that regulates gene expression. It is widely accepted that epigenetic factors, such as blood flow, combine with genetic programming to guide normal and abnormal heart development. However, the details and extent of this relationship continue to generate discussion and debate. Given the high prevalence of congenital heart defects and the ambiguities surrounding developmental processes in general, the conclusions are of practical importance to the medical and biological communities.

The main motivation for this research was to enhance our understanding of cardiogenesis by studying the development of cardiac structure and function. Our approach was to evaluate the dynamic relationship between cardiac contractile mechanics, hemodynamics, and morphogenesis. These efforts necessitated high resolution (both temporal and spatial) imaging of in vivo cardiac cell motions within a single heart beat and throughout cardiac development. Acquiring and analyzing data required demonstrations of principles from interdisciplinary studies, including biology, engineering, optics, and image processing to provide several quantitative measurements and qualitative descriptions of embryonic cardiac mechanics.

Utilizing novel imaging tools and four-dimensional visualization protocols (Liebling et al. 2005), we propose a new mechanism of valveless pumping in the embryonic heart tube via elastic wave propagation and reflection (Forouhar et al. 2006). We arrived at this conclusion by studying the structure of the embryonic heart tube, the dynamic motions of endocardial and myocardial cells, the natural relationship between heart wall motions and blood cell motions, and the experimental response of blood cell motions to changes in contractile dynamics. This comprehensive analysis of cardiac function at one stage of development provides a protocol for extending studies to more advanced stages and more complicated structures. It also provides one step in establishing the dynamic relationship between structure and function.

In order to connect how fluid dynamics may help orchestrate cardiac morphogenesis, we studied one region of the zebrafish (*Danio rerio*) heart, the developing atrio-ventricular (AV) canal, exposed to amplified hemodynamic forces. Our initial observations of blood flow through this region, the eventual site of the AV valve, revealed a clear transition from pulsatile unidirectional flow to oscillatory flow prior to valve formation, and then a return to unidirectional flow after the formation of functional valve leaflets. This was a particularly interesting phenomena for two reasons; (i) oscillatory flows are extremely biologically active, stimulating cell adhesion, proliferation, and death (Chappell et al. 1998; Haga et al. 2003; Sorescu et al. 2003; Sorescu et al. 2004), and (ii) the function of the derived structure, the AV valve, is to specifically prevent oscillatory flow. These two relationships furthered our curiosity, eventually prompting the question: do heart valves form in response to intracardiac oscillatory flow or is valve formation independent of flow patterns?

Many studies have successfully analyzed gene expression patterns in response to flow-induced forces in vitro but none has successfully duplicated the fidelity of these experiments in vivo. One significant challenge in studying fluid forces in vivo is non-invasively and acutely controlling blood flow through the intact heart. Several methods of manipulating blood flow in vivo include ligating vessels and chambers (Hogers et al. 1997; Hogers et al. 1999), occluding flow by inserting beads into the circulatory path (Hove et al. 2003), and studying mutants with altered cardiac contractile properties (Bartman et al. 2004). However, none of these specifically modulate oscillatory flow. Here we identify a relationship between oscillatory flow and contractile frequency, and manipulate embryonic heart rates to modulate oscillatory flow patterns through the developing AV canal. Our results suggest that oscillatory flows are essential for normal AV valve formation in the embryonic zebrafish heart. These results, along with the frequency-dependent nature of oscillatory flow, provide a mode for designing hemodynamic therapies to rescue congenital heart valve defects.

1.2 Organization

This thesis is a compilation of methods, data, and perspectives, some of which has been previously published in peer-reviewed journals. In cases where the thesis author is the sole first author of the published work, the text and figures have been included with appropriate references. In cases where the thesis author is either joint first author or a secondary author, the included text has been re-written but figures and figure legends may be included unaltered with appropriate references.

Chapter 2 provides essential background information for the research presented. We review heart development in vertebrates and explain why zebrafish are the model system of choice to study dynamic cardiac function. We provide evidence that hemodynamic forces contribute to normal and abnormal heart development and consider some of the questions that remain unanswered.

Chapter 3 introduces a number of tools and techniques used to study zebrafish heart biomechanics and hemodynamics. We describe protocols for imaging zebrafish hearts in vivo with brightfield and confocal microscopy. During the course of this study, technological improvements in confocal microscopy increased scan rates by two orders of magnitude, permitting observation of a wide range of dynamic cardiac motions. We briefly describe the technology employed by Carl Zeiss GmbH. in their preproduction prototype of the Zeiss LSM 5 LIVE high-speed confocal microscope (Liebling et al. in preparation). This prototype was used to obtain high speed two-dimensional scans of the beating zebrafish heart and blood flow through the heart. Next, we describe the correlation algorithm used to synchronize sequential two-dimensional scans to create dynamic four-dimensional cardiac data (Liebling et al. 2005). Among other things, this data can then be used to track cardiac cell motions, extract volume changes during the cardiac cycle, and analyze intracardiac flow patterns. Examples are provided.

In chapter 4 we examine endocardial, myocardial, and blood cell motions during early heart tube contractions and present evidence that contradicts peristalsis as a pumping mechanism in the embryonic heart. Instead, we propose a more likely explanation of early cardiac dynamics in which the pumping action is caused by suction due to elastic wave propagation and reflection in the heart tube (Forouhar et al. 2006).

We provide some perspective on how this pumping mechanism may be evolutionarily advantageous to peristalsis and may necessitate heart valve formation.

In chapter 5 we provide evidence in support of our hypothesis that oscillatory shear stress in the developing heart stimulates AV valve formation. We begin with a description of flow patterns throughout cardiogenesis, and illustrate the transition from unidirectional flow to bidirectional flow prior to valve formation (Leibling et al. in preparation). We identify and utilize an interesting relationship between heart rate and oscillatory flow to study the role of oscillatory shear stress on valve formation. Our results show that oscillatory flow is critical for normal AV valve formation (Forouhar et al. in preparation).

In chapter 6, we summarize the primary contributions of this work and discuss challenges and future opportunities in the field.

1.3 Goals

The major goal of this research is to improve our understanding of cardiac morphogenesis by studying the dynamic relationship between structure and function in the developing heart. Along the way, a number of intermediate goals were also established, including (i) quantitatively describing early heart wall and blood cell motions to understand how the heart tube pumps blood, (ii) extending our study of blood flow through the heart tube to later stages of cardiogenesis in order to describe blood flow patterns along with pumping mechanisms throughout heart development, (iii) deriving a non-invasive method to manipulate oscillatory flow through the intact heart, (iv) and

performing functional assays on heart valve formation to identify the results of altered oscillatory flow on valvulogenesis.

1.4 Chapter References

Bartman T, EC Walsh, KK Wen, M McKane, J Ren, J Alexander, PA Rubenstein, DY Stainier, *PLoS Biol*. **2**, E129 (2004).

Chappell DC, SE Varner, RM Nerem, RM Medford, RW Alexander, *Circ Res*. **82**, 532 (1998).

Forouhar AS, M Liebling, AI Hickerson, A Naisrei-Moghaddam, HJ Tsai, JR Hove, SE Fraser, ME Dickinson, M Gharib, *Science*. **312**, 751 (2006).

Forouhar AS, M Liebling, J Vermot, JR Hove, SE Fraser, M Gharib. Oscillatory Flow and Valvulogenesis, In preparation.

Haga H, A Yamashita, J Paszkowiak, BE Sumpio, AJ Dardik, *J Vasc Surg*. **37**, 1277 (2003).

Hogers B, MC DeRuiter, AC Gittenberger-de Groot, RE Poelmann, *Circ Res*. **80**, 473 (1997).

Hogers B, MC De Ruiter, AC Gittenberger-de Groot, RE Poelmann, *Cardiovasc Res*. **41**, 87 (1999).

Hove JR, RW Koster, AS Forouhar, G Acevedo-Bolton, SE Fraser, M Gharib, *Nature*. **421**, 172 (2003).

Liebling M, AS Forouhar, M Gharib, SE Fraser, ME Dickinson, *J Biomed Opt*. **10**, 054001 (2005).

Liebling M, AS Forouhar, R Wolleschensky, B Zimmermann, R Ankerhold, SE Fraser, M Gharib, ME Dickinson. Rapid three-dimensional imaging and analysis of the beating embryonic heart reveals functional changes during development, In preparation.

Sorescu GP, M Sykes, D Weiss, MO Platt, A Saha, J Hwang, N Boyd, YC Boo, JD Vega, WR Taylor, HJ Jo, *Biol Chem*. **278**, 31128 (2003).

Sorescu GP, H Song, SL Tressel, J Hwang, S Dikalov, DA Smith, NL Boyd, MO Platt, B Lassegue, KK Griendling, HJ Jo, *Circ Res*. **95**, 773 (2004).

CHAPTER 2: Vertebrate Heart Development

2.1 Introduction

Understanding the root of congenital heart and valve defects requires precise knowledge of the processes involved in cardiogenesis. Research in this field has been motivated by medicine and embryology alike. Current descriptions of heart and valve morphogenesis are largely composed from snapshots of static hearts. As Christine Seidman cleverly illustrated (Harvey and Rosenthal, 1999), this is like watching a play in which you can view the performance of the actors but can not hear the dialogue. In the context of heart morphogenesis, the dialogue is the interplay between structure and function: how the cellular components of the heart compile genetic and epigenetic information to design blueprints for the cardiac pump. In this chapter we introduce a few things we do know, many we do not know, and some we hope to find out regarding heart and valve development.

2.2 Vertebrate Heart Morphogenesis

The structure and function of the vertebrate heart has been the subject of studies for centuries. Some of the earliest contributions to the field were made by Leonardo DaVinci (1452-1519) in the 15th century. His drawings illustrate the anatomy of the mature human heart and valves. DaVinci created models of the heart and documented the flow patterns of millet seeded water through his models (Keele 1979). Since then, a wealth of knowledge on heart morphogenesis has been acquired, but much less is known about the development of blood flow patterns in the maturing heart.

As perhaps expected, the complexity of vertebrate heart development has increased throughout evolution. However, despite the differences in adult cardiac structure, many of the genes involved in regulating heart development are conserved amongst vertebrates, suggesting many features of cardiogenesis are also conserved (Cripps et al. 2002; Zheng et al. 2003). In a very brief description of heart morphogenesis, we consider vertebrate species above, and including, fish on the evolutionary ladder (i.e., amphibians, reptiles, and mammals). Heart development consists of four conserved stages: (i) heart tube formation, (ii) looping, (iii) chamber formation, and (iv) valve formation (reviewed by Moorman et al. 2003). The first functional shape of the heart is a linear tube composed of enodocardium and myocardium. Peridic myocardial contractions begin shortly after the tube is formed and blood circulation commences. The next stage of cardiogenesis consists of right-handed bending of this tube into a "C" shape. Chamber boundaries become marked first by endocardial cushions (ECs) and finally by valve leaflets, aiding the unidirectional flow of blood through the heart. The duration of cardiac morphogenesis, number of chambers, and final shape of the mature heart are specific to each species.

2.3 Embryonic Zebrafish as a Model

The zebrafish, named appropriately for its black-and-white stripes, is a tropical fresh water fish native to the Ganges River. This species has recently garnered significant interest in the clinical and biological communities as a model to study normal and abnormal vertebrate heart development. Eggs are externally fertilized and embryos can be rendered transparent, providing optical access to the earliest stages of heart development

(Fig. 2.1A-C). The small size of the embryo also makes it a candidate for confocal laser scanning microscopy (CLSM). Zebrafish embryos develop extremely rapidly (the heart reaches its mature configuration within 5 dpf (days post fertilization) and matings can produce several hundred embryos at a time, considerably enhancing the experimental throughput in comparison to other vertebrate models such as chicks or mice.

Zebrafish do not become critically dependent on a functional heart for several dpf, relying instead on diffusion alone to attain nutrients. Unlike in other larger vertebrate models, this unique characteristic of the zebrafish facilitates the study of heart malformations for a considerable period of development since the mutations are not immediately embryonic lethal. Perhaps the most generally appealing characteristic of zebrafish is their use as a genetic tool. The genome has been sequenced, and two large scale mutant screens have produced hundreds of mutants with a variety of cardiac phenotypes (Stainier et al. 1996; Chen et al. 1996), many of which resemble human cardiac malformations. In addition, a number of transgenic strains have been derived expressing fluorescent proteins (i.e, GFP, RFP, etc.) in tissue specific cell types (Long et al. 1997; Huang et al. 2003; Motoike et al. 2000), making zebrafish a powerful model for imaging as well.

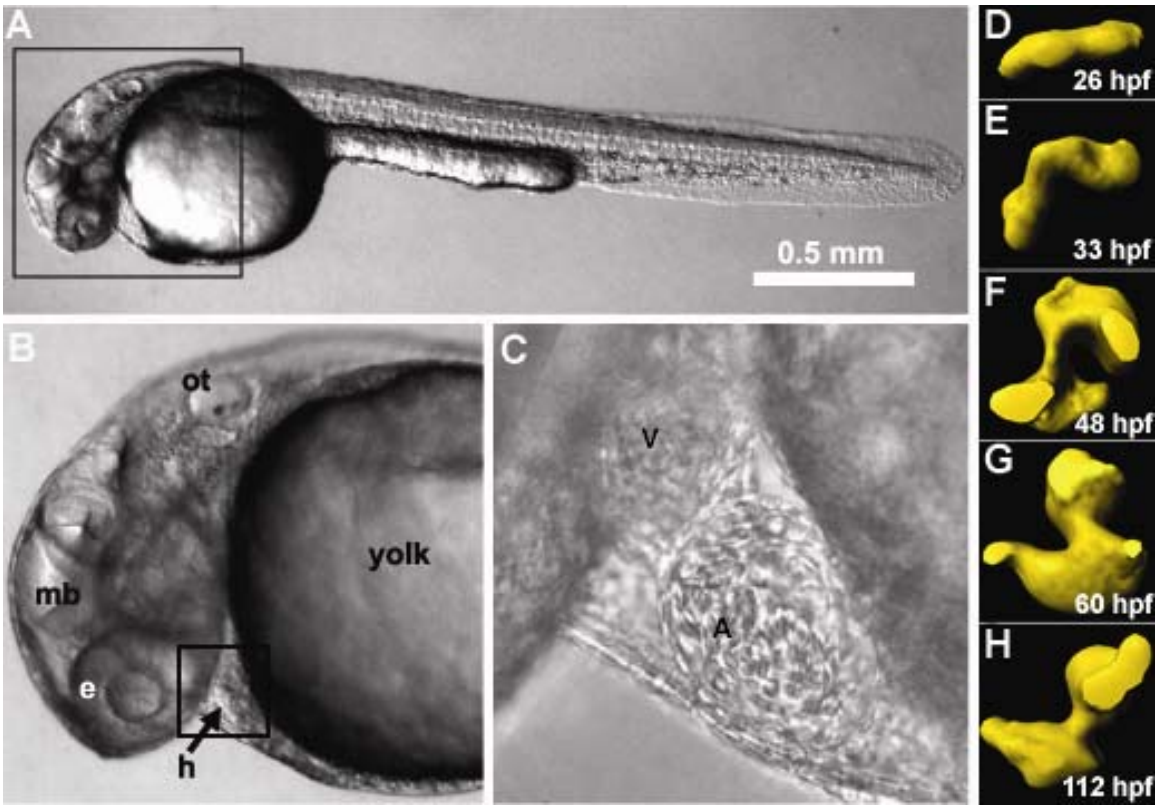

Figure 2.1. Embryonic zebrafish and heart development. (A,B) The small size and optical clarity of the embryonic zebrafish are evident through brightfield microscopy. The heart (h), midbrain (md), otic vesicle (ot), and eye (e) are labeled. (C) In a higher magnification image of the heart, the atrium (a), and ventricle (v) are visible. (D-H) Rapid heart development is illustrated by molds of the zebrafish heart throughout cardiogenesis. The zebrafish heart matures in 5 dpf. Stages of development in hours post fertilization (hpf) are included. (adapted from Liebling et al. 2005).

2.3 Zebrafish Heart Morphogenesis

The cardiovascular system is the first functional organ system to develop in vertebrate embryos. In its earliest stages is consists of a primitive heart tube that drives blood through a simple vascular network. During zebrafish heart morphogenesis, the linear heart tube rapidly loops and bends into a dynamic multichambered organ, all the while sustaining circulation (Fig. 2.1D-H). Despite the departure between the

morphology of the adult zebrafish heart and the adult human heart, many fundamental features of cardiac morphogenesis are conserved between the two vertebrate species.

The embryonic zebrafish heart tube originates from myocardial precursors that converge at the midline and fuse to form a cone by the 21 somite stage (19.5 hours post fertilization, hpf) (Yelon et al 1999; Stainier et al. 1993). This cone transforms into a linear heart tube consisting of concentric rings of endocardium and myocardium separated by an elastic cardiac jelly, and moves from the dorsal-ventral axis (D-V) to the anterior-posterior (A-P) axis of the embryo along the ventral midline (Trinh and Stainier, 2004). The A-P polarity conveniently positions the heart near the ventral plane of the embryo and within the light scattering limits of confocal microscopy. The initial myocardial contractions (22 hpf) are sporadic and do not effectively drive circulation. By 24 hpf, cells near the inflow tract adopt a pacemaker role and initiate periodic contractions (~1 Hz) that suck blood through the heart tube.

During the next 24 hours of development, the zebrafish heart undergoes rapid morphological changes. The linear heart tube loops to the right (31 hpf) and adopts an intermediate “C” shape. Several hours later (~36 hpf), distinct chambers begin to emerge. The ventricle is positioned to the right of the atrium and the heart transforms from a “C” to a more advanced “S” configuration. The ventricle becomes lined by an additional layer of myocardial cells (Hu et al. 2000) (48 hpf) and the boundary between the two chambers becomes defined by a constriction known as the AV canal, the site of the future AV valve. Over the course of heart development, pacemaker cells that initiate atrial contractions increase their firing rate, causing the heart rate to increase from ~1Hz to ~3Hz.

By 5 dpf, the zebrafish heart matures to its adult configuration. The atrium and ventricle are separated by a functional bicuspid valve, supporting unidirectional circulation through the heart. The ventricle transforms from a hollow structure to a densely trabeculated chamber. The atrium remains untrabeculated and repositions dorsal to the ventricle. The rapid and well-characterized development of the zebrafish heart is an asset for cardiogenetic studies.

2.5 Factors Influencing Cardiogenesis

2.5.1 Genetic Contributions

Explant studies in the early 20th century showed that information guiding specific stages of heart formation was pre-programmed in cardiac cells. Some of the earliest experiments were performed in amphibians in the 1920's (Ekman 1921, 1924; Stohr 1924; Copenhaver, 1926) and have since been extended to chicks (Rudy et al. 2001) and mice (reviewed by Zaffran et al. 2003). These studies demonstrated that many characteristics of normal cardiac development (i.e., looping and chamber formation) and dynamics (i.e., contractions) could be maintained despite removing the heart from its natural environment.

With contemporary molecular biology, specific genes influencing cardiogenesis have been identified through random mutation screens, gene ablations, and mRNA knock downs. In zebrafish, random mutations through chemical mutagenesis (Solnica-Krezel et al. 1994; Driever et al. 1996) are used to isolate fish with single gene mutations. Individuals with mutant phenotypes of interest are selected to retrospectively identify the mutated gene. Many genes critical to heart development in zebrafish have been identified

through two large scale screens published in 1996 (Stainier et al 1996; Chen et al 1996). Some of the creatively named cardiac mutants derived from these screens include *santa* (enlarged heart, no valves), *hip hop* (cardiac rhythm mutation), *dead beat* (reduced ventricular contractility), and *silent heart* (no heart beat). In cases where the sequence of a gene is known, gene ablations (reviewed by Rajewsky et al. 1996) and knockdowns (reviewed by Heasman 2002) can identify the developmental role of the targeted gene. Specific genes can be removed or inactivated at particular stages using conditional knockout strategies in mice (reviewed by Rajewsky et al. 1996). This class of studies has similarly revealed a number of genes necessary for normal heart development in mice (McFadden et al. 2005).

Collectively, explant studies, random mutation screens, and specific gene ablations provide a large body of evidence supporting the genetic basis for cardiogenesis, a platform that does not generate much debate. However, all aspects of heart development cannot be explained through genetic programming alone.

2.5.2 Epigenetic Contributions

The contributions of hemodynamic forces in cardiogenesis have been debated for some time. Early experiments examining cultured endothelial cell responses to fluid forces found that endothelial cells, which form the interface between the lumen of the developing heart and flowing blood cells, can sense their fluid dynamic environment and transduce mechanical stimuli, such as shear stress, into changes in gene expression, cell shape, and cell arrangement (reviewed by Davies, 1995; Davies et al. 1984, 1986; Garcia-Cardena et al. 2001). Dewey et al (1981) showed that bovine aortic endothelial cells

exposed to laminar shear stresses of 5 dynes/cm^2 for 24 hours changed from a polygonal to ellipsoidal shape and oriented in the direction of flow. Since then, experiments have explored the magnitudes and types (laminar, turbulent, oscillatory) of shear stresses that induce cellular responses. With the advent of microarray chips, studies now compliment morphological investigations with global gene expression responses to fluid dynamic forces (Ohura et al. 2003; reviewed by McCormick et al. 2003). Many of the genes known to influence cardiogenesis have independently been shown to respond to shear stresses.

A series of in vivo experiments have further validated claims that fluid dynamic forces influence cardiogenesis. Endocardial cells near the atrial boundary of the AV canal and in the developing AV cushions (Icardo, 1989) in the chick heart orient with the direction of flow. Fluid forces in these regions of the heart are amplified due to increased blood velocities. Consistent with "flow molding" theories, the two faces (ventricular and atrial) of the semilunar valve in chicks (Hurle and Colvee, 1983) and humans (Maroon and Hutchins, 1974) are marked by distinct cell shapes and alignments. During systole, blood jets across the semilunar valve generating large shear stresses on the ventricular surface of the leaflets. Elongated endocardial cells on the ventricular surface orient parallel to the flow direction. In contrast, systolic blood flow creates vortices on the arterial side of the leaflets, leaving endocardial cells irregularly shaped and without any recognizable orientation.

A number of techniques have also been utilized to perturb blood flow in vivo to study flow related cardiac anomalies. Some studies have included ligating vessels or chambers (Jafee, 1965; Hogers et al. 1997, 1999) to alter flow patterns. Another

technique employed to alter flow in vivo is the injection of magnetic particles into the blood stream (Acevedo-Bolton, 2005). The position of the particles can be manipulated through an external magnet. This technique still requires refinement for precise control of blood flow, but results indicate blocking flow into the heart stunts development at the heart tube stage. In addition, the *silent heart* (*sih*) zebrafish mutant has been used to show that the absence of blood flow through the heart leads to incomplete heart development and the absence of heart valve leaflets (Bartman et al. 2004). The consensus result is that abnormal blood flow through the intact heart leads to abnormal heart and valve development.

In another case specifically involving zebrafish cardiogenesis, Hove et al (2003) demonstrated that occluding flow out of and into the 37 hpf heart tube with 50 μm glass beads caused the heart to develop abnormally (Fig. 2.2; Appendix A). In both cases, generating high and low cardiac pressures respectively, chambers and valves did not form completely, the inflow and outflow tracts fused, and the heart did not reposition to its mature configuration. Control embryos with inserted beads not blocking blood flow through the heart developed normally. These results again demonstrate hemodynamic forces are an essential epigenetic factor in cardiogenesis. One of the common threads shared among embryos exposed to a variety of hemodynamic perturbations is that many of the cardiac anomalies include heart valve defects (Fig. 2.2J-L).

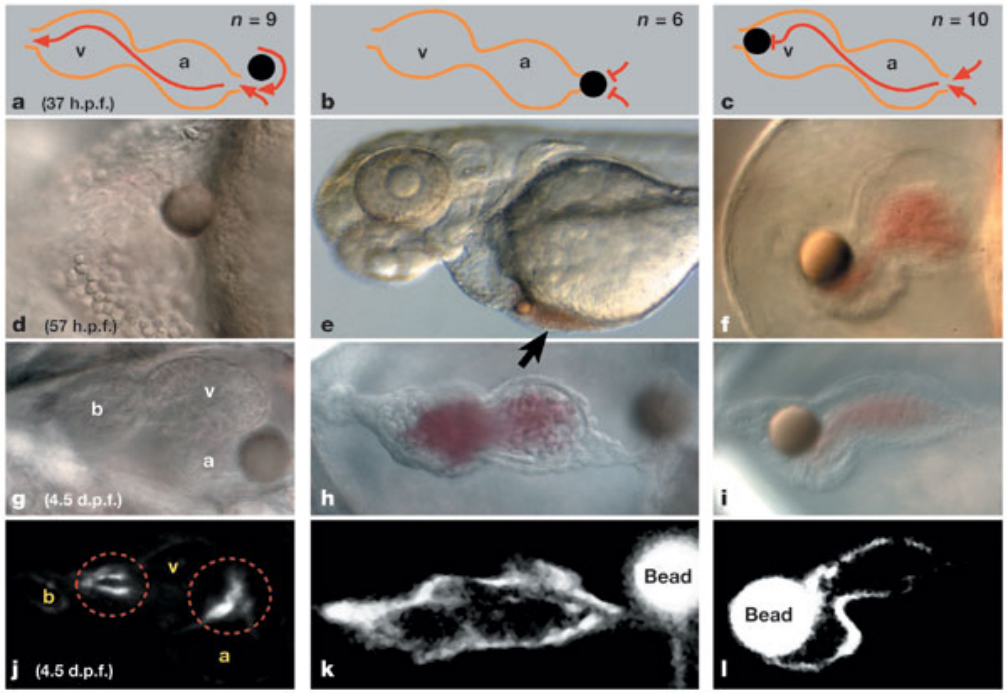

Figure 2.2. Hemodynamic forces are essential for proper cardiogenesis. (A-C) Schematic illustrating three different bead positions. (A) Control embryo with bead not blocking flow into or out of heart. (B) Embryo with bead blocking flow into heart (low pressure). (C) Embryo with bead blocking flow out of heart (high pressure). (D-F) Brightfield images of wild type zebrafish hearts with implanted beads at two developmental stages. (J-I) Fluorescent images of *Tg(tie2:GFP)* fish show blood flow is also critical for normal valve development. (adapted from Hove el al, 2003).

2.6 Discussion

The nature of the experiments implicating hemodynamic forces as contributing factors towards cardiogenesis have understandably generated heated debate and raised many more questions. They have also motivated a number of follow-up studies. For example, in response to the experiments described by Hove et al (2003), Bartman et al (2004) attempted to differentiate between myocardial function and abnormal hemodynamics by studying two cardiac contractile mutants (*sih* and cardiofunk, *cfk*) that lack EC formation. They complemented these experiments by pharmacologically altering contractile mechanics in wild type embryos. Through their analysis, they suspected

myocardial function was more influential in cardiogenesis than blood flow, however they concluded that the distinct contributions of myocardial function and hemodynamics could not be definitively separated. We extend their results to propose that the cardiogenetic effects of myocardial function and blood flow are indistinguishable because myocardial function and hemodynamics themselves are inseparable.

The dynamic relationship between structure and function in the developing heart imposes many constraints on the types of experiments that can be performed. Often times, experimental manipulations provoke questions regarding which effects are primary. Any hemodynamic perturbations using the intact heart in wild type embryos will undoubtedly cause changes in contractile mechanics, since the two are causally related. The challenge is to conduct experiments through relatively subtle changes in mechanics and flow.

In this work, we show that heart valve anomalies result from small perturbations in cardiac mechanics that lead to significant changes in intracardiac flow. We think these results will continue to advance the running dialogue surrounding the genetic and epigenetic contributions to cardiogenesis.

2.7 Chapter References

Acevedo-Bolton G, *Blood flow effects on heart development and a minimally invasive technique for in vivo flow manipulation*. PhD thesis, California Institute of Technology (2005).

Balcells M, MF Suarez, M Vazquez, ER Edelman, *J Cell Physiol*. **204**, 329 (2005).

Bartman T, EC Walsh, K Wen, M McKane, J Ren, J Alexander, PA Rubenstein, DY Stainier, *PLoS Biol*. **2**, 673 (2004).

Chappell DC, SE Varner, RM Nerem, RM Medford, RW Alexander, *Circ Res*. **82**, 532 (1998).

Chen JN, P Haffter, J Odenthal, E Vogelsang, M Brand, FJ van Eeden, M Furutani-Seiki, M Granato et al., *Development*. **123**, 293 (1996).

Copenhaver WM, *Amblystoma punctatum J. Exp. Zool*. **43**, 321 (1926).

Cripps RM, EN Olson, *Dev Biol*. **246**, 14 (2002).

Davies PF, CF Dewey, SR Bussolari, EJ Gordon, MA Gimbrone, *J Clin Invest*. **73**, 1121 (1984).

Davies PF, A Remuzzi, EJ Gordon, CF Dewey, MA Gimbrone, *Proc Natl Acad Sci USA*. **83**, 2114 (1986).

Davies PF, *Physiol Rev*. **75**, 519 (1995).

Dewey CF, SR Bussolari, MA Gimbrone, PF Davies, *J Biomech Eng*. **103**, 177 (1981).

Driever W, L Solnica-Krenzel, AF Schier, SC Neuhauss, J Malicki, DL Stemple, DY Stainier, et al., *Development*. **123**, 37 (1996).

Ekman G, *Oevers. Fin. Vetensk. Soci. Foerh. A*. **63**, 1 (1921).

Ekman G, *Wilhelm Roux' Arch. Entwicklungsmech. Org.* **106**, 320 (1924).

Forouhar AS, Liebling M, Hickerson A, Nasiraei-Moghaddam A, Tsai HJ, Hove JR, Fraser SE, Dickinson ME, Gharib M, *Science*. **312**, 751 (2006).

Garcia-Cardena G, J Comander, KR Anderson, BR Blackman, MA Gimbrone, *Proc Natl Acad Sci USA*. **98**, 4478 (2001).

Haga M, A Yamashita, J Paszkowiak, BE Sumpio, A Dardik, *J Vasc Surg*. **37**, 1277 (2003).

Harvey RP, N Rosenthal, *Heart Development*. (Canada: Academic Press, 1999).

Heasman J, *Dev. Biol*. **243**, 209 (2002).

Hogers B, MC DeRuiter, AC Gittenberger-de Groot, RE Poelmann, *Circ. Res*. **80**, 473 (1997).

Hogers B, MC DeRuiter, AC Gittenberger-de Groot, RE Poelmann, *Cardio. Res*. **41**, 87 (1999).

Hove JR, RW Koster, AS Forouhar, G Acevedo-Bolton, SE Fraser, M Gharib, *Nature.* **421**, 172 (2003).

Hu N, D Sedmera, JH Yost, EB Clark, *Anat. Rec*. **260**, 148 (2000).

Huang CJ, CT Tu, CD Hsiao, FJ Hsieh, HJ Tsai, *Dev. Dyn*. **228**, 30 (2003).

Hurle JM, E Colvee, *Anat. Embryol*. **167**, 67 (1983).

Icardo JM, *Anat. Rec*. **225**, 150 (1989).

Jaffee OC, *Anat. Rec.* **151**, 69 (1965).

Keele KD, *Yale Journal of Biology and Medicine*. **52**, 376 (1979).

Liebling M, AS Forouhar, M Gharib, SE Fraser, ME Dickinson, *J. Biomed. Optics* **10**, 054001 (2005).

Liebling M, AS Forouhar, R Wolleschensky, B Zimmermann, R Ankerhold, SE Fraser, M Gharib, ME Dickinson, *Rapid three-dimensional imaging and analysis of the beating embryonic heart reveals functional changes during development*, in preparation.

Long Q, A Meng, H Wang, JR Jessen, MJ Farrell, S Lin, *Development*. **124**, 4105 (1997).

Maroon BJ, GM Hutchins, *Am. J. Pathol*. 74,331 (1974).

McCormick SM, SR Frye, SG Eskin, CL Teng, CM Lu, CG Russell, KK Chittur, LV McIntire, *Biorheology*. **40**, 5 (2003).

Moorman AF, VM Christoffels, *Physiol Rev*. **83**, 1223 (2003).

McFadden DG, AC Barbosa, JA Richardson, MD Schnieder, D Srivastava, EN Olson, *Development*. 132, 189 (2005).

Motoike T, S Loughna, E Perens, BL Roman, W Liao, TC Chau, CD Richardson, *Genesis*. **28**, 75 (2000).

Ohura N, K Yamamota, S Ichioka, T Sokabe, H Nakatsuka, A Baba, M Shibata, *J Atheroscler Thromb*. 10, 304 (2003)

Rajewsky K, H Gu, R Kühn, UAK Betz, W Müller, J Roes, F Schwenk, *J Clin Invest*. **98**, 600 (1996).

Remuzzi A, CF Dewey, PF Davies, MA Gimbrone, *Biorheology*. **21**, 617 (1984).

Rudy DE, TA Yatskievych, PB Antin, CC Gregorio, *Dev Dyn*. **221**, 61 (2001).

Sato M, N Ohshima, *Biorheology*. **31**, 143 (1994).

Solnica-Krezel L, AF Schier, W Driever, *Genetics*. **136**, 1401 (1994).

Sorescu GP, H Song, SL Tressel, J Hwang, S Dikalov, DA Smith, NL Boyd, MO Platt, et al., *Circ Res*. **95**, 773 (2004).

Sorescu GP, M Sykes, D Weiss, MO Platt, A Saha, J Hwang, N Boyd, et al., *J Biol Chem*. **278**, 31128 (2003).

Stainier DY, RK Lee, MC Fishman, *Development*. **119**, 31 (1993).

Stainier DY, B Foquet, JN Chen, KS Warren, BM Weinstein, SE Meiler, MA Mohideen, et al., *Development*. **123**, 285 (1996).

Stoh P, *Arch. Mikrosk. Anat. Entwicklungsmech*. **102**, 426 (1924).

Trinh LA, DY Stainier, *Methods Cell Biology*. **76**, 455 (2004).

Yelon D, SA Horne, DY Stainier, *Dev Biol*. **214**, 23 (1999).

Zaffran S, R Kelly, A Munk, N Brown, M Buckingham, *Journal de la Societe de Biologie*. **197**, 187 (2003).

Zheng B, J Wen, M Han, *Biochemistry*. **68**, 795 (2003).

Chapter 3: Cardiac Imaging Tools and Techniques

3.1 Introduction

In vivo three-dimensional data can provide structural information on genes, cells, and organ systems. Dynamic data provide information on how things move. Collectively, they can teach us how proteins fold, cells move, and organs form. Optimal live imaging requires tools and techniques specifically tailored to the observed model system. The zebrafish naturally offers a beautiful window to view cardiogenesis and valvulogenesis, but the dynamic nature of heart contractions and morphogenesis presents a number of imaging challenges. Simply put, hearts are microscopic and cardiac cell motions are rapid. Here, we discuss techniques employed to optimize in vivo cardiac imaging using contemporary confocal microscopy and four-dimensional visualization tools. Together they allow us to view dynamic cardiac motions at previously unmatched spatial and temporal resolutions and acquire novel qualitative and quantitative data to assess early cardiac structure and function. In this chapter we present diagnostic tools and techniques used to study heart morphogenesis and the effects of blood flow through the developing heart.

We begin our discussion with a general protocol on zebrafish embryo collection and preparation for imaging. Three transgenic zebrafish strains that fluorescently label endocardium, myocardium, and blood cells, along with a vital dye that provides contrast to simultaneously view cardiac tissue and blood cells are introduced. We briefly describe the technology behind the pre-production prototype of the Zeiss LSM 5 LIVE employed to observe dynamic cardiac motions along with the synchronization algorithm

implemented to obtain dynamic four-dimensional (three-spatial dimensions and time) data of the beating heart. These tools enabled us to assemble a unique library of heart development data. As a result, we now have access to a number of embryonic cardiac diagnostics, including cardiac volume estimations, four-dimensional cardiac cell tracking, and more complete descriptions of blood flow throughout cardiogenesis. We end this chapter with a discussion of two quantitative methods, digital particle imaging velocimetry (DPIV) and particle tracking, to describe intracardiac flow in zebrafish.

3.2 Zebrafish Preparation

Adult zebrafish are housed in the biological imaging center and cared for by faculty, staff, and students in accordance with Westerfield (2000). Wild type, transgenic, and mutant zebrafish lines are separated into small tanks and fed brine shrimp and flake food multiple times daily. The fish room is maintained at 28.5 ºC and under a strict photoperiod (14 hours of light, 10 hours of darkness). Zebrafish embryos can be spawned from a pair of adults multiple times per week, with each mating producing hundreds of offspring. Externally fertilized embryos are collected in the morning in mating cages designed to separate fertilized eggs from adults, preventing adults from feeding on embryos. Embryos are raised in artificial pond water and staged according to (Kimmel et al. 1995).

A number of techniques are available to facilitate in vivo zebrafish imaging. Embryos can be treated with 0.003% phenylthiourea (PTU) between 12 and 24 hpf to prevent pigment formation (Fig. 3.1). In order to specifically prevent pigment formation blocking the ventral view of the heart, PTU can be added to the artificial pond water as

late as 40 hpf. Experimental embryos imaged prior to 48 hpf are manually dechorionated using forceps. If desired, dechorionated embryos can be stained with vital dyes illuminating specific structures. Minutes prior to imaging, embryos are anesthetized in 0.0175% tricaine methanesulfonate (Argent). Embryos can remain anesthetized for up to 24 hours with no adverse affects.

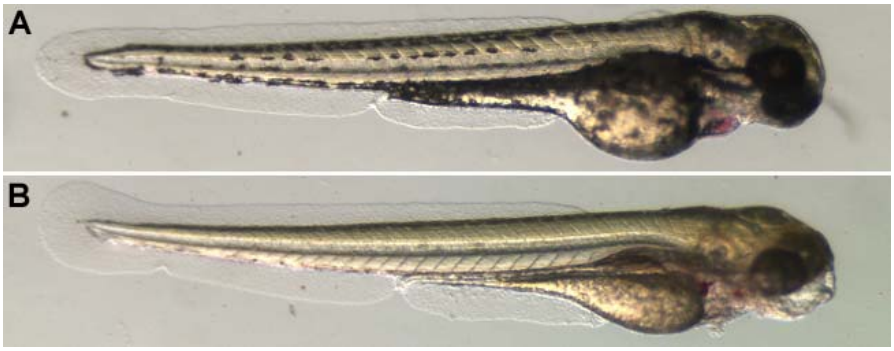

Figure 3.1. Blocked pigment formation in PTU-treated zebrafish embryos. (A) 72 hpf embryo with normal pigment formation. Often times pigment obscures views of internal structures. (B) Embryo treated with PTU does not form pigment.

Multiple techniques are available for immobilizing zebrafish for cardiac imaging. The appropriate technique depends on the imaging method, imaging duration, and developmental stage of the embryo. In the simplest case, for brightfield imaging done on an inverted microscope with an adjustable stage, embryos can be placed in a small drop of artificial pond water on a cover slip and directly viewed without anesthesia. Embryos older than 72 hpf are stable on their ventral surface. Simply touching an embryo's tail with a small Eppendorf microloader will cause the fish to swim briefly and eventually come to rest on the ventral surface. The liquid drop size restricts the motion of the swimming embryo. The stage is then adjusted so that the heart is in the field of view.

For confocal imaging, alternate methods are used since laser light causes the fish to escape from the excitation path. Embryos viewed with confocal microscopy must be

anesthetized. When multiple views of a single embryo are desired from an upright confocal micrscope, the best positioning method is to place embryos in small wells etched in agarose. Wells are made by pouring 30 mL of 1.5% molten agarose (Invitrogen) into a Petri dish (100 x 15 mm, VWR). A plastic mold is then placed on the molten agarose before it cools. When the agarose cools to room temperature (20 ºC) and hardens, the plastic mold is removed, leaving the desired pattern etched into the agarose gel. An elaborate series of plastic molds are available with patterns designed for a variety of developmental stages and embryo orientations (Megason et al. in preparation). In our case, simple block wells etched into agarose (750-900 μm wide) are sufficient. Embryos are placed into these wells and anesthetized with tricaine. Until ~5 dpf, embryos are negatively buoyant and sink to the bottom of the wells. The embryos can then be positioned manually using a small Eppendorf microloader. A detailed analysis of the best viewing angles for cardiac imaging at various developmental stages, along with detailed positions of the chambers and valves, is provided in Appendix B. One convenient feature of this positioning method is that a single embryo can be viewed from multiple angles. The major drawback is that if the embryo moves during imaging, *z*-sections cannot be correctly registered.

If a more rigid immobilization is desired, embryos can be positioned in small beads of agarose that fix the embryo in a single position. In this method, embryos are contained in a small drop of low melting point agarose (Sigma) stored at 28.5 ºC and placed on a Petri dish. An Eppendorf microloader is used to position the embryo before the agarose gels (20ºC). Once the agarose hardens, the embryo position is fixed. Artificial pond water is poured around the porous agarose so that the embryo receives nutrients

throughout immobilization. Embryos can be immobilized in agarose beads for up to 24 hours. The main advantage of this method is that the embryo position is fixed during imaging and can be maintained throughout long imaging periods. The drawback is that only one position can be viewed without removing the embryo from the bead.

3.3 Fluorescent Contrast Agents

In order to optically visualize static or dynamic structures, contrasting spectral properties between the observed structures and background must exist. Light focused on a sample is absorbed, transmitted or reflected, and this combination defines the appearance. Sometimes cells and structures are autofluorescent, but often times contrast is artificially enhanced by adding fluorescent molecules into specific cells of interest. The spectral properties of the fluorescent markers determine the excitation and emission wavelengths of the fluorophores and appropriate filters are utilized to collect emitted light from the sample. Multiple fluorophores can be used in a single sample as long as their spectral properties are sufficiently discernable. Two common ways to label cellular, or subcellular, structures in a living organism are through transgenic strains with fluorescent proteins inserted into the genome and fluorescent vital dyes. We employ both to visualize cardiac structures in the developing zebrafish.

3.3.1 Transgenics

Deriving transgenic strains offers the opportunity to acutely label tissue specific cell types. This can be achieved by integrating a DNA sequence coding a fluorescent protein (i.e., green fluorescent protein, GFP, red fluorescent protein, RFP, etc.) whose

expression is driven by a selected promoter. The primary requirement to create a transgenic is that the promoter sequence must be known. When this is the case, a much wider variety of cells can be labeled in comparison to vital dyes. Deriving transgenic lines requires a significant initial investment to create stable strains, but requires no additional sample preparation since the fluorescent proteins are expressed in the offspring. Stable transgenic lines can also be crossed with mutant strains to label specific cells in mutant embryos. A variety of zebrafish transgenic strains has been derived to observe cardiac cells, some of which we describe in the following sections.

3.3.1.1 *Tg(gata1:GFP)*

In order to observe intracardiac blood flow patterns with confocal microscopy, we imaged *Tg(gata1:GFP)* zebrafish provided by Shuo Lin (UCLA). These fish express GFP behind the GATA-1 promoter, an erythroid-specific transcription factor (Long et al. 1997). We visualized GFP in blood cells throughout development (Fig. 3.2), and to a lesser extent, endocardial and myocardial cells early in heart development (until ~72 hpf). GFP expression within an individual embryo varied greatly, some blood cells appeared large and bright while others appeared smaller and dimmer. The variations in brightness and size may be partially due to imaging thin sections with confocal microscopy. The ellipsoidal blood cells with the long axis in the imaging plane appear brighter and larger. Imaging blood flow in *Tg(gata1:GFP)* embryos allowed us to connect cardiac structure and function (Chs. 4, 5).

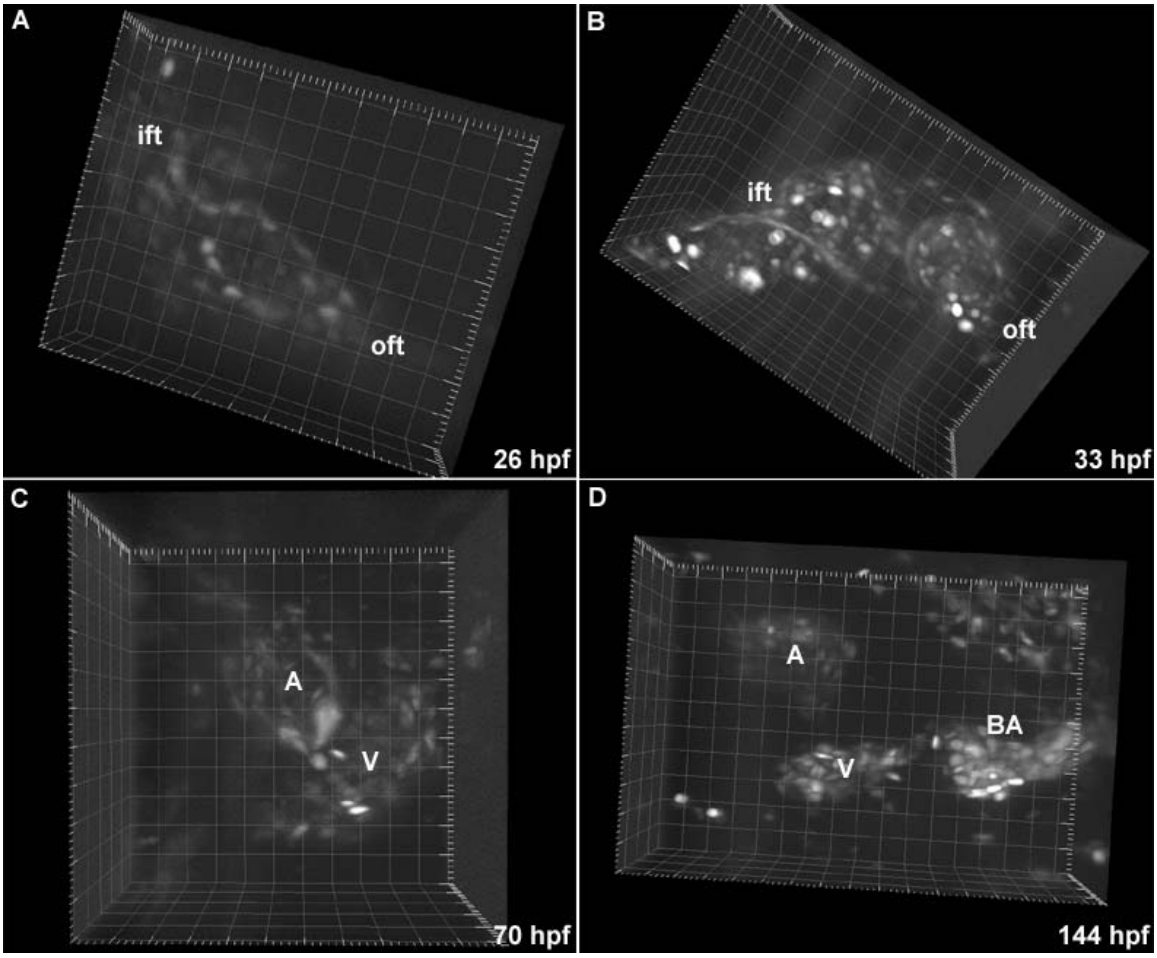

Figure 3.2. Heart morphogenesis in *Tg(gata1:GFP)* embryos. (A-D) Blood cells are fluorescently labeled, permitting visualization of blood flow and intracardiac volumes. The inflow tract (ift), outflow tract (oft), atrium (A), ventricle (V) and bulbus arteriosus (BA) are labeled. Grid spacing is 20 µm.

3.3.1.2 *Tg(cmlc2:GFP)*

In order to observe cardiac mechanics, we imaged *Tg(cmlc2:GFP)* provided by Huai-Jen Tsai (National Taiwan University). These fish express GFP behind the myosin light chain-2 (MLC-2) promoter, a myocardial specific gene (Huang et al. 2003). GFP expression was consistenly bright in myocardial cells throughout cardiogenesis and *Tg(cmlc2:GFP)* embryos were the most suitable transgenic strain for imaging due to the high signal-to-noise ratio (Fig. 3.3). The fluorescent label permits high resolution

visualization of morphological changes during cardiogenesis (i.e., looping in Fig. 3.3A,B, trabeculation in Fig. 3.3E,F) as well as biomechanics within a single cardiac cycle (i.e., myocardial strain, etc.).

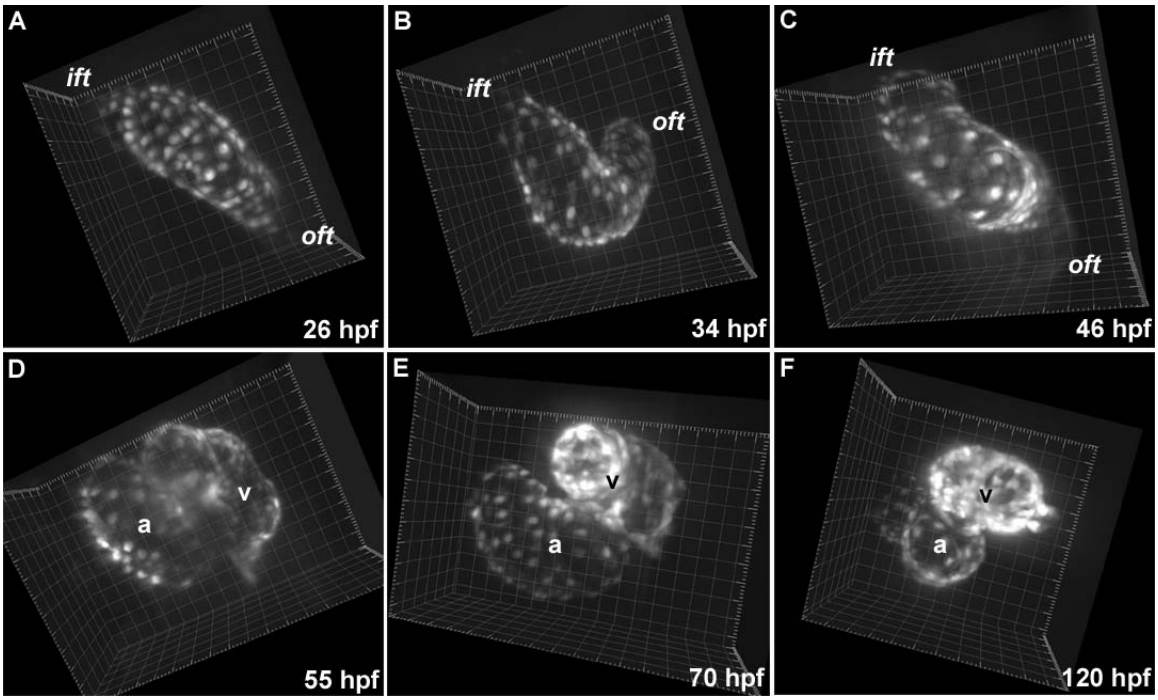

Figure 3.3 Heart morphogenesis in *Tg(cmlc2:GFP)* embryos. Fluorescently labeled myocardium permits visualization of cardiogenesis and contractile mechanics. (A-C) Observing embryonic hearts between 26 and 46 hpf provides a detailed description of heart tube looping in vivo. The primitive heart tube loops to the right, forms a "C" by 34 hpf and eventually forms an "S" by 46 hpf. (D) Well defined chambers are evident by 55 hpf. (E,F) Ventricular trabeculation is evident between 70 and 120 hpf. Grid spacing is 20 µm.

3.3.1.3 *Tg(tie2:GFP)*

In order to observe endocardial cell motions and valve dynamics, we imaged *Tg(tie2:GFP)* zebrafish provided by the Stainier Lab (UCSF). These fish express GFP behind an endothelial-specific receptor tyrosine kinase, tyrosine kinase with immunoglobulin and epidermal growth factor homology domain-2, tie2 (Motoike et al. 2000). In the early stages of cardiogenesis, a single endothelial cell layer is evident lining

the lumen of the primitive heart tube. Endothelial cells later invade the ECs, making the AV canal significantly brighter. Endocardial cells in growing valve cushions, and eventually leaflets, continue to express GFP throughout valvulogenesis. GFP expression in valves is much brighter than endocardium, and poses a problem for dynamic imaging. In order to observe the atrial and ventricular endocardium, the laser must be operated at high power which saturates the signal in the valve regions, making fine structures and delicate motions challenging to resolve.

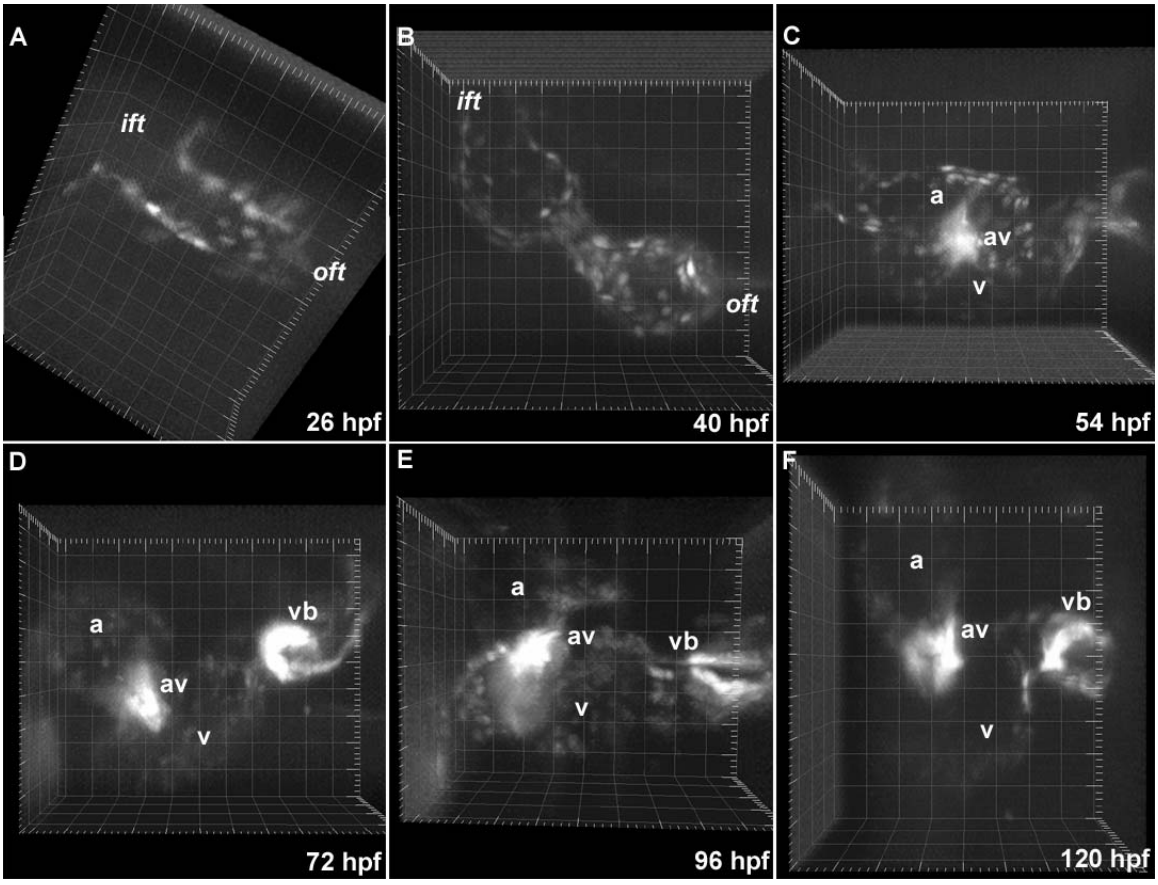

Figure 3.4. Heart morphogenesis in *Tg(tie2:GFP)* embryos. (A) A single layer of endothelial cells lines the 26 hpf heart tube. (B) Chamber formation is evident by 40 hpf. (C) By 55 hpf, endothelial cells invade the ECs, making the AV boundary (av) much brighter than the surrounding endocardium. (D-F) GFP expression continues to be much brighter in the developing AV and ventriculo-bulbar (VB) valves. Grid spacing is 20 µm.

3.3.2 Vital Dyes

Vital dyes are an important tool for labeling cells and structures in wild type animals. For zebrafish heart imaging, it provides a method to label cells within the beating heart with a variety of colors. The major advantage in using vital dyes is the short sample preparation time, and for our purposes, non-tissue-specific staining. Since the fluorescent marker is not integrated into the genome, it permits viewing structures in wild type, transgenic, and mutant embryos in the short time it takes the dye to penetrate the cells.

In order to provide contrast between the heart, serum, and blood cells, we soaked embryos in BODIPYFL C_5-ceramide (Molecular Probes), a fluorescent lipid membrane dye (Fig. 3.5). We initially suspected the dye would stain blood cell membranes, but instead it fluorescently labeled the blood serum, leaving the blood cells and cardiac tissue unlabeled. Despite creating the inverse of what we expected, BODIPY-ceramide staining allowed simultaneous visualization of dynamic heart wall, heart valve, and blood cell motions in the beating heart at all stages of development (Fig. 3.5B). The protocol for this technique is to place 1 µl of 4mM BODIPY-ceramide in a centrifuge tube with 0.2 ml of artificial pond water along with up to ten embryos. Embryos are soaked for at least 4 hours prior to imaging and retain the dye for at least 24 hours after removal.

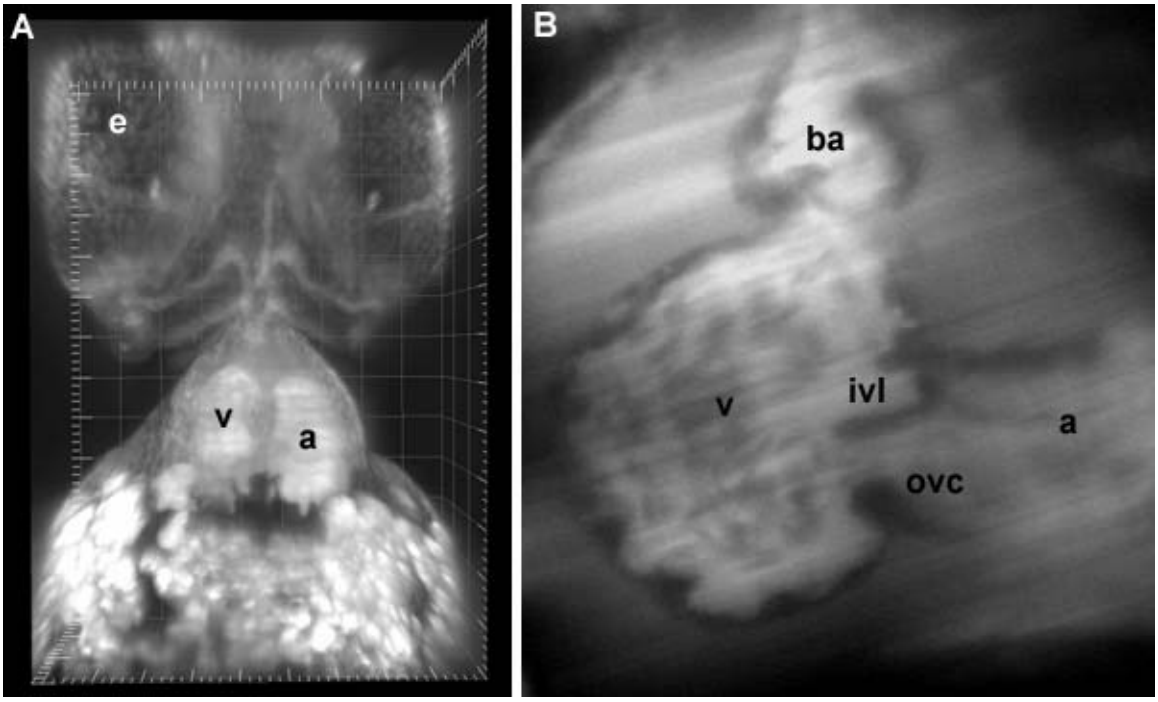

Figure 3.5. BODIPY-ceramide stained embryos reveal non-tissue specific fluorescent contrast. (A) 20X view of a 96 hpf zebrafish embryo illustrates the variety of observable structures. The atrium (a), ventricle (v), and eye (e) are labeled. Grid spacing is 50 µm. (B) 63X view of the heart shows fluorescently labeled blood serum. Serum labeling provides contrast to view the atrium (a), ventricle (v), inner ventricular leaflet (ivl) and outer ventricular cushion (ovc). Unlabeled blood cells can be seen in the ventricle.

3.4 High Speed Confocal Microscopy

(adapted from Liebling et al. in preparation)

A significant amount of data presented in this work has been collected through high-speed confocal microscopy, specifically acquired from a pre-production prototype of the Zeiss LSM 5 LIVE, Carl Zeiss GmbH. Therefore, it is appropriate to briefly discuss some specifications of this prototype along with the technology that has increased confocal scan rates by two orders of magnitude.

Confocal microscopy has significantly improved three-dimensional imaging by allowing high resolution scans to be acquired in vivo. The basic principle of confocal imaging is to illuminate, and collect, emitted light from a very thin section of a

fluorescently marked sample. The thickness of the field of view is controlled by a pinhole aperture that limits signal contribution from out of focus light (i.e., from a plane other than the desired imaging plane). Traditional laser scanning confocal microscopes employ a laser that illuminates a single point on the specimen and, with a pair of vibrating mirrors, scan this point across the imaging plane (scan time is approximately 1 frame per second, fps, for a 512x512 pixel image). The collected light is then detected by a photomultiplier and used to create the image.

The rate-limiting step in acquiring confocal scans is the laser scan time. The LIVE prototype employs a novel line-scanning, as opposed to point-scanning, technique that significantly increases frame rates without sacrificing resolution. Rather than focusing light to a point, the laser beam is shaped to illuminate a full line of pixels and the galvanometer-based mirror is required to scan in only one direction to image a plane, significantly increasing frame rates to 175 fps for a 256x256 pixels image.

Confocal imaging parameters and techniques specific to our applications are presented here. In most cases, we were interested in collecting rapid two-dimensional scans at various optical planes. Using the Zeiss LSM AIM software, a specified number of planar confocal scans were taken at a fixed frame rate (typically between 85 and 175 fps) and time interval between scans (0 seconds). The *z*-positions were registered with the stage control feature of the software, and the *z*-plane could be adjusted by moving the stage manually or through the computer, to optically section through the sample. Before acquiring scans, the excitation wavelength (488 nm for GFP) and appropriate filters (505 nm long pass filter for GFP) were specified. The laser power used depended on the brightness of the fluorescent marker and the amount of GFP expression. The maximum

frame rates depended on the scan mode (bidirectional or unidirectional) and image size (256x256, 512x512, or 1024x1024 pixels). The fastest frame rates possible on the Zeiss LSM 5 LIVE prototype were 175 fps for a 256x256 pixels bidirectional scan. All imaging was done with water-immersion lenses (Achroplan 20x/0.5, 40x/0.8, 63x/0.9). The x,y aspect ratio for each pixel was approximately 1:1.4. The x,y sampling step for the 256x256 pixels image taken with the 40x objective was 0.9 μm x 1.3 μm.

3.5 Four-Dimensional Reconstructions

(adapted from Liebling et al. 2005)

Although embryonic ECGs are available for synchronizing confocal scans, they are cumbersome to acquire while imaging. Short working distance objectives put tight spatial restrictions on electrode positions and orientations, and acquiring ECG data requires additional apparatus to collect and record signals. Therefore, a more convenient method for synchronizing confocal scans acquired at unknown intervals was desired. This is a common challenge in four-dimensional cardiac MR imaging and many solutions have been developed. Some solutions rely on secondary signals such as ECGs to gate slice sequences (prospective gating), and others are capable of synchronizing non-gated data retrospectively by acquiring a reference signal along with the image signal, via specific pulse sequences.

For our purposes, an ideal candidate would (i) not put any additional constraints on imaging logistics, (ii) be robust enough to process large amounts of data quickly, (iii) specifically handle imaging artifacts due to confocal microscopy (i.e., noise, photobleaching, etc.), and (iv) provide reliable data independent of the fluorescent marker

used (i.e., GFP, BODIPY-ceramide, etc.) and cell type labeled (i.e., myocardium, heart valves, blood cells, etc). The solution came through an in-house, wavelet based, post-acquisition synchronization program. A brief summary of the procedure, requirements, and limitations of the synchronization process are provided here, but details can be found in Liebling et al. (2005).

3.5.1 Data Collection

First and foremost, the four-dimensional reconstruction algorithm processes data post-acquisition, increasing experimental throughput and placing no additional restrictions on the imaging setup. High-speed confocal scans (x,y,t) are acquired at one imaging plane (z_1), starting at an arbitrary time in the cardiac cycle. The imaging plane is then moved manually to a proximal imaging plane (z_2) of known distance (Δz) and the scan is repeated, again starting at some unknown time in the cardiac cycle (Fig. 3.6). At least two periods must be recorded at each z-section, preferably many. The sections must be named in an ordered fashion that describes their z-position (i.e., 30hpfGATA_100, 30hpfGATA_105, etc.) so the software can recognize sequential sections. The data are recorded using the LSM AIM software which also records the frame rate, number of frames collected, objective used, and z-position in the LSM formatted files.

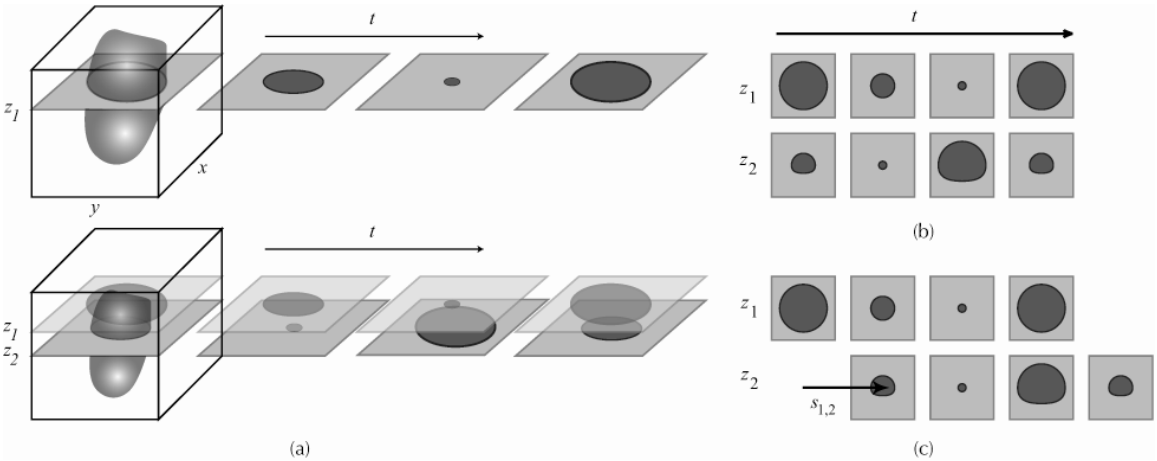

Figure 3.6. Acquiring and synchronizing nongated motions in sequential optical planes (A) Non-synchronized scans at sequential optical sections (z_1, z_2) are recorded. (B) The time interval between recordings at different optical planes is unknown, leaving data naturally unsynchronized. (C) After synchronization, data are shifted to produce aligned volumes. (adapted from Liebling et al. 2005).

3.5.2 Algorithm

The first step in synchronizing slice sequences is to determine the period. An initial guess of the number of frames corresponding to one period (±10%) must be provided by the user and can be obtained utilizing the region of interest (ROI) (Fig. 3.7A,B) function in the AIM software. This function takes the average intensity of a selected group of pixels over time. If the motion is periodic and the region of interest is fixed, the average intensity plot will also be periodic with a small decay due to photobleaching. This first approximation provided by the user is not precise enough to compute the real period. The synchronization software uses the entered period length (number of frames) along with a phase dispersion minimization technique (Stellingwerf et al. 1978) to determine a closer estimate of the period. Briefly, this technique computes the mean intensity of a region at every time point over several periods. For a candidate period, it then shifts (mode locks) the time coordinate of these values onto the first

period. A function, $f(t)$, is computed that connects the phase locked intensity values. A close estimate of the period is obtained when $f(t)$ is minimized (Fig. 3.7C).

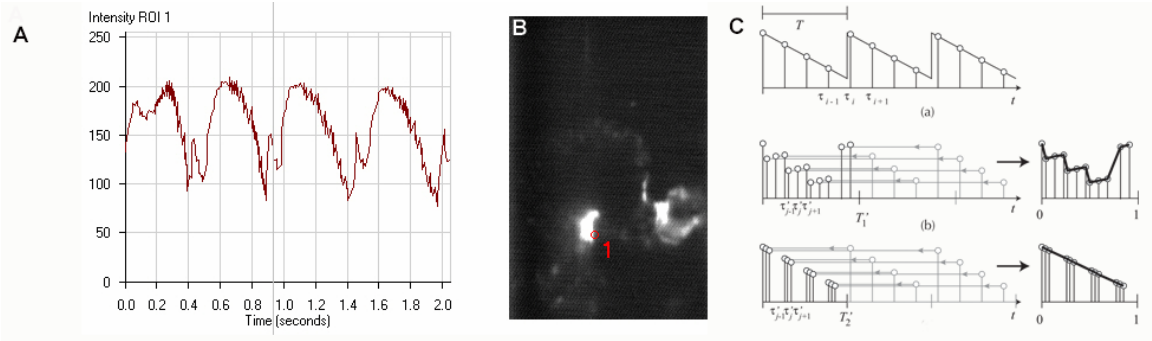

Figure 3.7. Period determination in the zebrafish heart. (A) When heartbeats are periodic, the average pixel intensity of a region of interest (ROI) as a function of time is also periodic, with a small decay due to photobleaching. (B) The ROI should be placed over a bright structure. Here, the ROI is over the AV valve. (C) Period estimations from the ROI are used to determine the actual period. (adapted from Liebling et al. 2005)

Before the relative time shifts between slice sequences are computed, the image data, which is defined by the local intensity $I(x,y,z,t)$, undergo a spatial two-dimensional wavelet transform. The wavelet transform is a multiresolution technique that decomposes periodic functions into space and frequency components. Unlike the Fourier transform, which can only reveal what frequencies are present, the wavelet transform can provide information on where these frequencies occur. One advantage of working in the wavelet domain is that representation of natural images is sparse (i.e., most of the signal energy is concentrated in a small number of coefficients). Data can be greatly reduced in size (roughly corresponding to band pass filtering) by removing specific wavelet coefficients, while preserving relevant image features. For our specific application, we remove fine resolution coefficients corresponding to sharp variations in intensity, such as at the edges of individual blood cells. This greatly reduces the size of our dataset, and significantly

decreases the computation time. We also discard low resolution coefficients thus removing artifacts associated with confocal microscopy (i.e., non-uniform background, photobleaching, etc.).

The computed wavelet coefficients are then used in conjunction with an image registration technique based on the minimization of image intensity differences in a least-squares sense (Thevenaz et al. 1988) to determine the similarities between sequential slice sequences. Time shifts are computed to maximize the similarity between sequential slice sequences. Once the appropriate time shifts are chosen, the slices are shifted in time and reconstructed to four-dimensional datasets.

3.5.3 Limitations

The implemented synchronization technique is very robust, can handle large amounts of information quickly, and is particularly suitable for use with confocal imaging. However, existing limitations need to be considered. The dataset, $I(x,y,z,t)$, must be periodic, and the period must remain constant throughout the different slice sequences. Reconstructed datasets with non-periodic motions can easily be recognized since they are initially synchronized but then quickly fall out of phase (Fig. 3.8).

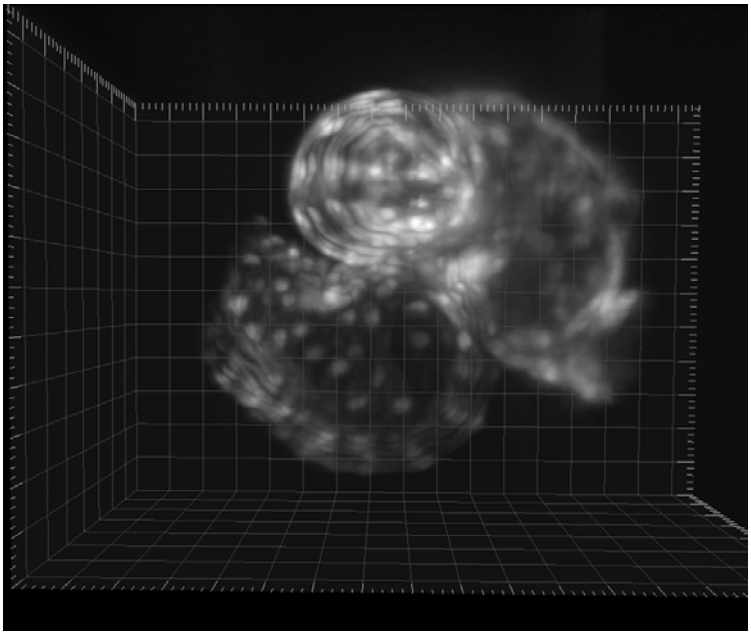

Figure 3.8. Realignment artifacts due to non-periodic cardiac cylces. In this 72 hpf heart, the heart rate was not consistent. While the initial part of the reconstructed cycle is aligned, the non-periodic nature of the data causes the later phases to become unaligned. This is evident by the discernable layers in the atrium and ventricle at the time point shown.

The second limitation restricts the axial sampling step. Sequential scans acquired at different depths must be separated by intervals (Δz) smaller than the axial extent of the point spread function (PSF) (in our case, just over 5 μm). When this case holds, sequential slice sequences share fluorophore excitation information. When the axial sampling step is larger than the axial PSF, sequential slice sequences can be considered disconnected.

Alternatively deformations in the *z*-axis, between sequential optical planes, need to be homogeneous. For example, the algorithm might not accurately re-align two sequences if one sequence is shrinking while the other is expanding and the two samples are larger than the point spread function extent. Future modeling simulations are required to comprehensively determine all the limiting cases.

3.5.4 Conclusions

Four-dimensional data of the beating embryonic heart provide a new perspective to view cardiac biomechanics throughout cardiogenesis. Transforming data into the wavelet domain provides a number of advantages including robustness in dealing with a variety of four-dimensional datasets. Dynamic heart data from three transgenic lines, *Tg(gata1:GFP)*, *Tg(tie2:GFP)*, and *Tg(cmlc2:GFP)*, with GFP-labeled blood cells, endocardium, and myocardium, respectively as well as BODIPY-ceramide stained embryos has been studied. The versatile synchronization method filters data so that various imaging resolutions are analyzed. In cases where motions are not strictly periodic (i.e., blood cells occupy different positions during different periods), filtering the appropriate wavelet coefficients provides acceptable correlation functions. Data extracted from four-dimensional reconstructions are used to characterize cardiac dynamics throughout this work.

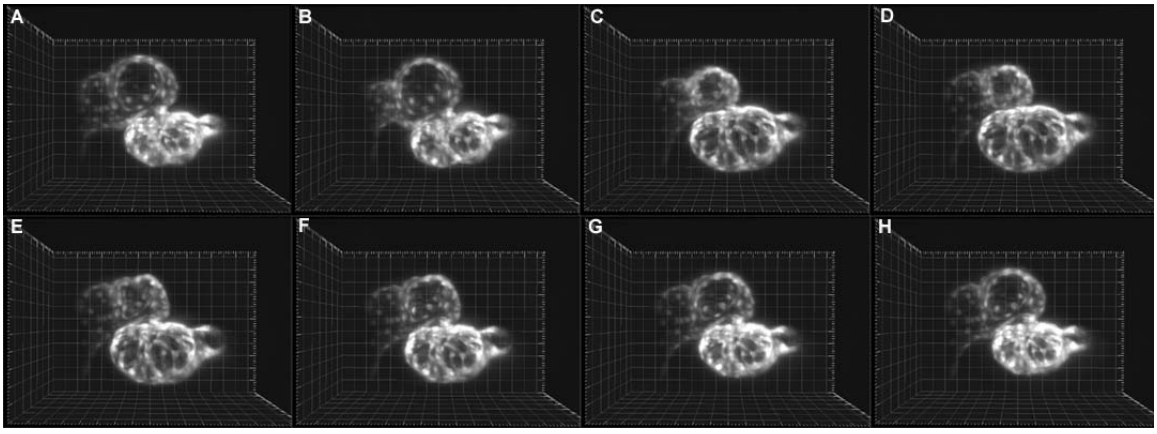

Figure 3.9. Four-dimensional data of heart contractions in *Tg(cmlc2:GFP)* embryos. (A-H) Images of one complete cardiac cycle in a 96 hpf embryo are displayed. The cycle begins with ventricular diastole as seen by the increasing volume of the ventricle. Subsequent changes in atrial and ventricular volumes throughout the cycle are evident.

3.6 Four-Dimensional Data Analysis

The range of dynamic processes that can be observed depends on the spatial and temporal resolutions of the imaging system. With high speed confocal microscopy and four-dimensional reconstruction techniques (Liebling et al. 2005) we can study a variety of dynamic cardiac motions. With the appropriate analysis software, a wealth of data relating structure and function in the developing heart is now available. We present a very small sample of the possibilities here.

3.6.1 Volume Measurements

Heart volume measurements are essential for a number of characteristic cardiac parameters including cardiac output, stroke volume, and ejection fraction. These metrics are often associated with clinical diagnoses. Less direct information on cardiac structure, such as muscle fiber orientation, can also be gleaned from volume data. In the embryonic heart, cardiac volume data could be used to estimate the efficiency of the developing heart as a function of morphology and dynamics.

Through the use of appropriate fluorescent markers, and in conjunction with in vivo four-dimensional reconstructions, atrial and ventricular volume curves can now be calculated in the developing heart. These data can be attained when there is adequate contrast between the intracardiac volume (i.e., blood cells and plasma) and the heart wall. Two candidates for imaging cardiac volumes are *Tg(gata1:GFP)* embryos with GFP-labeled blood cells and BODIPY-ceramide stained embryos with fluorescently labeled plasma. In both cases, the heart wall is much darker than the intracardiac volume. With *Tg(gata1:GFP)* embryos, the challenge is to find hearts that do not express GFP in the

endocardium (typically embryos that are older than 48 hpf) and have bright blood cells. With BODIPY-ceramide staining, fluorescence is much brighter and becomes localized inside the heart, always providing adequate contrast.

Using analysis tools available through Imaris (Bitplane AG), intracardiac isosurface renderings reveal atrial and ventricular volume curves. The first step is to manually create a contour surface around the region of interest, in this case the inner-chamber boundary. This requires finding the *z*-sections that contain the chamber, and drawing a contour that contains the volume throughout the cardiac cycle. In order to calculate atrial and ventricular volume changes independently, two contour surfaces are needed. Once the contour surfaces have been designated, isosurface renderings are fit to the specified areas. The challenge in acquiring repeatable volume data is in establishing a consistent method for creating isosurfaces, which depends heavily on the marker used.

Using *Tg(gata1:GFP)* embryos, our volume data was very inconsistent. Stroke volumes and ejection fractions had large standard deviations. This is most likely due to varying levels of GFP expression between fish, intricate ventricular trabeculations that are not accounted for, and variations in heart sizes and *z*-positions which influence light scattering. However, in multiple cases, we found that ventricular ejection fractions exceeded 60%. This is noteworthy for two reasons: (i) the human left ventricular ejection fraction is approximately 60% (Guyton and Hall, 2000), and (ii) ejection fractions exceeding 49%, based on a 20% muscle fiber contraction length, indicate that the heart has a helical muscle fiber orientation pattern (Sallin, 1969). A conserved ventricular muscle fiber structure between the human heart and the embryonic zebrafish heart lends

further credibility to studies that seek information on human cardiogenesis from zebrafish cardiogenesis.

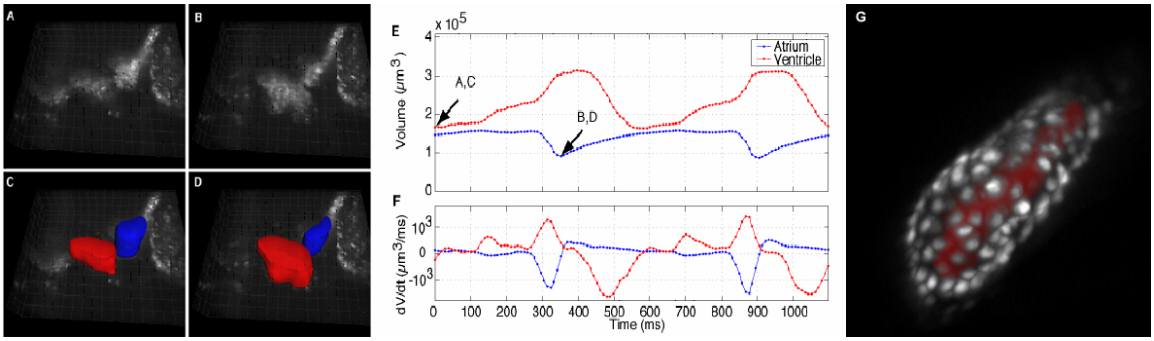

Figure 3.10. Embryonic cardiac volume renderings (A-D) Isosurface renderings of the atrium (blue) and ventricle (red) in 148 hpf embryos. (E) Atrial and ventricular volume changes as a function of time are shown. (F) The derivative of the volume changes can also be calculated. The two peaks in the ventricular volume derivative curves correspond to E and A waves (Sec. 5.4.1.1). (G) Volume renderings can also be used to artificially enhance images. Here we add a red blood volume to the heart tube in a *Tg(cmlc2:GFP)* embryo.

3.6.2 Cardiac Cell Tracking

Four-dimensional heart reconstructions can also provide detailed information on how cardiac cells, and structures such as valves, move throughout the cardiac cycle. This can provide information on myocardial structure and dynamics, endocardial structure and dynamics, and heart valve structure and dynamics. Again, these are common metrics to describe cardiac function in the human heart. Tagged MRI is often used to observe myocardial motions and evaluate cardiac failure (reviewed by Prasad et al. 2004). Echocardiography has been used to examine heart valve motions and appears to be a method to diagnosis particular heart failures, such as ischemic mitral regurgitation (Ahmad et al. 2004). With four-dimensional reconstruction techniques, these studies can now be extended to embryonic heart function and failure. In developmental studies, three-dimensional cardiac tracking (two spatial dimensions and time) has been used to

measure mechanical forces during cardiogenesis (Alford et al. 2003; Taber et al. 1994; Tobita et al. 2000). With four-dimensional reconstruction techniques, these studies can now be extended to three spatial dimensions.

The transgenic lines utilized to track cardiac cell motions were *Tg(gata1:GFP)*, *Tg(cmlc2:GFP)*, and *Tg(tie2:GFP)*. In each case, four-dimensional reconstructions were used to track cell positions in three dimensions throughout the cardiac cycle. Cell positions were registered using the spot tracking feature in Imaris (Bitplane AG). The user input requires an estimated particle size and maximum distance traveled from frame to frame to place spots on the dataset. After spots are placed, the user can manually remove, add, or reposition spots. In order to connect spots between frames, and track trajectories, a tracking method is required. Generally, an autoregressive gap closed tracking method is utilized. Once cell trajectories are computed, spot positions, velocities, and accelerations along the path can be recorded.

Analyzing endocardial and myocardial cell trajectories, we studied wave propagation in the embryonic heart tube and obtained results that refute peristalsis as a pumping mechanism in the heart tube (Ch. 4). An extensive study of embryonic myocardial mechanics is presented in (Nasirei-Moghaddam et al. submitted). As a proof of concept, we also quantified heart valve dynamics throughout the cardiac cycle (Fig. 3.12).

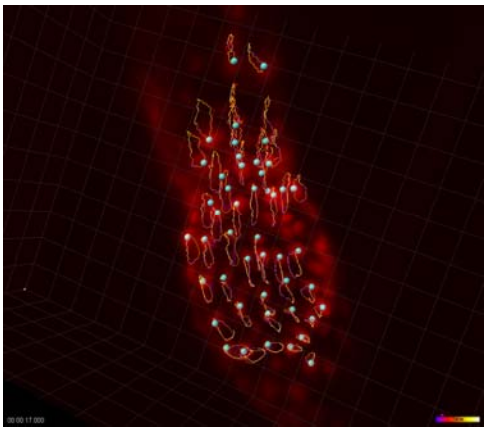

Figure 3.11. Cardiac cell tracking in *Tg(cmlc2:GFP)* embryos. Myocardial cells in the 26 hpf heart tube are identified with small white spheres. Myocardial cell trajectories throughout the cardiac cycle can be traced.

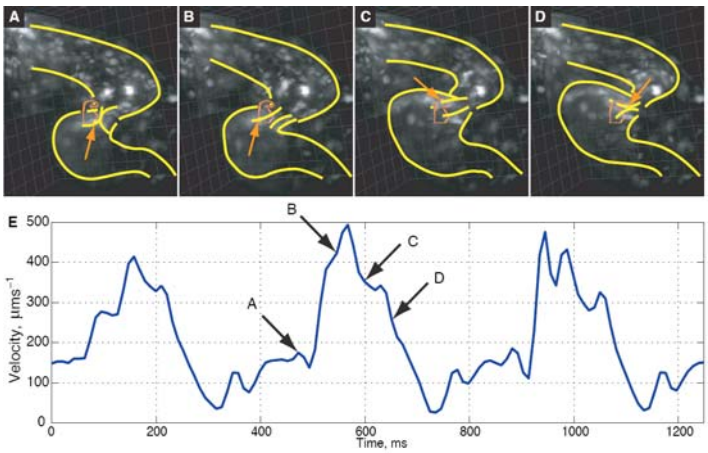

Figure 3.12. Quantitative description of endocardial cushion dynamics. (A-D) Confocal scans of a 48 hpf *Tg(gata1:GFP)* embryo heart. Endocardial cushions trajectories are marked. (E) Velocity of cushion motions at each time point are shown.

3.6.3 Qualitative Flow Analysis

During some phases of the cardiac cycle, confocal scan rates (151 fps) are fast enough to acquire quantitative blood flow data. In cases where scan speeds are not fast enough to extract qualitative data, we still have access to a wealth of information on intracardiac hemodynamics. Qualitative analysis of blood flow through the heart

provided many insights into the form and function of the developing heart and valves. Examining blood cell accelerations during heart tube contractions suggest that the heart tube does not act as a peristaltic pump (Ch. 4). Preliminary observations of flow through the heart tube indicate that pulsatile unidirectional flow quickly turns bidirectional during heart tube looping and retains a retrograde component until functional valve leaflets are formed (Ch. 5). Another property of intracardiac hemodynamics observed without quantitative flow tracking was that the duration of the retrograde component of oscillatory flow through the heart was frequency dependent (Ch. 5).

One of the limitations in this flow visualization method is that the *z*-resolution is much coarser than *x*,*y*-resolution and data collected at different optical sections are separated by multiple cardiac periods. Thus, true four-dimensional flow visualization appears to be limited by several obstacles, some of which are currently being investigated by others. While quantitative four-dimensional flow data would significantly advance our understanding of intracardiac hemodynamics, qualitative flow visualization has also provided a substantial amount of intracardiac blood flow data.

3.7 Blood Flow Visualization

Understanding the relationship between hemodynamic forces and cardiogenesis hinges on in vivo imaging methods that can reliably describe blood flow patterns in the developing heart (reviewed by Hove, 2004). Zebrafish are arguably the most suitable vertebrate model system to study intracardiac hemodynamics since transparent embryos provide optical access to moving blood cells. Here, we discuss the applicability of two

blood cell imaging techniques, DPIV (Willert and Gharib, 1991) and particle tracking, to qualitatively and quantitatively describe intracardiac blood flow.

3.7.1 Digital Particle Imaging Velocimetry

DPIV is a statistical correlation technique that computes the velocity and acceleration vectors for groups of particles in a flow field (Willert and Gharib, 1991). Typically, non-biological flow fields are seeded with small particles and imaged rapidly. The Fourier transform of a fixed region of the image, determined by the interrogation window size, is computed from consecutive frames and cross-correlated to calculate a mean displacement vector for that window. In biological samples, inserting particles without disturbing the flow field presents a number of challenges. Among many other considerations, particles must be (i) small enough to not disturb natural flow patterns, (ii) equal density as the fluid so they do not settle in the vasculature, (iii) neutrally charged so they do not stick to each other or to the vasculature, (iv) non-toxic, and (v) injected without damaging tissue. Optimizing these parameters is a significant task, and not within the scope of this project. Instead, we chose to use an endogenous marker, red blood cells, to trace blood flow. Our first attempt to use blood cell motions along with DPIV to quantify blood flow in zebrafish was in the dorsal aorta (DA) and posterior cardinal vein (PCV) (Fig. 3.13). We found that computed velocity vectors were consistent with visual inspection (pusatile flow with appropriate vector directions and positions).

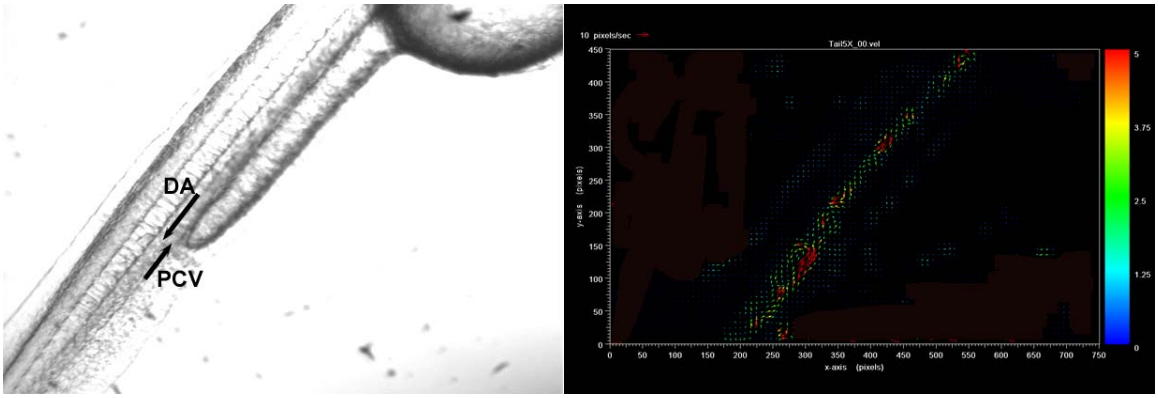

Figure 3.13. First use of DPIV to characterize blood flow in the embryonic zebrafish. (A) Brightfield image of a X hpf zebrafish embryo tail. The dorsal aorta (DA) and posterior cardinal vein (PCV) are labeled, along with the flow direction (black arrows). (B) DPIV of blood cell motions in the tail appear to be consistent with visual data.

Subsequent experiments were conducted to determine the feasibility of this method to quantify intracardiac blood flow. Initially, intracardiac data collected from a Kodak EktaPro high speed camera (500 fps) and processed with DPIV again appeared to be consistent with visual inspection. However, when velocity vector magnitudes were compared to blood cell tracking results, significant variations were found. Furthermore, when interrogation window sizes were changed, velocity vector magnitudes also changed; a result that could not be explained. In addition, velocity vector calculations integrated heart wall and blood cell movements together since cardiac chamber boundaries could not be identified automatically. We arrived at the conclusion that while DPIV could qualitatively describe flow patterns (pulsatility, flow reversal, regions of vorticity, etc.), it does not currently offer a reliable method to quantify intracardiac blood flow and hemodynamics because of inappropriate particle (blood cell) sizes.

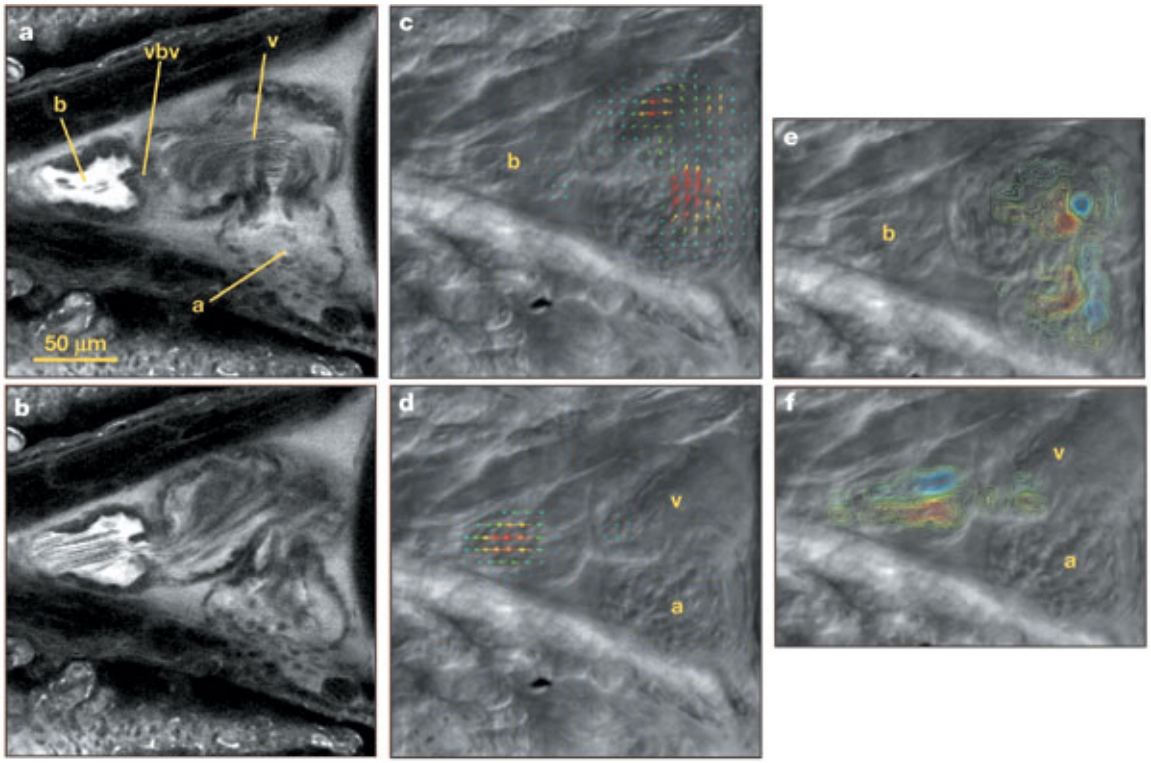

Figure 3.14 Intracardiac blood flow characterization utilizing DPIV. (A,B) Confocal scans of a 4.5 dpf zebrafish embryo during diastole (A) and systole (B). The atrium (a), ventricle (v), bulbus arteriosus (b), and ventriculo-bulbar valve (vbv) are labeled. (C,D) Velocity vectors computed using DPIV superimposed on the heart during diastole (C) and systole (D). (E,F) Vorticity plots computed using DPIV superimposed on the heart during diastole (E) and systole (F) (adapted from Hove al, 2003).

3.7.2 Particle Tracking

Particle tracking is a common technique used to quantify flow. In zebrafish circulation, blood cells can serve as tracer particles. Measurement accuracies depend on the ability to resolve particles in consecutive frames. Blood cells provide adequate contrast with brightfield microscopy, as do GFP-labeled blood cells with confocal microscopy, to be uniquely identified. In many cases, blood cell tracking provides a reliable method for flow quantification (Fig. 3.15). Results from blood cell tracking through the heart tube are discussed in Chapter 4.

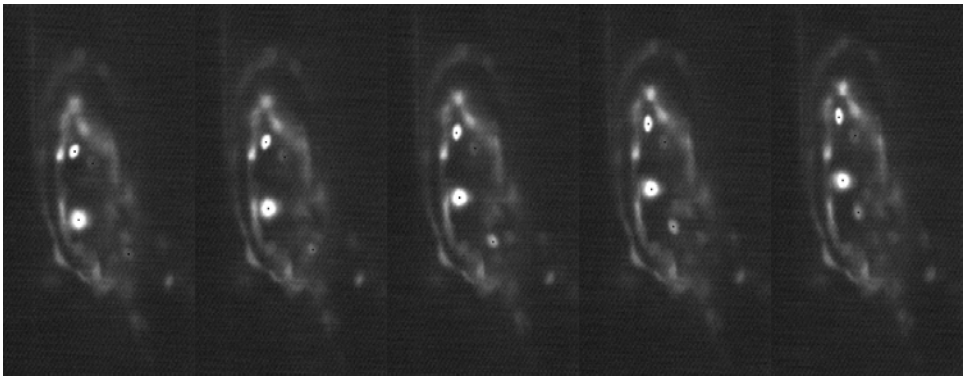

Figure 3.15 Blood cell tracking through a *Tg(gata1:GFP)* heart tube. We can compute blood cell velocities by tracking blood cell positions in sequential frames.

In some cases, however, intracardiac blood cell motions are too fast to be resolved at several hundred fps. This is clearly the case with blood flow across the developing AV valve during ventricular diastole. Thus, in older hearts, our acquisition frame rate prevents particle tracking from being a viable method for quantifying blood flow during the entire cardiac cycle. In such cases, we again defer to qualitative descriptions of intracardiac blood flow (Ch. 5).

3.8 Chapter References

Ahmad RM, AM Gillmoy, PM McCarthy, EH Blackstone, C Apperson-Hansen, Qin JX, D Alger, T Shiota, GM Cosgrove, *Ann Thorac Surg.* **78**, 2063 (2004).

Alford PW, LA Taber, *J Biomech*. **36**, 1135 (2003).

Guyton AC, JE Hall, *Textbook of Medical Physiology*. Saunders, Philadelphia, PA, (2000), p. 101.

Hove JR, RW Koster, AS Forouhar, G Acevedo-Bolton, SE Fraser, M Gharib, *Nature.* **421**, 172 (2003).

Hove JR, *Birth Defects Res C Embryo Today*. **72**, 277 (2004).

Huang CJ, CT Tu, CD Hsiao, FJ Hsieh, HJ Tsai, *Dev Dyn*. **228**, 30 (2003).

Kimmel CB, WM Ballard, S Kimmel, B Ullmann, TF Schilling, *Dev Dyn*. **203**, 253 (1995).

Liebling M, AS Forouhar, M Gharib, SE Fraser, ME Dickinson, *J. Biomed. Optics* **10**, 054001 (2005).

Long Q, A Meng, H Wang, JR Jessen, MJ Farrell, S Lin, *Development*. **124**, 4105 (1997).

Megason SG, LA Trinh, RY Tsien, SE Fraser, High-throughput systematic imaging of zebrafish embryogenesis, In preparation.

Motoike T, S Loughna, E Perens, BL Roman, W Liao, TC Chau, CD Richardson, et al., *Genesis*. **28**, 75 (2000).

Nasiraei-Moghaddam A, M Liebling, AS Forouhar, HJ Tsai, SE Fraser, M Gharib, A Lagrangian approach reveals the active and passive regions in the embryonic zebrafish heart. Submitted to *Biomechanics and Modeling in Mechanobiology.*

Prasad SK, P Kotwinski, R Assomul, *Expert Rev Cardiovasc Ther*. **2**, 53 (2004).

Sallin EA, *Biophys J*. **9**, 954 (1969).

Stellingwerf RF, *Astrophys J*. **224**, 953 (1978).

Taber LA, H Sun, EB Clark, BB Keller, *Circ Res*. **75**, 896 (1994).

Thevenaz P, UE Ruttimann, M Unser, *IEEE Trans Image Process*. **7**, 27 (1998).

Tobita K, BB Keller, *Am J Phys*. **279**, H959 (2000).

Westerfield M. *The Zebrafish Book*. Univ. of Oregon Press. Eugene, OR (2000).

Willert CE, M Gharib, *Exp. Fluids* **10**, 181 (1991).

Chapter 4: Embryonic Heart Tube Biomechanics (adapted from Forouhar et al. 2006)

4.1 Introduction

Internal flows in organisms can be propelled through a variety of pumping mechanisms. Peristaltic pumps push fluids by progressively reducing the surrounding volume (Vogel, 1994); the method utilized by the esophagus to squeeze food from the pharynx to the stomach. Cilia motions create fluid dynamic environments by rapidly rotating and forming small vortical structures; some believe these motions cause the first asymmetrical forces in the developing embryo, helping to establish embryonic polarity (reviewed by Wood, 2005). Even suction due to the evaporation of water at the tops of tree leaves can lift sap through vessels that are meters long (Vogel, 1994). Undoubtedly, Nature has designed a number of creative ways to transport fluids, only a few of which have been comprehensively characterized.

One of the elusive characteristics of human blood circulation has been the relationship between blood flow and pressure. As one might expect, the velocity amplitudes of arterial blood flow pulses decrease as they travel away from the heart. Surprisingly though, arterial pressure amplitudes increase as they travel away from the heart (Nichols and O'Rourke, 1988). It was eventually realized that increasing pressure amplitudes are due to wave reflections in the vasculature. Pressure waves periodically originate with each cardiac contraction and travel throughout the vasculature. When they reach a discontinuity, some portion of the wave is reflected (reviewed by O'Rourke and Kelly, 1993). Thus, incident and reflected pressure waves can add up to form larger

pressure wave amplitudes than the source, explaining the behavior of the pressure pulse amplitude as it travels away from the heart.

The wave reflection inducing discontinuities, as they relate to the vascular system, are due to changes in impedance. Impedance describes the relationship between pulsatile pressure and pulsatile flow across a small segment of the vasculature (Nichols and O'Rourke, 1988). Many properties of the vasculature can influence impedance, such as material elasticity, diameter, and curvature (Hickerson et al. 2005; Hickerson and Gharib, in press). Although these basic concepts have been used to explore circulation through the vasculature, they had previously not been extended to study flow through the heart tube.

At the core of understanding embryonic cardiac mechanics is identifying the dynamic relationship between structure and function. Insights into the earliest cardiac pumping mechanisms will undoubtedly shed light on cardiogenesis in general. Cardiac physiologists have long conjectured that the valveless embryonic heart tube drives circulation by means of peristaltic contractions (Fishman and Chien, 1997; Gilbert, 2000), a positive displacement pumping mechanism (Vogel, 1994). Confirmation of this pumping mechanism requires in vivo visualization and quantification of endocardial, myocardial, and blood cell motions, which is difficult to obtain with traditional imaging modalities. High speed imaging using brightfield microscopy does not provide adequate spatial resolution to clearly identify heart cell motions and traditional point-scanning confocal microscopes are limited by slow frame rates.

Improvements in confocal microscopy (Liebling et al. in preparation) and four-dimensional (three spatial dimensions and time) visualization (Liebling et al. 2005)

permit us to revisit heart tube biomechanics at much finer resolutions. Our results identify three biomechanical properties of embryonic heart tube contractions that contradict a peristaltic pumping mechanism in the embryonic heart tube, (i) a bidirectional, as opposed to a unidirectional, wave traverses the endocardial layer, (ii) blood cell velocities significantly exceed the instantaneous traveling wave speed through the heart wall, and (iii) the frequency-flow relationship is non-linear and exceeds the maximum estimated value for a peristaltic pump. These observations suggest an elastic wave resonance mechanism based on impedance mismatches at the boundaries of the heart tube as the likely pumping mechanism. We compared our in vivo results to the previously investigated mechanical impedance pump model (Hickerson et al. 2005) and in both cases we find: (i) resonance peaks in the frequency-flow relationship, (ii) mismatched impedance and visible wave reflections at the inflow and outflow boundaries of the heart tube, (iii) a pressure-flow relationship that exhibits a phase difference between the maximum acceleration of the blood and the highest local pressure gradient, (iv) and net flow reversal at different contractile frequencies.

4.2 Embryonic Heart Tube is Not Peristaltic

4.2.1 Bidirectional Wave

To test the nature of cardiac pumping we employed in vivo high-speed confocal imaging of zebrafish hearts prior to valve formation. Optical sections through 26 hpf *Tg(gata1::GFP)* zebrafish hearts, expressing GFP in blood cells, endocardium, and myocardium, were reconstructed into four-dimensional data sets (Fig. 4.1) (Liebling et al. 2005), which provide direct three-dimensional data on the position of myocardial and

endocardial cells throughout the cardiac cycle (Figs. 4.1C,D, 4.2). By tracking the position of the trailing edge of the endocardial wave crest during the cardiac cycle, we identified the speed and direction of the traveling wave through the heart wall. The wave originates in myocardial cells positioned near the inflow tract of the heart tube and upon contraction, a bidirectional wave propagates axially along the heart tube wall (Fig. 4.1A,B). The proximity of the pacemaker cells to the venous boundary of the heart tube, along with the speed of the traveling wave, combine to make this bidirectional wave undetectable through traditional imaging modalities.

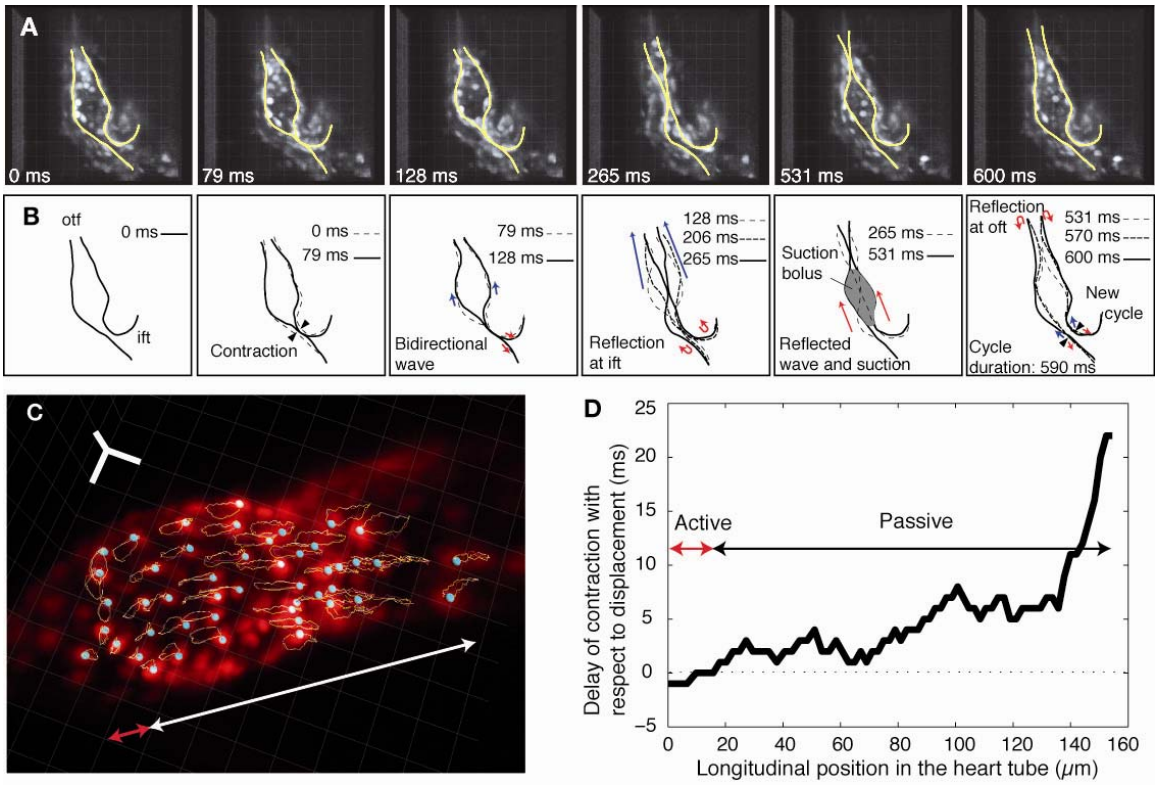

Figure 4.1. Biomechanics of embryonic heart tube contractions contradicts peristalsis as the main pumping mechanism. (A) Three-dimensional reconstruction of a 26 hpf *Tg(gata1:GFP)* zebrafish heart tube at six timepoints. Yellow lines denote the shape of the endocardial layer. (B) Superimposed outlines at different timepoints highlight bidirectional traveling wave (red and blue arrows). Black arrows indicate contraction location. Shaded gray region indicates suction bolus. Regions of mismatched impedance at the inflow and outflow boundaries of the heart tube are reflection sites. Grid spacing is 20 μm. (C) Three-dimensional reconstruction of a 26

hpf *Tg(cmlc2:GFP)* embryo. Myocardial cells are fluorescently labeled and their three-dimensional trajectories during two complete cardiac cylces are shown. The red line indicates the active pacemaker region and the white line the passive region. Grid spacing is 20 μm. (D) The active pacemaker region spans the first 20 μm of the heart tube. It was identified by calculating the time difference between the moment myocardial cells at a given position along the tube experience a 10-13% strain rate with neighboring cells and the time at which they reach 90% of their maximal displacement for each. When this time difference is nearly zero, the region experiences active contraction.

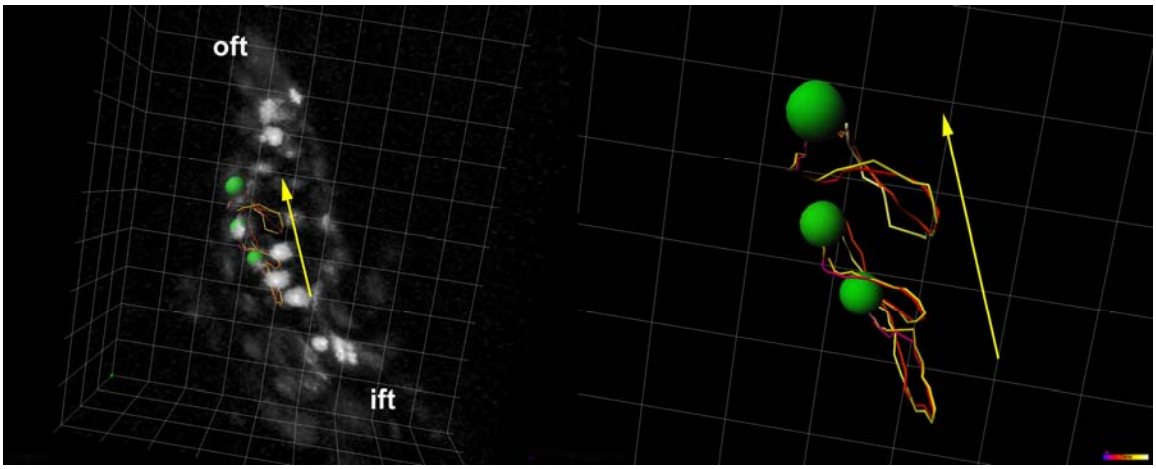

Figure 4.2. Endocardial cell trajectories during heart tube contractions contradict peristalsis. Three endocardial cells are tracked throughout the cardiac cycle. The direction of blood flow through the heart tube is also shown (yellow arrow). Blood cell positions never move downstream from their resting location. Grid spacing is 20 μm.

4.2.2 Blood Velocity Exceeds Heart Wall Wave Speed

In a peristaltic heart tube model, the net flow is exactly equal to the volume displaced during contractions. This dynamic imposes a direct relationship between the upstream blood velocity and the local traveling wave velocity. Specifically, since peristalsis is governed by static pressure rather than dynamic pressure (Vogel, 1994), it would imply that the upstream blood velocity in the zebrafish heart does not exceed the simultaneous local traveling wave velocity. However, in each of the cases observed

(n=5), the maximum velocity of the upstream blood accelerates to velocities exceeding the wall wave speed (Fig. 4.3).

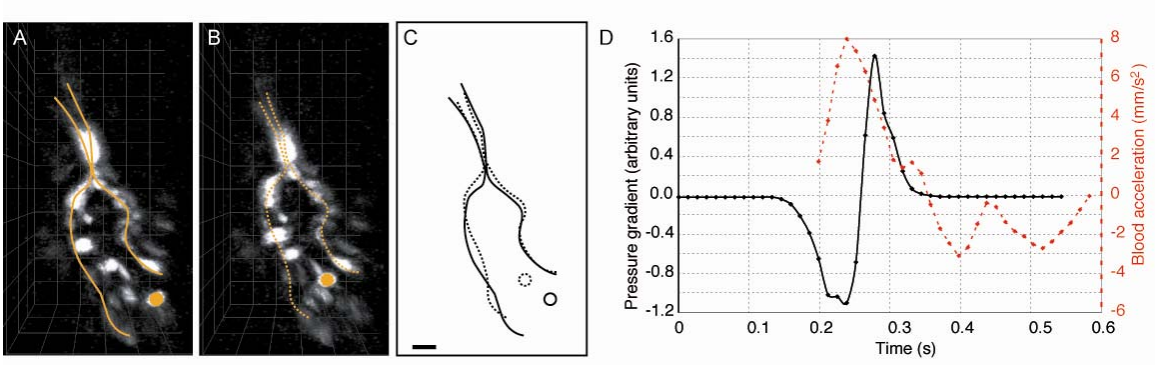

Figure 4.3. Blood cell velocities greatly exceed the traveling wave velocity. (A,B) Reconstruction of a 26 hpf *Tg(gata1::GFP)* embryo. The endocardial layer, along with a blood cell, have been marked in each image. (C) Superposition of schematics in A and B. Blood cell displacement is much greater than traveling wave crest displacement indicating that blood cells do not passively follow the traveling wave. Scale bar is 20 µm. (D) Blood cell accelerations and estimates of the pressure gradient as a function of time (see supplemental information). The maximum acceleration occurs when the pressure gradient is negative, indicating that the embryonic heart tube acts as a suction pump.

4.2.3 Nonlinear Frequency Flow Relationship

To investigate how the cardiac output varied with the contractile wave frequency in vivo, we altered temperature to manipulate heart rates, and tracked blood cells to determine the flow rate. In this temperature range (24 to 34 °C), fish develop normally, and we do not expect a non-linear change in blood viscosity. If the heart tube were a peristaltic pump, the cardiac output should increase linearly with the contractile wave frequency as long as the contraction amplitude is conserved between frequencies. However, we found that despite similar contraction amplitudes, the blood velocity response, and thus the net flow rate response, to a monotonic heart rate change is surprisingly non-linear (Fig. 4.4E).

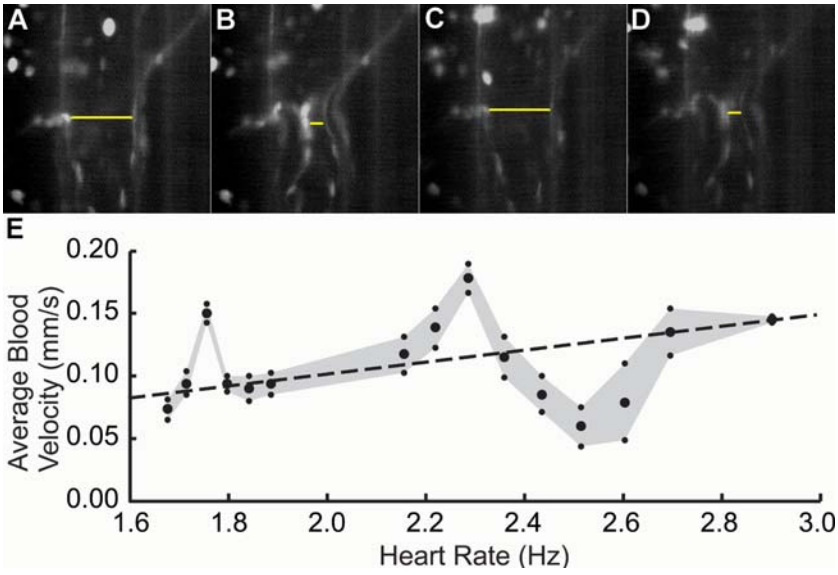

Figure 4.4. Non-linear frequency flow relationship for 26 hpf zebrafish heart tube despite similar contraction amplitudes. (A-D) Contraction amplitude of the heart tube is conserved at two different contractile frequencies. (A,B) The maximum and minimum distances between two endocardial cells on opposite sides of the tube are marked during a single cardiac cycle (~3 Hz), 50±1 μm and 10±1 μm respectively. (C,D) Same measurements when the heart beats at a slower frequency (~2 Hz) yields similar distances of 50±1 μm and 10±1 μm respectively. (E) Resonance peaks in the observed average blood velocity at 1.75 Hz and 2.3 Hz exceed the expected estimate for peristaltic pumping (dashed line).

4.3 Embryonic Heart is a Dynamic Suction Pump

4.3.1 Resonance Peaks in Frequency-Flow Relationship

These three observations indicate that the embryonic heart tube does not act as a peristaltic pump; instead, they seem consistent with a previously investigated hydroelastic impedance pump model (Hickerson et al. 2005; Hickerson and Gharib, in press). In this model of valveless pumping, the pumping action results from elastic wave propagation and reflection in the heart tube; resonance conditions arise at certain frequencies where the phase speed permits constructive interference between the incident and reflected pressure waves. Mechanical properties of the system such as the diameter,

length, elasticity, and pressure dictate the wave speed as well as the attenuation and reflection coefficients in the system. The impedance pump model exhibits a sensitivity of the generated flow to activation frequency that is similar in many ways to our in vivo observations, including non-linear flow with frequency, domains of negative slope, and resonance frequencies that allow higher flow rates than peristalsis (Fig. 4.4).

4.3.2 Reflections at Mismatched Impedance Sites

The impedance pump model requires mismatches in impedance to induce wave reflections at the boundaries of the pump element to build up suction and induce net flow (Hickerson et al. 2005). In zebrafish, many mechanical properties of the heart tube boundaries contribute to mismatched impedance. The most prominent feature at the inflow boundary of the heart tube is a drastic change in diameter (Fig. 4.5). The heart tube stems from the surface of the spherical yolk sac, acutely narrows to about 30 μm, and becomes lined by an additional layer of cells (myocardium) and cardiac jelly that alters the elasticity of the heart tube at the inflow boundary (Fig. 4.5). Our four-dimensional data confirms that this region of mismatch impedance is indeed a site of wave reflections. Pacemaker cell contractions initiate axial waves that travel along the heart tube until they reach the heart tube boundaries. When these waves reach the inflow and outflow boundaries they reflect in the form of sudden expansions and begin to travel back through the heart tube.

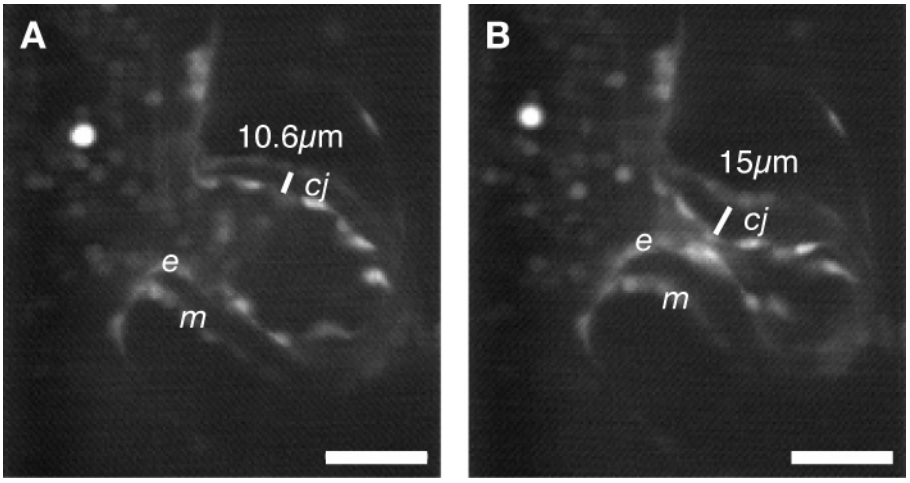

Figure 4.5. Hydroelastic nature of the embryonic heart tube wall. (A) Inflow region of a 26 hpf embryo. The distance between the myocardial (m) and endocardial (e) layers is marked. (B) Upon contraction, this distance increases. The expansion of the cardiac jelly (cj) at the site of contraction illustrates the elastic nature of the heart wall, a requirement of the impedance pump model. This observation contradicts the muscularly driven peristaltic mechanism since the concentric rings of endocardium and myocardium do not approach each other during contraction. Scale bars are 50 μm.

4.3.3 Pressure-Flow Relationship

The sudden expansions of the cardiac lumen at the reflection sites suck blood through the heart tube. In order to describe this suction mechanism in vivo, we looked at the pressure-flow relationship through the heart tube during the cardiac cycle. By measuring the radius of the cardiac lumen at two cross sections a short distance apart (Fig. 4.6), we deduced the pressure gradient at a point, dP_1/dt, (Nichols and O'Rourke, 1988) using the spatial pressure gradient dP/dz and Laplace's Law (see Section 4.3.4). In this region, blood cells first begin to accelerate when the pressure gradient is negative (i.e., when the pressure is decreasing), analogous to drinking liquid through a straw. Blood cells continue to accelerate, reaching a maximum as the pressure gradient climbs from negative values towards zero (i.e., as the pressure continues to decrease but at a slower rate). As the pressure gradient increases from zero to positive values, blood cells

continue to move forward, but with decreasing accelerations. Finally, when the pressure gradient reaches a maximum and begins to decrease, blood cells decelerate and oscillate around a resting point. Importantly, a phase difference between the maximum acceleration and the maximum pressure gradient exists. Specifically, blood reaches a maximum acceleration before there is a local maximum in the pressure gradient. This time lag between suction pressure and flow in the embryonic heart resembles the pressure-flow relationship of a fluid dynamic pump (Vogel et al. 1994) rather than a peristaltic mechanism where such a time lag should not exist.

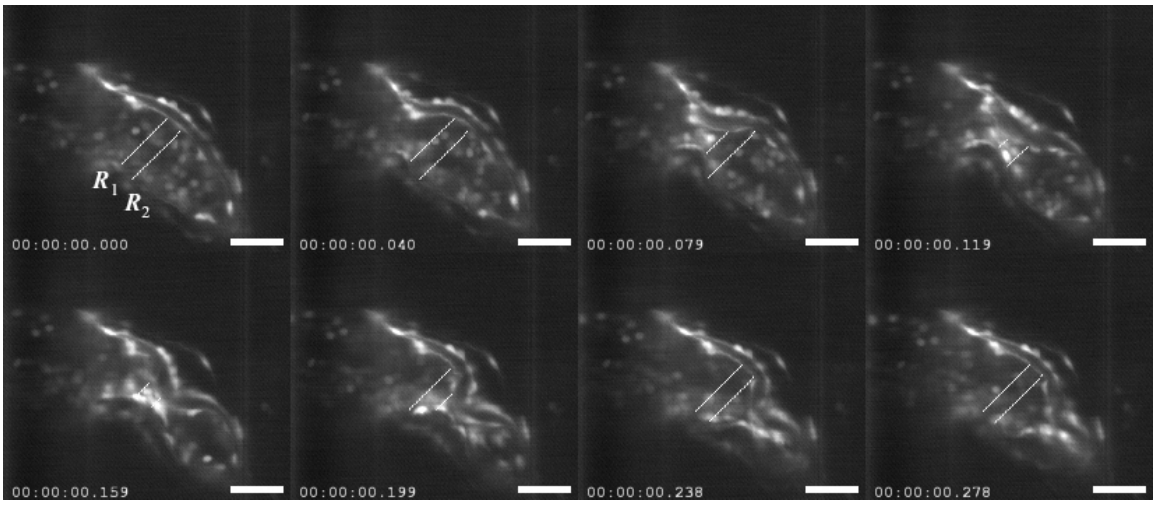

Figure 4.6. Pressure gradient estimations. A sequence of images during the cardiac cycle is shown with two measured radii (R_1, R_2). The difference in radii, R_1-R_2, is used to compute the temporal pressure gradient (Sec. 4.3.3).

4.3.4 Net Flow Reversal

One of the intriguing characteristics of impedance pumping is that the direction of net flow is a function of frequency (Hickerson et al. 2005). Contractions at a fixed location can drive flow in one direction, while contractions at the same location but with a different frequency can drive flow in the opposite direction. Here we discuss the frequency sensitivity of the net flow direction through the embryonic heart tube. In all

24-30 hpf fish examined (n>100) at room temperature, none exhibited a net flow from the outflow tract towards the inflow tract. In these fish, only one heart rate was examined, and fish were at a fixed temperature long before imaging. However, in the cases where we adjusted heart rate and examined flow immediately (n=10), we did find one zebrafish heart that exhibited a net flow reversal (Fig. 4.7). The flow rate through this particular heart was noticeably lower than other fish, but never the less, at 1.7 Hz, the net direction of blood flow was from the inflow tract towards to the outflow tract. We decreased the heart rate to 1.4 Hz and noticed that the flow direction changed. Net flow through the heart tube traveled from the outflow tract towards the inflow tract as shown through blood cell position tracking along the angular orientation of the heart. Although this was a rare example, it is another illustration of characteristics shared between in vivo heart tube dynamics and impedance pumping.

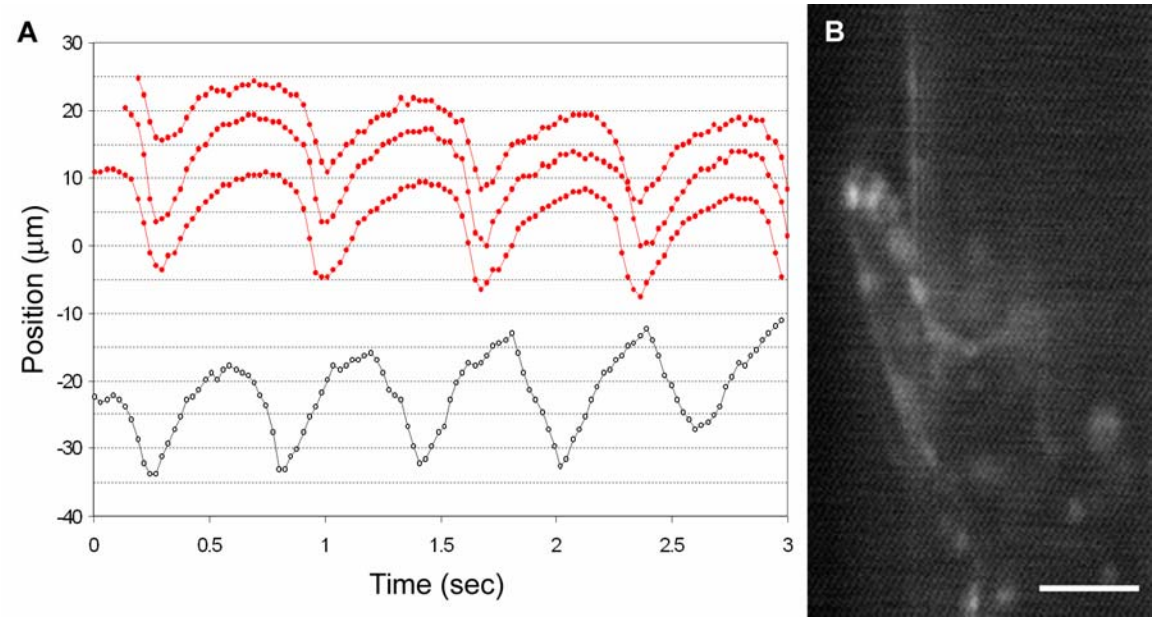

Figure 4.7. Net flow reversal in the heart tube at different contractile frequencies. (A) Blood cell tracking in the 26 hpf heart tube at 1.7 Hz (black) and 1.4 Hz (red). Blood cell positions increase as they travel from the inflow tract towards the outflow tract. At 1.7 Hz, net flow is positive since the maximum position increases with time. Three blood cells tracked in the same heart at a slower frequency (red) indicate a

flow reversal. Maximum blood cell positions decrease with time. (B) Confocal scan of the heart this data was obtained from. Scale bar is 50 µm.

4.4 Materials and Methods

4.4.1 Imaging Parameters

Embryos were raised at 28.5ºC and, unless otherwise noted, imaged at 24ºC. Bidirectional confocal scans (256x256 pixels) were taken at 151 fps. Time series were triggered at a random time in the cardiac cylce and taken for 300-500 frames. Upon completion of a two-dimensional time series at one z-section, the optical plane was moved 3-5 microns and the acquisition was repeated. Four-dimensional datasets were collected from 15-25 z-sections and did not exceed 100 microns in total depth.

4.4.2 Quantitative Flow Analysis

Blood cell velocities were computed from image sequences, 5-10 cardiac cycles in length, acquired in fish at temperatures between 24 ºC and 34 °C. For every sequence, we selected the same portion of the heart near the centerline of the tube at the venous boundary as a region of interest. We manually marked the first frame of each cardiac cycle in which compression occurs defining cycles of variable length, or equivalently, frequency. For every cardiac cycle, individual blood cell trajectories were tracked manually and pixel positions recorded over time. Cells were chosen that maintained their intensity values (indicating that their motion was largely in the focal plane) while traversing the region of interest. The instantaneous velocity of a cell was computed using the distance traveled between two frames along the angular orientation of the heart tube. For each cycle length, the velocities from sequences of corresponding duration were

merged to yield a minimum of one velocity and up to twelve velocity measurements for each time step (Fig. 4.8). For all data corresponding to one cycle length (± 0.007 seconds), a Monte Carlo sampling was performed. In this method, a velocity from each time step in a cycle is chosen at random. The average velocity for the given cycle length is then computed from these points. The random sampling is repeated 1000 times for each cycle length from which a mean and standard deviation of average velocities was computed (Fig. 4.4). We tested the sensitivity of our results to the number of velocity points at each phase by computing average velocities only from phases that had at least three data values. Even under these stringent conditions, the non-linear frequency-flow relationship is conserved. The anticipated peristaltic rate was determined by assuming the heart was cylindrical and estimating the length of the actively compressing component during each cardiac cycle. We determined the average flow velocity by dividing the flow rate, which is equal to the volume compressed multiplied by the compression frequency, by the cross-sectional area.

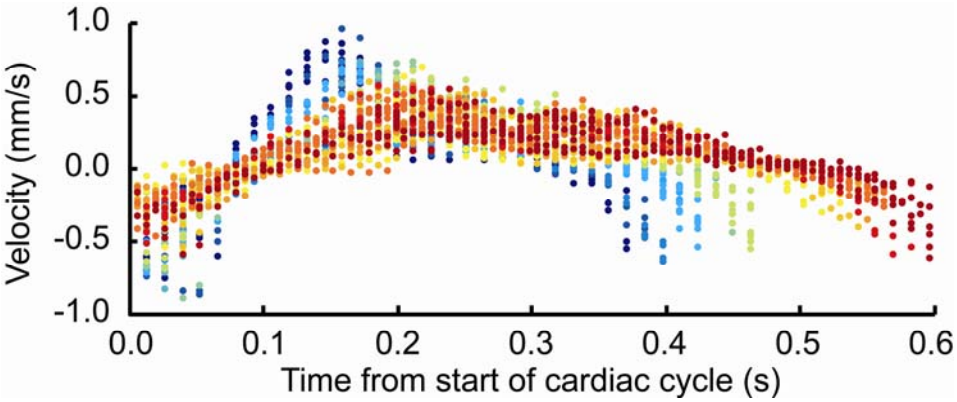

Figure 4.8. Blood cell velocity measurements over a range of frequencies. The set of velocities for each period is denoted by a unique color. Monte Carlo sampling of this data was used to compute the average velocity along with the standard deviation.

4.4.3 Pressure Variation Estimates

In steady Poiseuille flow, the net flow rate at a point is directly related to the pressure at that point. In oscillatory flow the pressure-flow relationship is a bit more complicated. Studies of pressure and flow in the canine femoral artery show that the maximum flow rate precedes the maximum pressure (Nichols and O'Rourke, 1988). An explanation for this phenomenon was provided by McDonald in 1955 (McDonald, 1955) when he discovered the flow rate was governed by the oscillatory pressure gradient, not pressure. He calculated the spatial pressure gradient, $\delta P/\delta z$, across a short length of the artery, δz, by subtracting the downstream pressure (P_2) from the upstream pressure (P_1) at all phases of the oscillatory cycle. As with any traveling pressure wave, this resulted in an oscillatory pressure gradient that can be described as follows: if we consider a sinusoidal pressure wave with a peak at some arbitrary location A, then the pressure difference (P_2-P_1) between point A and a second point a short distance downstream of A, A+δz, will be positive. When we consider the pressure difference between A and A+δz a short time later, as the pressure wave travels downstream, we find the pressure difference is negative. Thus, $\delta P/\delta z$ continues to oscillate around the mean pressure gradient.

A convenient relationship between the spatial and temporal pressure gradients exists in oscillatory flows. McDonald recorded the pressure at a site, P_1, as a function of time and calculated the temporal pressure gradient, dP_1/dt. He found that the spatial derivative, $\delta P/\delta z$, closely approximated dP_1/dt in the limiting case where dz is very small.

$$\delta P/\delta z \propto dP_1/dt \qquad (1)$$

The only difference between $\delta P/\delta z$ and dP_1/dt is a small phase difference due to the time the pressure wave takes to traverse δz. They experimentally supported this finding by measuring the pressure gradient, dP/dt, at a point in the canine femoral artery and with

the assumption that dP/dt = dP/dz, calculated the velocity. Their calculated velocity closely resembled the measured velocity, validating the assumption.

The next obstacle in developing a pressure-flow relationship in vivo is the challenge of recording two reliable pressure measurements a very small distance apart. In order to address this problem we utilized a known relationship between the pressure and radius of a chamber, Laplace's Law. This law states that the pressure (P) in a chamber is equal to the tension (T) divided by the radius (R). In our case, if we assume that the tension in the heart tube is linear, we can simplify the Laplace equation to (2).

$$P \propto 1/R \tag{2}$$

Combining equations (1) and (2) we obtain a relationship (3) between the pressure in the heart tube and the radii at two proximal locations (R_1 and R_2,where R_2 is downstream of R_1).

$$dP_1/dt \propto dP/dz \propto (R_1\text{-}R_2)/(R_1\, R_2) \tag{3}$$

We measured the latter radii over time (Fig. 3.6), and assuming a circular cross section, we determined changes in pressure in the embryonic heart tube.

We characterized blood flow behavior in this region by tracking blood cell positions (X) along the angular orientation of the heart throughout the cardiac cycle. The resulting X-T data was used to compute the instantaneous acceleration of the blood cells (n=25) at each phase of the cardiac cycle. We computed a single acceleration of the bulk flow by averaging all the accelerations calculated at a single phase. We combined this acceleration data with the pressure gradient estimation to uncover the pulsatile pressure-flow relationship in the embryonic heart tube (Fig. 4.3D).

4.5 Discussion and Perspectives

Using new in vivo imaging tools, we have taken a closer look at early cardiac structure and function and identify three biomechanical properties of embryonic heart tube contractions that contradict cardiac peristalsis: (i) a bidirectional, as opposed to unidirectional, wave traverses the endocardial layer, (ii) blood cell trajectories do not follow local endocardial wave trajectories and exhibit velocities significantly greater than those of the traveling wave, and (iii) the frequency-flow relationship is non-linear and exceeds the maximum flow rate possible for a peristaltic pump. Furthermore, we observed (i) resonance peaks in the frequency-flow relationship, (ii) mismatched impedance at the inflow and outflow tracts, and visible wave reflections at the heart tube boundaries, (iii) a pressure-flow relationship that exhibits a phase difference between the maximum acceleration of the blood and the maximum local pressure gradient, and (iv) a net flow reversal at different contractile frequencies. Thus, the valveless embryonic heart does not drive circulation through peristalsis. Instead, these observations suggest a hydroelastic impedance pump model based on elastic wave propagation and reflection (Hickerson et al. 2005).

The simple pumping mechanism we propose provides novel functions for cardiac structures. A single actuation site provided by the pacemaker region is sufficient to pump blood through the heart tube. Thus, we speculate that once a group of cells adopt a pacemaker role, they alone can provide the mechanical (wave propagation through cardiac tissue) and fluid dynamic (intracardiac blood circulation) stimuli needed for further heart development. This pumping mechanism also provides mechanical

robustness in the embryonic heart tube, permitting a range of pacemaker sizes, positions, and frequencies in the heart tube (Hickerson and Gharib, in press). In addition, we propose a critical function for the acellular cardiac jelly separating the myocardial and endcardial cell layers. Small contractions of myocardial pacemaker cells translate into much larger amplitude waves through the heart tube wall. The cardiac jelly, the elastic interface between the myocardial and endocardial layers, passively acts as an amplifier that converts a small isolated myocardial contraction into an oscillating volume displacement wave. Abnormalities of this cardiac jelly will likely lead to increased stiffness and limit the efficiency of the pump. This paradigm provides a new model for computer simulations evaluating early cardiac function, establishing new variables to describe blood flow and wall motions in the heart tube.

The frequency-dependent flow rate and flow direction of the heart tube pumping mechanism suggests that such valveless pumping may not be suitable for post-embryonic circulation in ectotherms. Unlike normal valved hearts, increasing the heart rate does not guarantee an increase in flow rate, and in extreme cases could lead to flow reversals. This demonstrates one reason why heart valves may be necessary for further development. We also speculate through preliminary observations of Drosophila (Rolf Bodmer, UCSD) and *Ciona instestinalis* (Brad Davidson, UCSB) that many lower vertebrate hearts exhibiting bidirectional flow (Pass, 2000), and previously considered peristaltic, may also use an impedance-based pumping mechanism. The presented characterization of early cardiac biomechanics should provide the foundation to re-visit many aspects of embryonic cardiogenesis and illustrates the first evidence for an embryonic root to the observed

suction action of the adult heart (Torrent-Guasp et al. 2001). Our in vivo observations have also inspired new designs for mechanical impedance pumps.

4.6 Chapter References

Torrent-Guasp P, GD Buckberg, C Clemente, J Cox, C Coghlan, M Gharib, *Semin. Thorac. Cardiovasc. Surg.* **13**, 301 (2001).

Forouhar AS, M Liebling, A Hickerson, A Nasiraei-Moghaddam, HJ Tsai, JR Hove, SE Fraser, ME Dickinson, M Gharib, *Science*. **312**, 751 (2006).

Fishman MC, *Science*. **294**, 1290 (2001).

Fishman MC, KR Chien, *Development* **124**, 2099 (1997).

Gilbert SF, *Developmental Biology*. Sinauer, Sunderland, MA, (2000).

Hickerson AI, D Rinderknecht, M Gharib, *Exp. in Fluids* **38**, 534 (2005).

Hickerson AI, M Gharib, *J Fluid Mech*. in press.

Hove JR, RW Koster, AS Forouhar, G Acevedo-Bolton, SE Fraser, M Gharib, *Nature.* **421**, 172 (2003).

Liebling M, AS Forouhar, M Gharib, SE Fraser, ME Dickinson, *J. Biomed. Optics* **10**, 054001 (2005).

McDonald DA, *J Physiol*. **127**, 533 (1955).

Nichols WW, MF O'Rourke, *McDonald's Blood Flow in Arteries*. Oxford Univ. Press, New York, (1988) pp. 98-102.

O'Rourke MF, RP Kelly, *Journal of Hypertension*. **11**, 327 (1993).

Pass G, *Ann Rev of Entomology*. **45**, 495 (2000).

Stainier DY, *Nat. Rev. Genet*. **2**, 39 (2001).

Vogel S, *Life in Moving Fluids*. Princeton Univ. Press, New Jersey, (1994), pp. 323-9.

Wood WB, *PLoS Biol*. **3**, e292 (2005).

Chapter 5: Oscillatory Flow and Valvulogenesis

5.1 Introduction

Growth and development of vertebrate embryos is critically dependent on efficient cardiac function to sustain blood circulation. In multi-chambered hearts, unidirectional intracardiac circulation can only be maintained with functional heart valves. However, congenital heart valve defects remain one of the most prevalent manifestations of cardiac dysmorphology. Mitral valve defects occur in almost 1% of live human births (Chauvaud, 2004).

Why are proper heart valves necessary? Systolic contractions reduce the ventricular volume and force deoxygenated blood to exit the ventricle towards the atrium or outflow tract. Only blood traveling through the gills (or lungs in humans) via the outflow tract is re-oxygenated. AV valve closure isolates the atrium from the ventricle, ensuring blood is directed towards the outflow tract.

Ultimately, the need for heart valves is the product of having multiple cardiac chambers. Thus, a more fundamental question may be: why do vertebrates need an atrium and a ventricle? The ventricle is the workhorse of the heart, providing high pressure to drive blood through the circulatory system. In a way, the ventricle operates like a spring, imparting maximum pressure to the blood only after it has been adequately loaded (preload) by the diastolic blood volume (Guyton and Hall, 2000). Since venous pressures are low, this would take a considerable amount of time without an auxiliary pump. The atrium provides the auxiliary pump. Atrial suction collects blood from the veins during systole and rapidly loads the ventricle during diastole, providing the preload necessary to sustain normal ventricular ejection fractions.

In order to understand the normal valvulogenetic process, recent studies have identified a number of genes and transcription factors that govern heart valve formation (Beis et al. 2005; Walsh and Stainier, 2001). Many of these genes are regulated by epigenetic factors such as fluid forces (Appendix C). The ability to create and identify mutant genes affecting heart development is one of the primary assets of zebrafish in cardiogenetic studies. One example is the silent heart mutant (*sih*) which does not have a contracting heart due to a mutation of cardiac troponin T (Sehnert et al. 2002). Since the heart does not contract, there is no blood circulation, but embryos can survive for up to 7 days through diffusion alone. *Sih* embryos undergo normal heart development until 32 hpf (Sehnert et al. 2002). Embryonic hearts start out as a tube, loop to the right, and undergo the initial stages of chamber formation. It is reasonable to assume that none of these stages of cardiogenesis is guided by hemodynamic forces since they occur in the absence of intracardiac circulation. However, the later stages of AV boundary specification are not completed in *sih* embryos (Fig. 5.1). Upregulation of Tie2 is not seen at the AV boundary, nor are any subsequent stages of AV valve formation (Bartman et al. 2004). Since the mutation only effects cardiac contractility, the stages of cardiogenesis that are halted may very well depend on transvalvular blood flow.

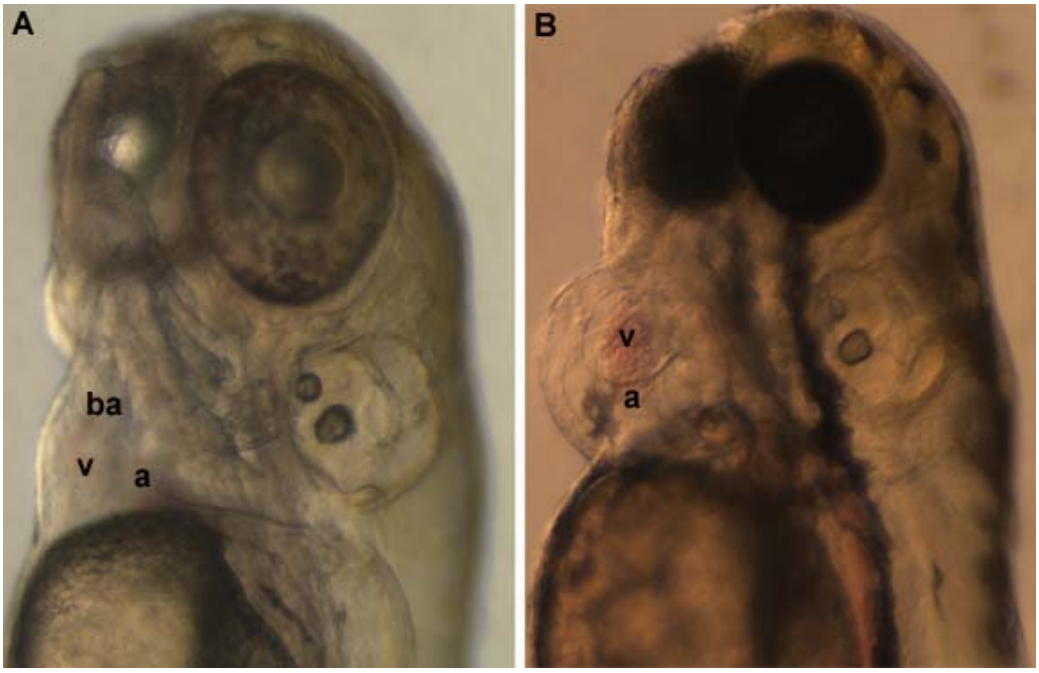

Figure 5.1. Silent heart mutants undergo incomplete cardiogenesis. (A) 72 hpf wild type embryo with atrium (a), ventricle (v), and bulbus arteriosus (ba) labeled. (B) Silent heart mutant undergoes incomplete looping along with stunted chamber and valve formation.

Traditional imaging modalities are either too slow, or do not have the spatial resolution to appropriately describe blood flow across the developing heart valves. Previous studies have considered normal flow through the developing AV canal in zebrafish to be unidirectional (Beis et al. 2005). In contrast to their observations, by examining flow through the developing zebrafish heart, we reported that normal blood flow through the developing valve region has an oscillatory component (Liebling et al. in preparation).

In this chapter, we qualitatively describe blood flow patterns during AV valve formation. With knowledge of how blood normally courses through the developing heart, we implemented a non-invasive method of perturbing oscillatory flow during cardiogenesis and carried out functional assays on in vivo heart valve formation.

5.2 Methods

5.2.1 High-Speeed Confocal Imaging

The Zeiss LSM 5 LIVE was used to image *Tg(gata1:GFP)* and BODIPY-ceramide stained embryos to visualize blood flow and valve formation. Embryos were anesthetized prior to imaging and placed in agarose wells. All images were taken with a 40x/0.8 Achroplan water immersion lens. Scans were acquired at 151 fps.

5.2.2 Brightfield Imaging

To confirm that observed flow patterns in the developing heart were not due to confocal imaging conditions (i.e., Tricaine or laser light excitation), unanesthetized embryos were viewed under brightfield imaging. We mounted a high speed camera (Kodak EktaPro Imager Model 1000HR) to an inverted microscope (Nikon Eclipse TE2000-S) and imaged free swimming embryos (500 fps) on a coverslip.

5.2.3 Discrete Flow Representation

Transvalvular blood flow was discretely characterized as positive, negative, or absent (no flow) by analyzing blood cell motions across the developing valve (i.e., cushions or leaflets). This region was fixed relative to the atrium and ventricle and moved with the valve plane during the cardiac cycle. Blood flow direction was marked in every frame of the cardiac cycle. The percentage of retrograde flow per cycle was determined by summing up the total number of frames exhibiting retrograde flow and dividing by the total number of frames per period.

5.2.4 Methods to Control Heart Rate

5.2.4.1 Lidocaine Treatment

Heart rates of experimental embryos were decreased according to dosage dependent exposure to lidocaine (1% stock, Abbott Laboratories). Lidocaine was drawn from the stock solution with a 1 ml syringe (Becton, Dickinson and Company) and placed directly in wells containing artificial pond water and approximately 5 embryos. Embryos were exposed to lidocaine for 24 hours (31 to 55 hpf). Surviving embryos (>80%) were washed three times, placed in artificial pond water, and incubated at 28.5 ºC until being imaged (4 dpf).

5.2.4.2 Temperature

Zebrafish heart rates are regulated by ambient temperature. Unless otherwise noted, embryos were incubated at 28.5 ºC (VWR Scientific, model 2030). To decrease and increase heart rates, a low temperature incubator (Fisher Scientific) at 22ºC and a higher temperature (32-34°C) incubator (Thermolyne, model 37900) were used.

5.2.5 Valve Development Assay

BODIPY-ceramide stained embryos were anesthetized and analyzed with high speed confocal microscopy (151 fps). A random sample of experimentally manipulated embryos were imaged at 4 dpf and scored based on the presence of valve leaflets. In cases where leaflets were difficult to identify (<2%), the presence or absence of transvalvular retrograde flow was used to determine abnormal or normal valvulogenesis, respectively.

5.3 Intracardiac Flow Patterns

A requirement for studying the role of fluid dynamic forces on developing valve tissue is to determine what flow patterns constitute normal conditions. Many cardiac mutant phenotypes have been classified by hemodynamic observations (Walsh and Stainier, 2001; Lee et al. 2006; Stainier et al. 1996). Since it was generally accepted that normal flow through the heart was unidirectional, the presence of retrograde flow across the developing AV valve was used in a forward genetic screen to identify cardiac valve mutants (Beis et al. 2005). However, to the best of our knowledge, all of this data has been collected at sub-video frame rates (<30 fps). It is our impression that the utility of studying intracardiac flow to identify normal and abnormal cardiac development depends on much higher resolution (spatial and temporal) data. Using high-speed confocal microscopy (151 fps), two-dimensional scans and four-dimensional reconstructions reveal that normal blood flow across the developing AV and VB valves has an oscillatory component, refuting unidirectional flow as a phenotype for normal cardiac function.

In order to characterize transvalvular flow during heart development we tracked the direction of blood cells moving between the atrium and ventricle. During some phases of the cardiac cycle, individual blood cell positions are slow enough to track in sequential frames, permitting velocity measurements and derivations of hemodynamic forces such as shear stress. However, at our acquisition speed, this does not hold true for the entire cardiac cycle. During some phases, such as middiastole, blood cells move too fast to be tracked in consecutive frames. Although blood cell velocities cannot be measured at all times, the direction of blood cell trajectories traveling across the developing AV valve

(i.e., anterograde, from the atrium to ventricle, or retrograde, from the ventricle to atrium) are resolvable. Here we provide two graphical representations of blood flow during heart development: (i) a color coded superposition of multiple phases that shows the direction of flow at various stages, during select phase sequences (Fig. 2), and (ii) a discrete representation of transvalvular flow at all phases of the cardiac cycle (Fig. 5.2).

Using both illustrations, it is evident that unidirectional flow transitions to bidirectional flow before the emergence of valve leaflets, and returns to unidirectional flow after the formation of functional valve leaflets. The valveless embryonic heart (26 hpf) is able to sustain unidirectional flow through the heart tube (n=10) by the suction mechanism described in Chapter 4. As the heart tube loops, forms chambers, and increases systemic resistence (33 hpf, 48hpf, 60hpf, and 72hpf), blood flow through the AV canal exhibits a prominent oscillatory component (n=6, 10, 10, and 10, respectively). Atrial contractions and ventricular suction, force blood into the ventricle, elevating ventricular pressure (Pelster and Burggren, 1996). When the ventricular pressure becomes large enough, blood is expelled from the ventricle. Since the AV cushions do not completely isolate the ventricle from the atrium, blood from the ventricle can travel to lower pressure regions in the bulbus arteriosus as well as back into the atrium. In many cases, and at many stages, over 50% of the cardiac cycle is marked by retrograde flow from the ventricle to the atrium (Fig. 5.2F). Retrograde flow continues during the later stages of AV valve formation (96 hpf, n=7 of 11) and ultimately remains until functional valve leaflets are formed (111 hpf, n=11), effectively isolating the atrium from the ventricle during systole.

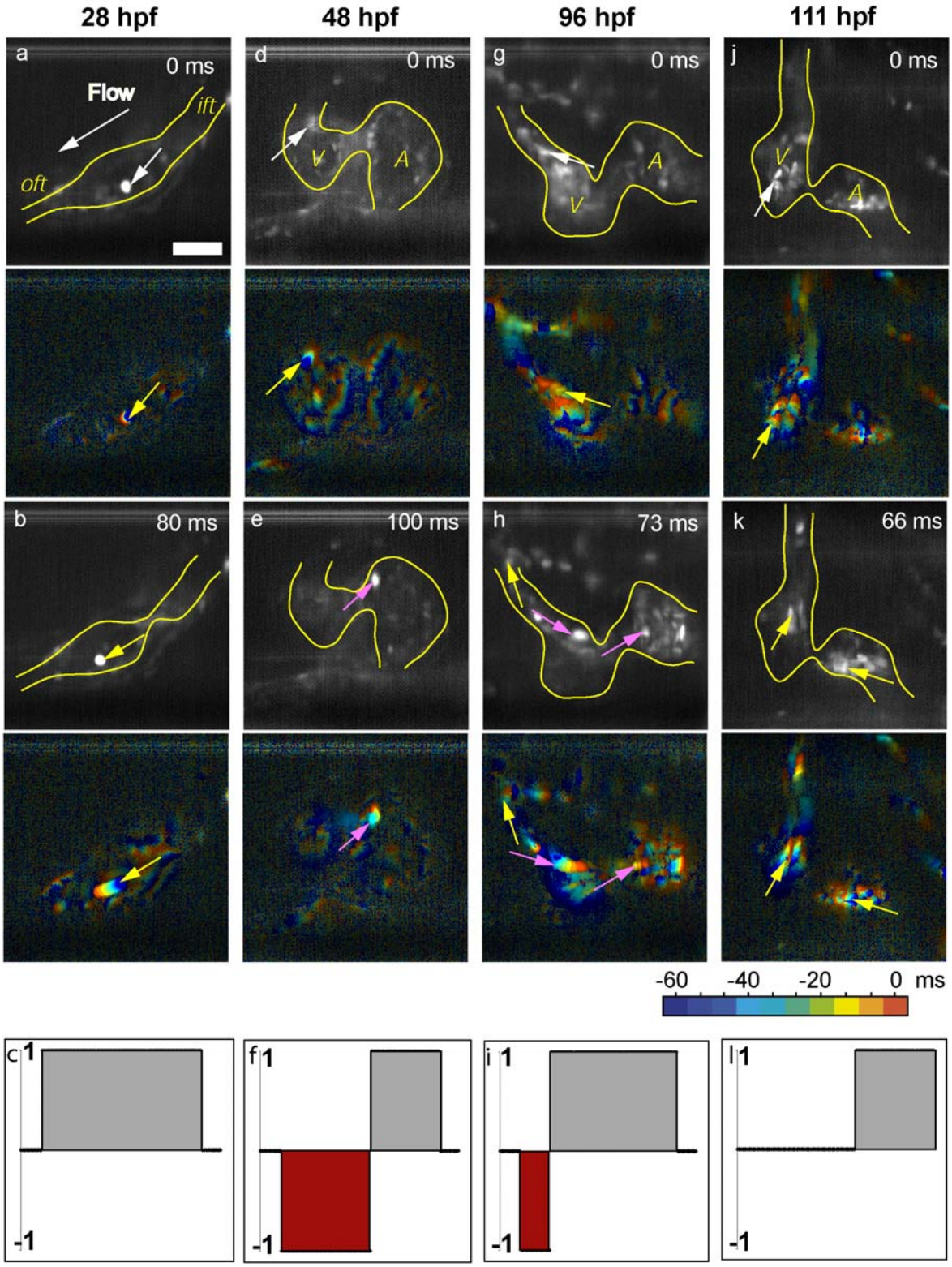

Figure 5.2. Oscillatory flow across the developing valve. Dynamic slice sequences of the developing *Tg(gata1:GFP)* heart. Each column corresponds to a single age. Color coded superpositions of consecutive time frames (10 frames per image).

Yellow arrows mark cells moving forward, purple arrows mark cells moving backwards. Only slower moving cells during particular phases are resolvable using this method. (C, F, I, L) Discrete representation of blood flow across the developing valve. This method allows flow to be characterized during all stages of the cardiac cycle. One cycle is shown in each image. Positive flow (gray region, +1), negative flow (red region, -1), and no flow (black line, 0) phases are depicted. Through both representations it is evident blood flow through the heart tube is initially unidirectional (28 hpf), develops an oscillatory component (48 and 96 hpf), and finally becomes unidirectional (111 hpf) when functional leaflets emerge.

5.4 Zebrafish Valvulogenesis

5.4.1 Valve Morphogenesis

Zebrafish hearts develop bicuspid valves at three positions, between the sinus venosus and atrium, atrium and ventricle, and ventricle and bulbus arteriosus. This description of valve formation will concentrate on the AV valve which prevents backflow from the ventricle to the atrium. BODIPY-ceramide stained embryos were used to visualize in vivo valve morphogenesis (Fig. 5.3).

The initial stages of chamber formation (36 hpf) produce a small constriction at the boundary between the developing atrium and ventricle (Fig. 5.3A). This constriction, known as the AV canal, is a circular orifice separating the atrium and ventricle. Cellular changes in shape and adhesion accompany this gross morphological change. A single endocardial cell in this region transforms from a squamous to cuboidal shape and can be identified by Dm-grasp expression, a cell-surface adhesion molecule (Beis et al. 2005). Together, these characteristics mark the first morphological signatures of AV canal formation, and differentiate AV endocardial cells from their neighboring atrial and ventricular endocardial cells.

Between 36 hpf and 55 hpf, an additional five to six endocardial cells in the AV canal become cuboidal and express Dm-grasp (Beis et al. 2005). By 60 hpf, endocardial

cells migrate into the cardiac jelly, between the endocardium and myocardium, and undergo an epithelial to mesenchymal transition (EMT). This transition forms a pair of ECs, small mesenchymal protrusions in the AV canal. These ECs are the thick black structures separating the atrium and ventricle (Fig. 5.3C,D)

The ECs continue to thicken and by 84 hpf, the cushions begin to break off from the ventricular side of the canal while remaining attached at the atrial side. We consider this the first morphological indication of leaflet formation. Interestingly, there appears to be temporal asymmetry in leaflet formation between the two valves (i.e., the inner ventricular leaflet and outer ventricular leaflet). In many cases, the inner ventricular leaflet breaks off earlier than the outer ventricular leaflet (Fig. 5.4A-D). In other cases, a more subtle asymmetry in leaflet formation can be observed by examining the difference in leaflet lengths (Fig. 5.4E-H). This developmental asymmetry may be partially due to asymmetrical flow patterns across the valve and in the ventricle.

The leaflets elongate and become lined by two layers of endocardial cells separated by fibronectin (Beis et al. 2005) (~96hpf). Separation of the leaflets from the ventricular EC completes and the bi-valve hinges from the atrial portions of the ECs, appearing as a two “u” shaped strucutres (Fig. 5.3G-J). At this stage, the valve leaflets largely resemble their mature form.

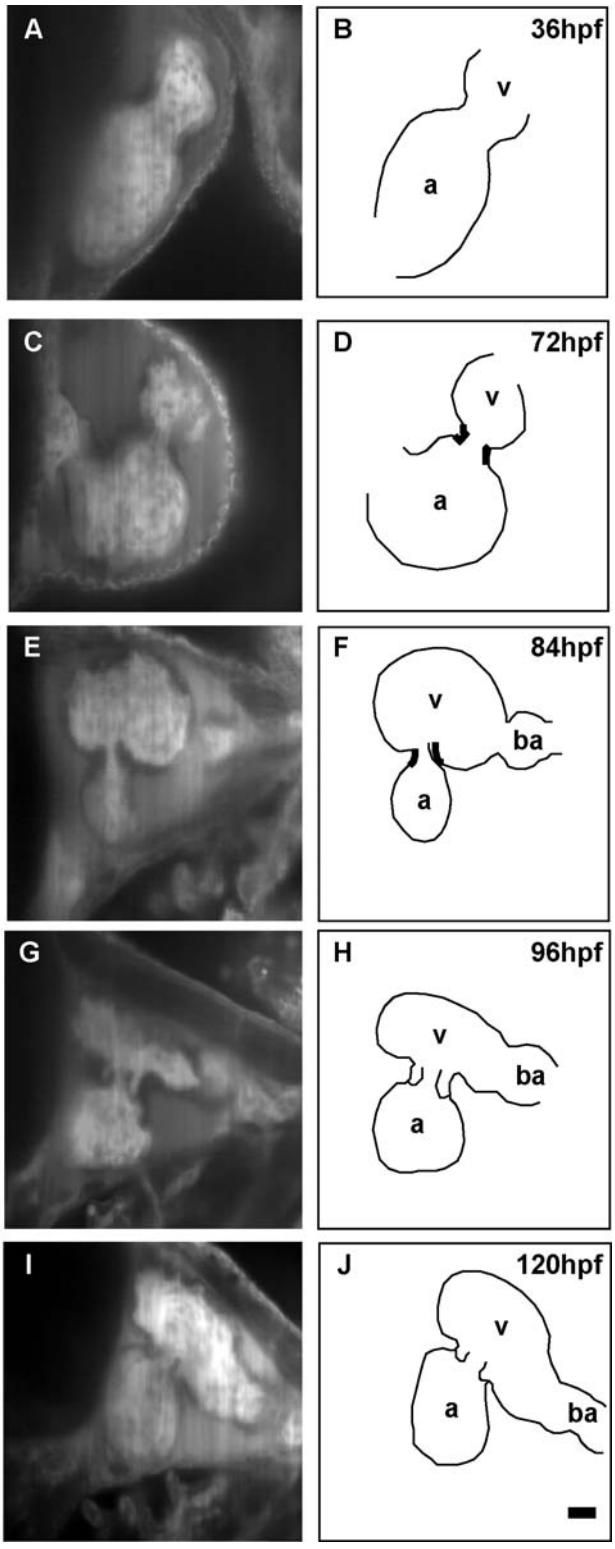

Figure 5.3. AV valve morphogenesis in BODIPY-ceramide stained embryos. Chamber formation is evident by 36 hpf (A, B). Endothelial cells migrate into the cardiac jelly to form ECs (C, D). Leaflet formation commences with detachment at the ventricular region (E, F), eventually giving way to mature leaflets (G-H).

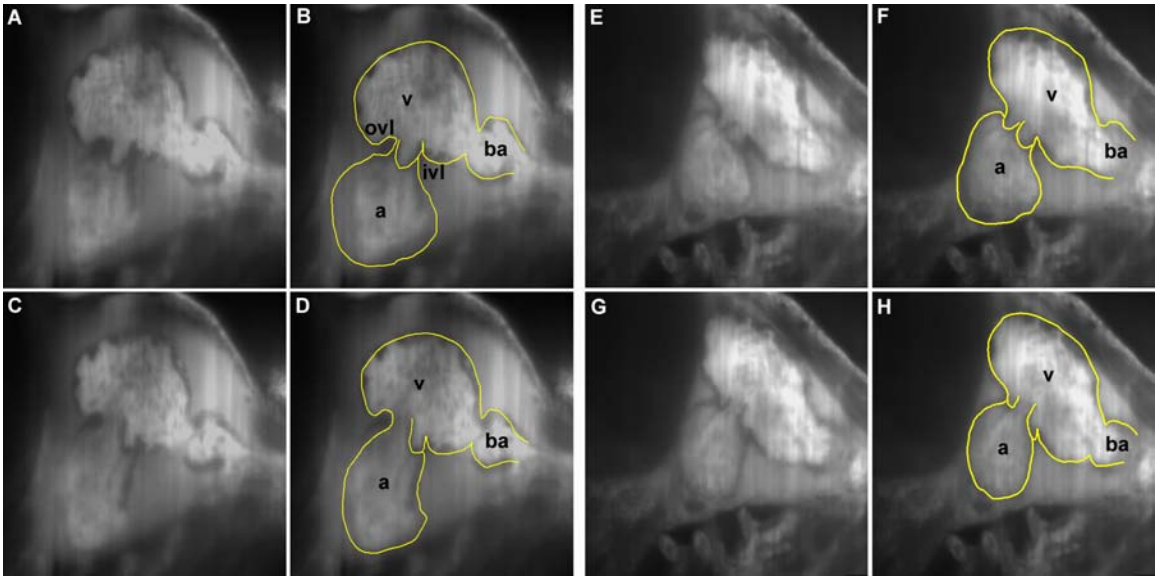

Figure 5.4. Temporal asymmetry in valve leaflet formation. The inner ventricular leaflet (ivl) appears to form before the outer ventricular leaflet (ovl). Sometimes this asymmetry is extreme (A-D), and other times it is more subtle (E-H). The atrium (a), ventricle (v), and bulbus arteriosus (ba) are labeled.

5.4.2 Valve Dynamics

Observing the dynamic nature of the AV valve during the cardiac cycle and throughout valvulogenesis, in conjunction with flow patterns, provides the opportunity to analyze the functional characteristics of heart valves. Here, we present diagrams of valve motions during the cardiac cycle along with a discrete representation of transvalvular blood flow (Sec. 5.1.3).

During the initial stages of chamber formation, the heart is little more than a tube with two bulges. As blood enters the atrium, the atrium expands and the AV canal slides towards the ventricle (Fig. 5.5 J, N). At the onset of diastole, the orifice diameter increases and blood is expelled from the atrium into the ventricle (Fig. 5.5K, O). During later stages of diastole, the AV orifice remains expanded and recoils towards the atrium (Fig. 5.5L, P). At the beginning of systole the orifice constricts, although not completely,

to prevent the ventricular blood volume from re-entering the atrium (Fig. 5.5I, M). The morphological constraints imposed by the AV canal dimensions and closing mechanics prevent the heart from maintaining unidirectional flow during systole.

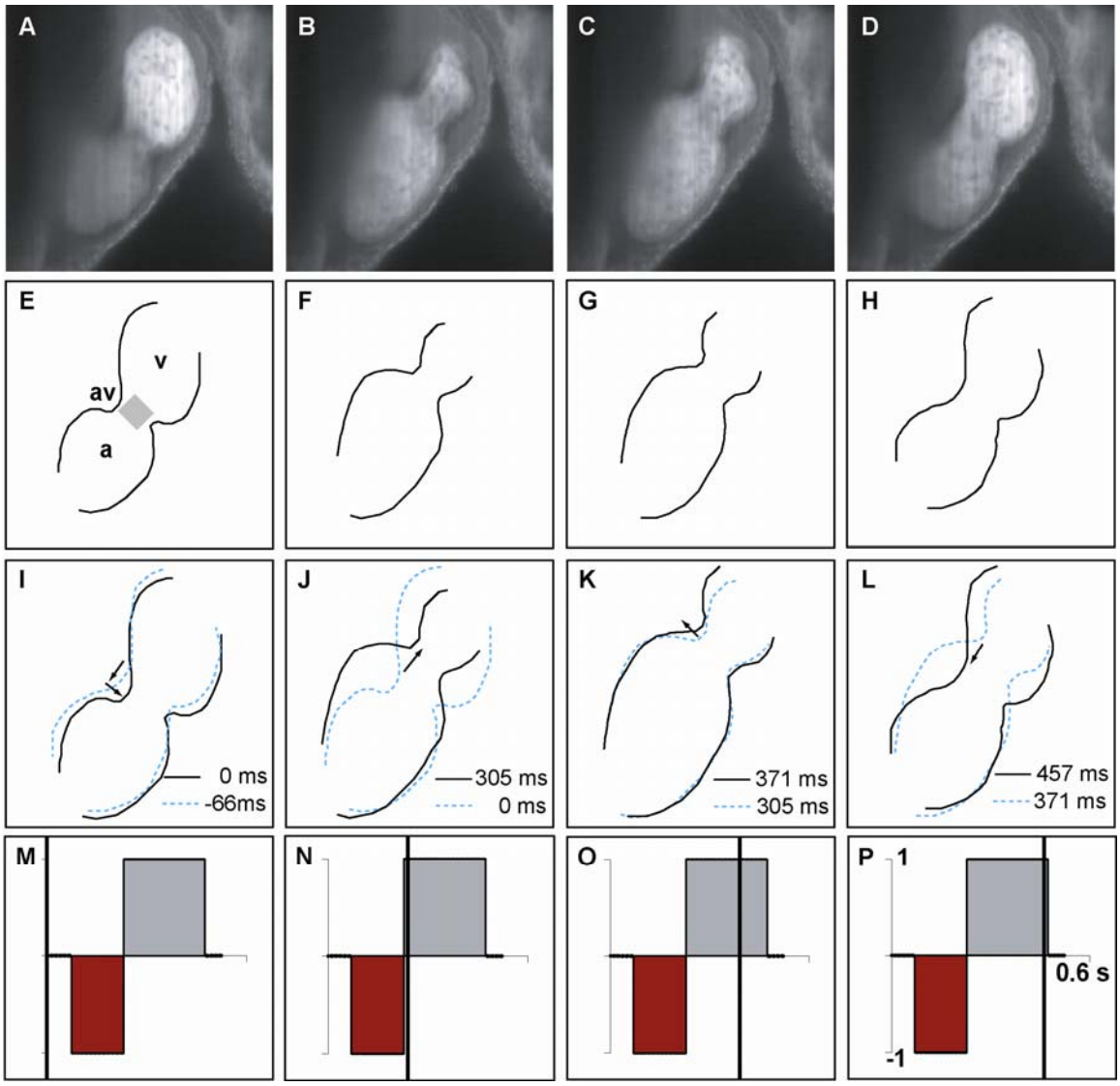

Figure 5.5. Valve dynamics and blood flow in 36 hpf embryos. (A-D) Sequence of confocal scans during one cardiac cycle. Outlines of each image are provided (E-H). The gray box (E) indicates the location of blood flow characterization. Sequential images are superimposed upon each other to show cardiac cushion motions (I-L) along with timestamps. The black arrows indicate the motion of the cushion. (M-P) Binary representation of flow during one cardiac cycle. Vertical black line indicates the time point images (E-H) were recorded. See text for details of dynamics.

At 72 hpf, atrial filling commences with the valve cushions in close proximity to each other, but still separated by a short distance (Fig. 5.6I). Atrial filling occurs synchronously with ventricular systole. Blood fills the atrium, sliding the ECs towards the ventricle, while allowing a small volume of blood to flow backwards through the small opening from the ventricle to the atrium (Fig. 5.6J,N). During diastole, the valve cushions separate and move back towards the atrium, allowing blood to pass from the atrium to ventricle (Fig. 5.6K,O). The end of diastole features the ECs once again approaching each other, but not making complete contact (Fig. 5.6L). Although not evident in the discrete blood flow representation, the heart is becoming a more efficient pump, allowing a smaller blood volume to regress from the ventricle to the atrium. However, further valve development and advanced dynamics are still required to prevent retrograde flow altogether.

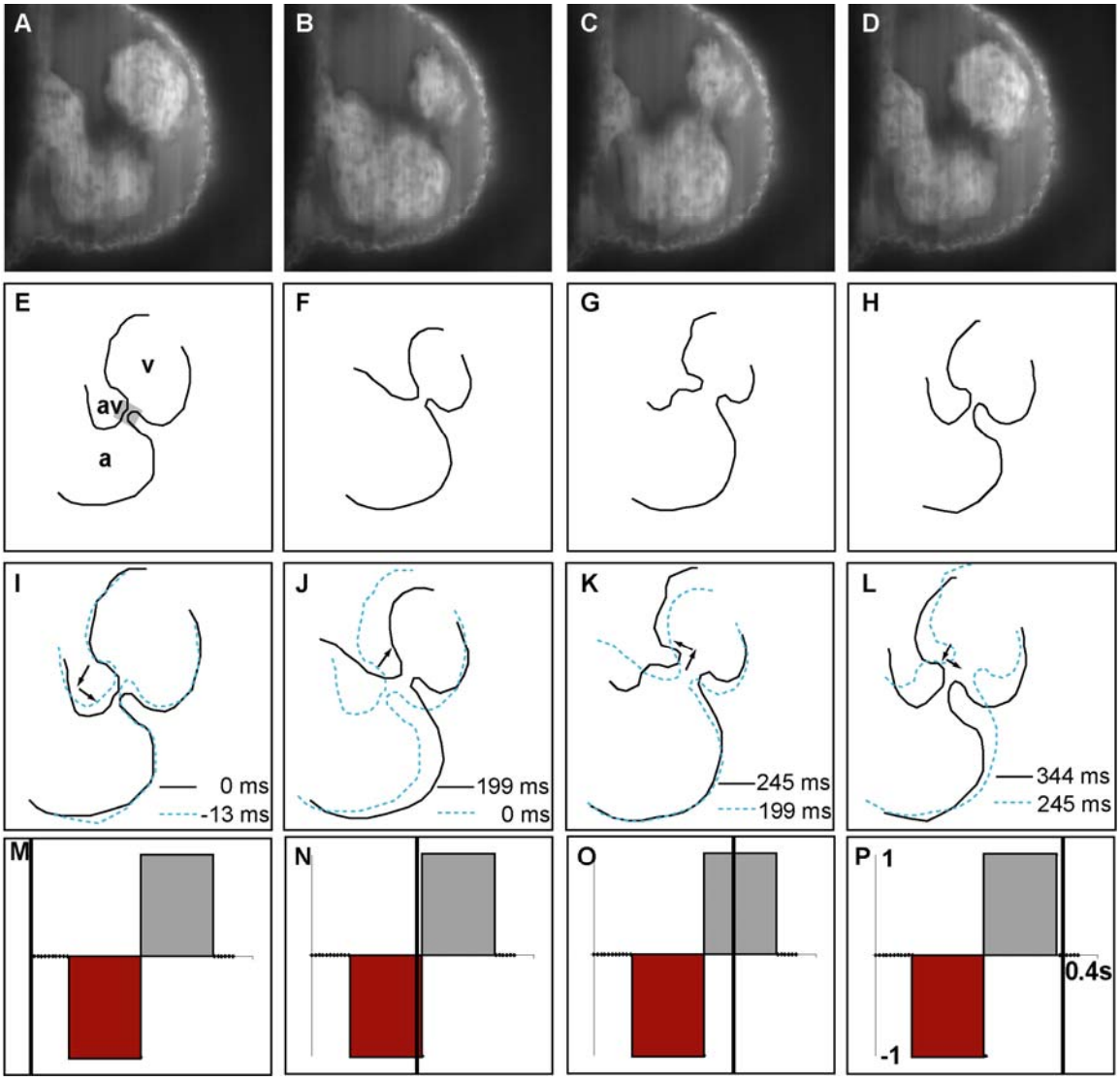

Figure 5.6. Valve dynamics and blood flow in 72 hpf embryos. (A-D) Sequence of confocal scans during one cardiac cycle. Outlines of each image are provided (E-F). Sequential images are superimposed upon each other to show cardiac cushion motions (I-J) along with timestamps. The black arrows indicate the motion of the cushion. (M-P) Binary representation of flow during one cardiac cycle. Vertical black line indicates the time point images (E-H) were recorded. See text for details of dynamics.

By 84 hpf, maturing leaflet dynamics continue to improve cardiac pumping efficiency. As mentioned previously, valve leaflets are hinged on the atrial side and free moving on the ventricular side. During atrial filling and ventricular systole, the valve

leaflets approach each other and appear to make contact, but not cohesively enough to prevent retrograde flow (Fig. 5.7J, N). The atrial volume increases while the ventricular volume decreases, and the valve plane moves towards the ventricle. During diastole, the leaflets separate and the valve plane recoils towards the atrium (Fig. 5.7K, L, O, P). Decreased retrograde flow across the valve is evident during the later stages of systole and is present because the valve leaflets are not yet capable of completely sealing the atrium from the ventricle.

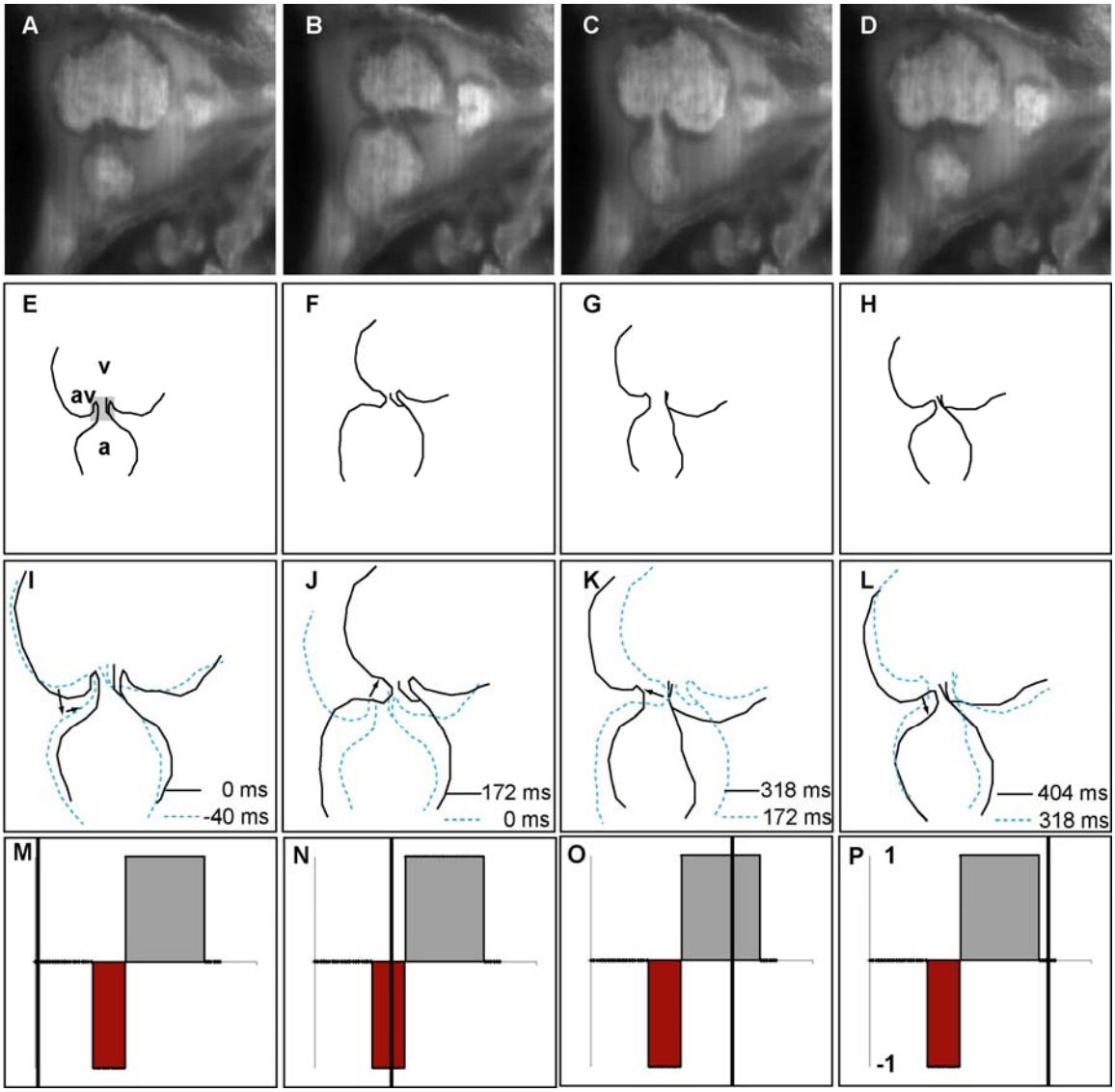

Figure 5.7. Valve dynamics and blood flow in 84 hpf embryos. (A-D) Sequence of confocal scans during one cardiac cycle. Outlines of each image are provided (E-F). Sequential images are superimposed upon each other to show cardiac cushion and leaflet motions (I-J) along with timestamps. The black arrows indicate the motion of the cushion and leaflet. (M-P) Binary representation of flow during one cardiac cycle. Vertical black line indicates the time point images (E-H) were recorded. See text for details of dynamics.

By 120 hpf, valve leaflets are fully functional and retrograde flow between the ventricle and atrium is no longer evident (Fig. 5.8M). At the onset of atrial filling, valve leaflets make contact at the atrial hinge while the free edges (ventricular portions) of the valves are still separated (Fig. 5.8I). Blood continues to enter the atrium, the chamber expands, and the contact point between the leaflets moves towards the free edge (Fig. 5.8J). At the later stages of atrial filling, the valve plane moves towards the ventricle (Fig. 5.8K). During diastole, the leaflets separate and allow blood flow from the atrium to ventricle (Fig. 5.8L, P). The ventricular volume increase, the atrial volume decreases, and the valve plane recoils towards the atrium (Fig. 5.8I, M). The leaflets are long enough to make contact throughout systole, preventing retrograde flow across the valve region.

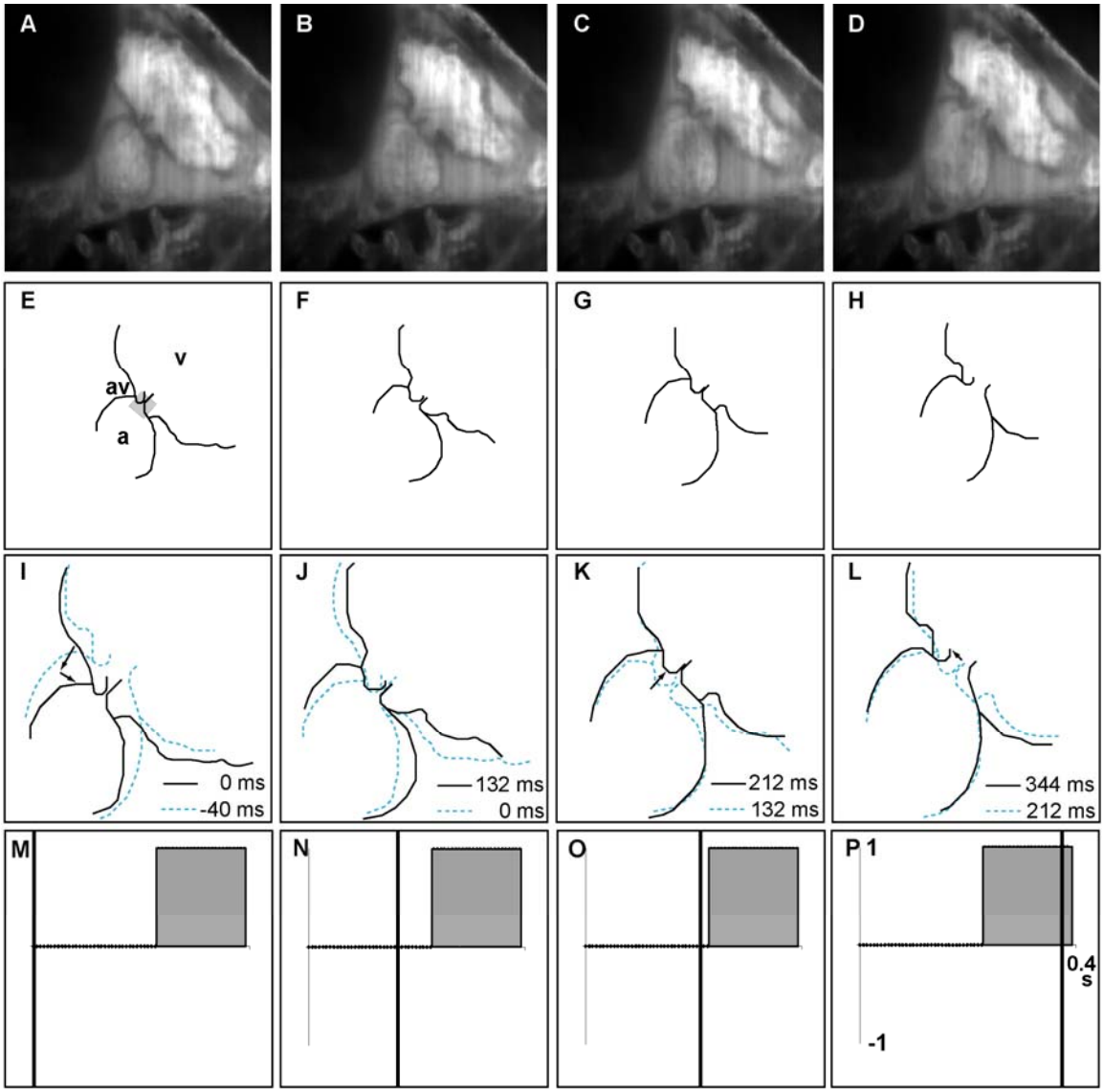

Figure 5.8. 120 hpf valve dynamics and blood flow. (A-D) Sequence of confocal scans during one cardiac cycle. Outlines of each image are provided (E-F). Sequential images are superimposed upon each other to show valve leaflet motions (I-J) along with timestamps. The black arrows indicate the motion of the leaflet. (M-P) Binary representation of flow during one cardiac cycle. Vertical black line indicates the time point images (E-H) were recorded. See text for details of dynamics.

5.5 Frequency and Flow

5.5.1 Decreased Heart Rate

In vivo experiments designed to study the effects of retrograde flow on heart valve formation require a non-invasive method to modulate oscillatory flow. Studies relating negative near-wall shear stress in the human aorta and congestive heart failure lead to in vitro experiments that identified a relationship between retrograde flow and frequency (Gharib and Beizaie, 2003). A decrease in frequency eliminated retrograde flow through the model aorta. These results motivated us to explore the relationship between retrograde flow and frequency in the developing heart.

Here, we show similar in vivo results in the embryonic zebrafish heart. At all stages examined (36 to 72 hpf), a decrease in heart rate resulted in a decreased duration of the retrograde component of oscillatory flow (Fig. 5.9). Thus, manipulating embryonic heart rates provide a method to modulate the duration of retrograde flow during the cardiac cycle. The two methods we employ to manipulate heart rates are ambient temperature control and exposure to lidocaine, a bradycardia- (slow heart rate) inducing drug.

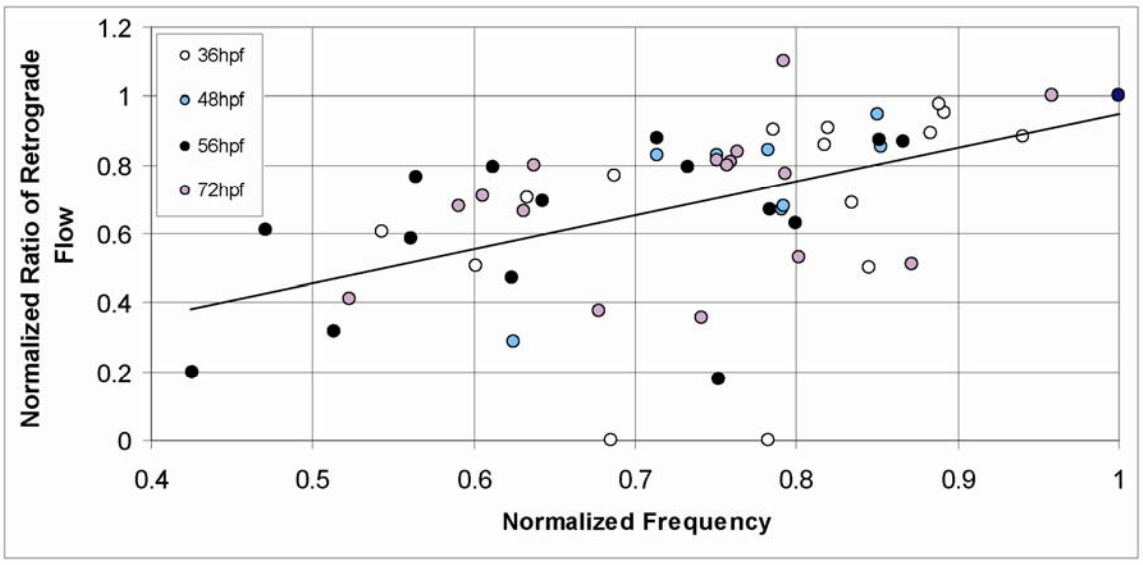

Figure 5.9. The duration of retrograde flow decreases with decreased heart rate. (A) Each point on the chart is a comparison of an embryo under experimental

conditions (exposure to lidocaine) compared with itself under normal conditions. The vertical axis is a ratio of the percentage of the cycle marked by retrograde flow in both cases. A number less than 1 indicates that the percent of the cycle exhibiting backflow has decreased. Combining all the data points for fish between 36 and 72 hpf, we display a trendline that shows retrograde flow decreases as a function of frequency. The trendline for each age decreases similarly (data not shown).

5.5.2 Oscillatory Flow Reduction Mechanism

Since valve leaflets are not contractile, the mechanisms by which heart valves open and close appear to be controlled by mechanical forces in the heart (i.e., pressure differences between chambers and contractile motions). Diastolic blood flow from the atrium into the ventricle of the adult human heart can be separated into two sections: (i) early diastolic filling (E wave), and (ii) filling due to atrial contraction (A wave). During atrial filling, the atrial pressure increases and eventually exceeds the ventricular pressure, causing the AV valve to open (commencement of E wave). The valve opening allows blood to pass from the atrium to the ventricle in order to equilibrate the pressure between the chambers (i.e., decrease atrial pressure and increase ventricular pressure). The second part of diastolic filling occurs when the atrium contracts, further increasing the atrial pressure, forcing more blood into the ventricle (A wave). These are the two main driving forces behind heart valve opening.

E and A waves are also apparent in the embryonic heart, and contribute to embryonic EC dynamics. When the pressure in the atrium exceeds the pressure in the ventricle, diastolic filling commences. Shortly after, the atrium contracts and assists ventricular filling. When the heart rate is decreased, the portion of the cardiac cycle between early diastolic filling and atrial contraction is lengthened. In cases where the period is only marginally extended, the duration of positive flow (E wave plus A wave), negative flow, and no flow are all increased but the ratio of the duration of negative flow

to the whole period decreases (from 40% to 35%). In more extreme cases, increasing the period can separate the E and A waves, causing cessation of flow from the atrium to ventricle during diastole (Fig. 5.10c). In these cases, the duration of retrograde flow can decrease substantially (from 40% to 24%).

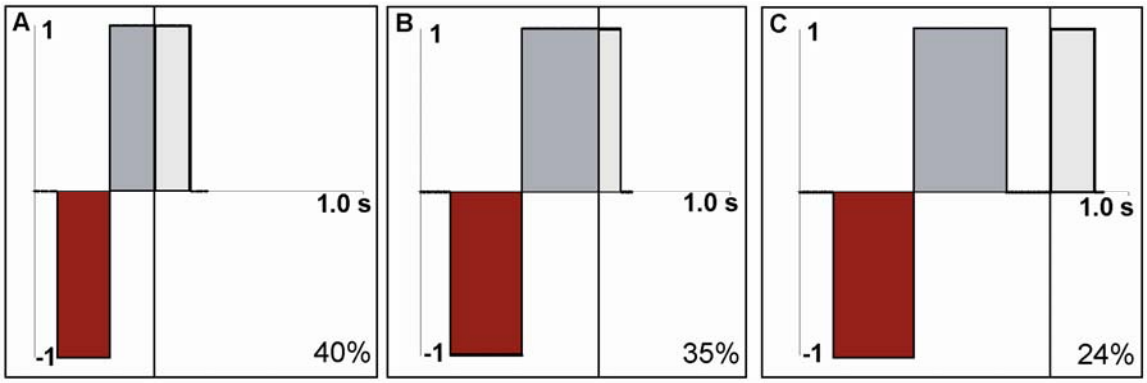

Figure 5.10. Oscillatory flow reduction mechanism. Flow through a single heart beating at different frequencies is shown. (A-C) As the heart rate decreases, the duration of retrograde flow also decreases (duration is shown in bottom right corner of each box). The black line indicates the beginning of atrial contraction and onset of the A wave (light gray region). Lengthening the cardiac cycle causes the time interval between early diastolic filling and atrial contraction to increase. During this interval atrial and ventricular pressures equilibrate.

5.5.3 Lidocaine Treatment

In developmental studies, and in the absence of reliable embryonic cardiac pacing, perhaps the most appropriate mode of controlling heart rate for extended periods of time is through exposure to drugs with specific target sites. Lidocaine decreases heart rate by blocking sodium channels. Cardiac sodium channels help maintain normal heart rates by allowing sodium to enter the myocytes, depolarizing the cell and causing an action potential. Multiple mechanisms by which lidocaine decreases heart rate have been proposed including sterically blocking sodium channels (Wang et al. 1997), increasing

the duration of the inactivation state (Balser et al. 1996; Fan et al. 1996), or preventing channels from opening altogether (Kambouris et al. 2000).

Fish were soaked in various concentrations of lidocaine (0.15%, 0.12%, 0.09%, 0.06% from a 1% stock solution) diluted in embryo medium. Changes in heart rate were evident within minutes of exposure. The relationship between lidocaine concentration and heart rate is shown in Fig. 5.11. The data indicates that the effects of lidocaine are relatively consistent over 24 hours of exposure. However, when comparing the effect of the treatment dosage to different clutches of embryos, the response varied. Three trials of 0.12% lidocaine (n=5 for each trial) gave normalized heart rates of 0.82±0.02, 0.55±0.04, and 0.47±0.07.

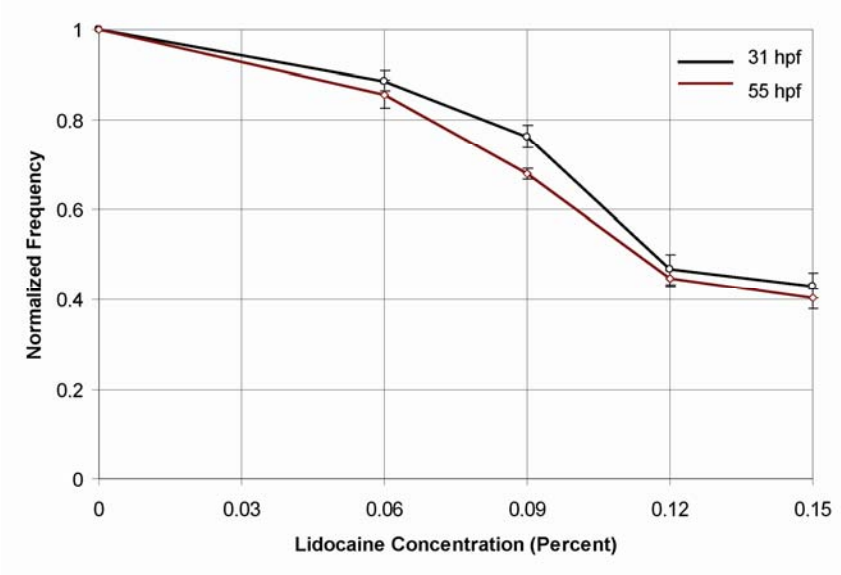

Figure 5.11. Lidocaine decreases heart rate. Heart rate as a function of lidocaine concentration and exposure. Each data point consists of 5 individuals. Heart rates measured 15 minutes (black line) and 24 hours (red line) after exposure to lidocaine.

5.6 Reduced Oscillatory Flow Induces Valve Defects

We initiated our oscillatory flow perturbations at 31 hpf, the developmental stage marked by the natural transition from unidirectional to bidirectional transvalvular blood

flow. Previous studies have shown that shear stress can cause actin cytoskeleton remodeling in cultured endothelial cells within minutes (Osborn et al. 2006) and induce cell alignment to flow in 24 hours (Dewey et al. 1981). In order to study in vivo effects, we perturbed flow in the developing zebrafish heart for 24 hours of development (31-55 hpf). We decreased heart rates up to approximately one-half the natural frequency, and created conditions in which oscillatory flow decreased substantially (Fig. 5.11).

5.6.1 Range of Valve Defects

In fish exposed to a range of concentrations of lidocaine, and thus a shorter duration of oscillatory flow, a variety of valve abnormalities were evident (Fig. 5.12) (the only other morphological changes evident were cardiac edema and changes in tail curvature). Sometimes subtle defects were observed in which cushions were present but valve leaflets did not separate (Fig. 5.12C,D) and in more extreme cases the heart remained a tube and cushions were not apparent (Fig. 5.12E,F). Valve abnormalities were accompanied by functional inadequacies as well, allowing significant back flow at 4 dpf.

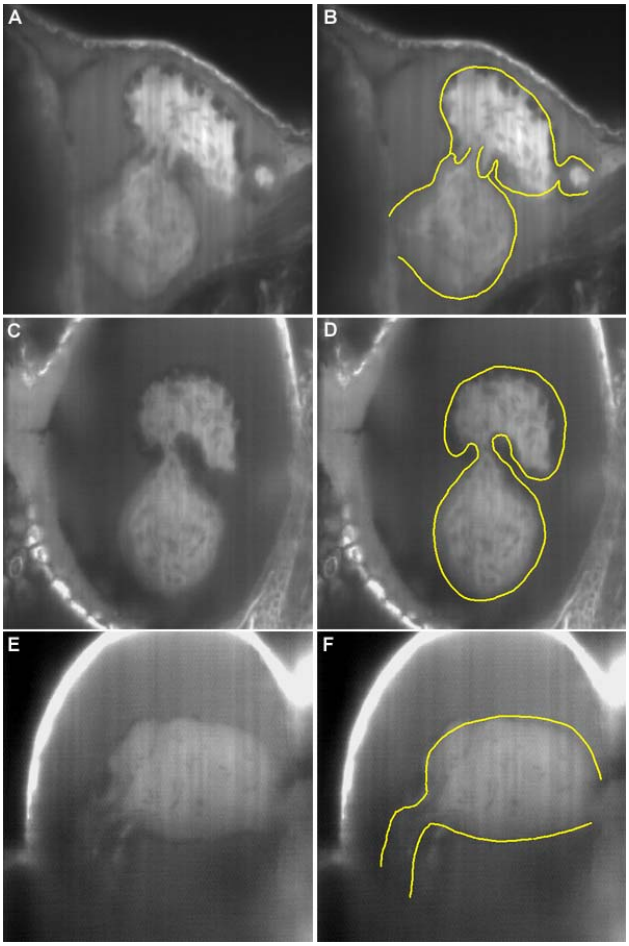

Figure 5.12. Range of valve dysmorphology at 96 hpf. (A,B) Control embryo with evident valve leaflets. (C,D) Experimental embryo with cardiac cushions but no apparent leaflets. (E,F) Experimental embryo with severe dysmorphology. Heart remains in tube form.

5.6.2 Incidence of Valve Dysmorphology

The incidence of valve dysmorphology increased with decreasing oscillatory flow (i.e., decreased heart rate and increased exposure to lidocaine), consistent with our hypothesis that oscillatory flow is critical for normal AV valve formation. Combined results from 4 trials are shown in Fig. 5.13. Dysmorphologies were scored by the absences of valve leaflets at 4 dpf (Fig. 5.12 C-F).

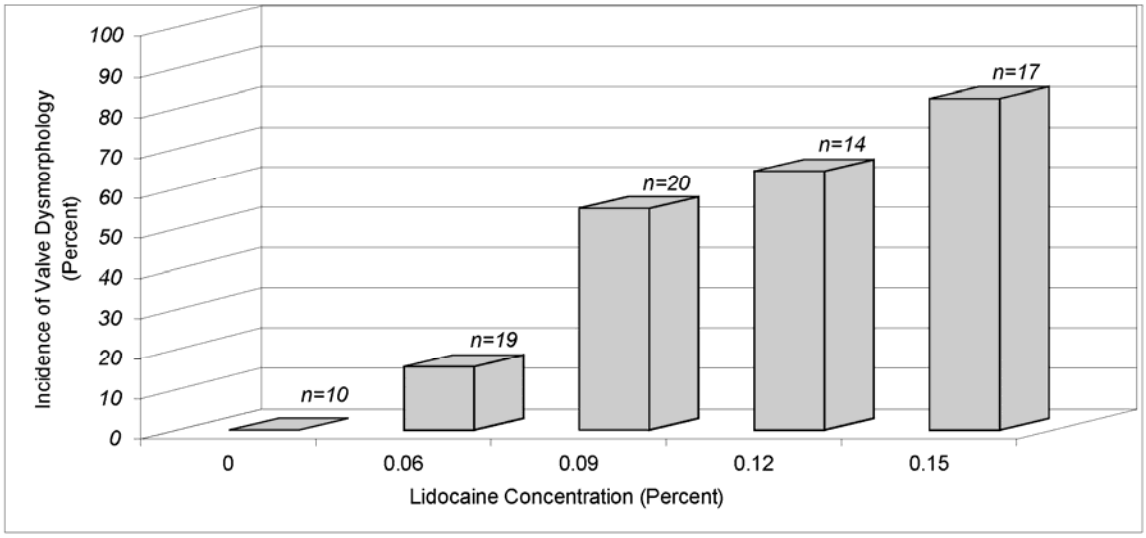

Figure 5.13. Incidence of valve dysmorphology. 4 dpf embryos treated with various concentrations of lidocaine. Decreased oscillatory flow (i.e., increased doses of lidocaine) induces increased valve dysmorphology. In all cases, scored dysmorphologies included the absence of prominent valve leaflets. For relationship between lidocaine concentration and heart rate, and subsequently oscillatory flow, see Figs. 5.11 and 5.9 respectively.

5.7 Control Experiments

To confirm the occurrence of oscillatory flow in the developing heart was not due to our imaging conditions (i.e., Tricaine, laser light excitation, or fluorescently labeled embryos) we observed flow in un-anesthetized wild type embryos under brightfield imaging. Results were consistent with those obtained from the Zeiss LSM 5 LIVE. Oscillatory flow was observed in all 48 hpf (n=6) and 72 hpf (n=7) embryos. Although faster frame rates can be obtained in conjunction with brightfield microscopy compared to laser scanning confocal microscopy, the fluid-structure interactions are not as clear since the imaging field is much thicker.

In a second control experiment, we used ambient temperature control to confirm that intracardiac flow patterns, and not the blockage of the sodium channels, caused the valve abnormalities. Since the internal temperature of zebrafish is directly controlled by

ambient temperature, enzymatic activity in zebrafish is also controlled by ambient temperature. Heart rates are accelerated at increased temperatures, and decelerated at lower temperatures (Barrionuevo and Burggren, 1999). This provides a simple method to control heart rate for long periods of time with no adverse developmental effects.

In our original experiments, fish exposed to 0.15% lidocaine for 24 hours displayed the highest portion of valve dysmorphology (88%, 15 of 17). In order to see if we could prevent abnormal valve development despite exposure to 0.15% lidocaine from 31-55 hpf, we incubated fish during the drug treatment at an elevated temperature (34º±0.5ºC) to bring the heart rate back within a normal range (Barrionuevo and Burggren, 1999). Through two trials, we found that at 4 dpf, 0 out of 20 embryos displayed AV valve anomalies (i.e., all had at least one valve leaflet), suggesting the drug was not driving the dysmorphology (Fig. 5.14). We supported this conclusion by similarly rescuing valve anomalies in fish exposed to 0.09% lidocaine and incubated at 32.5°±0.5°C during exposure. This data was collected from a single trial.

We also evaluated fish incubated (31-55 hpf) at 22.0º±0.5ºC to see whether this mechanism of oscillatory flow control (~40% decrease in heart rate) also caused valve defects at 4 dpf. Unlike embryos exposed to lidocaine, embryos with reduced heart rates due to lower temperatures did not display valve anomalies (n=7). It may be possible that normal magnitudes of oscillatory shear stress are maintained due to the increased blood viscosity resulting from decreased temperature.

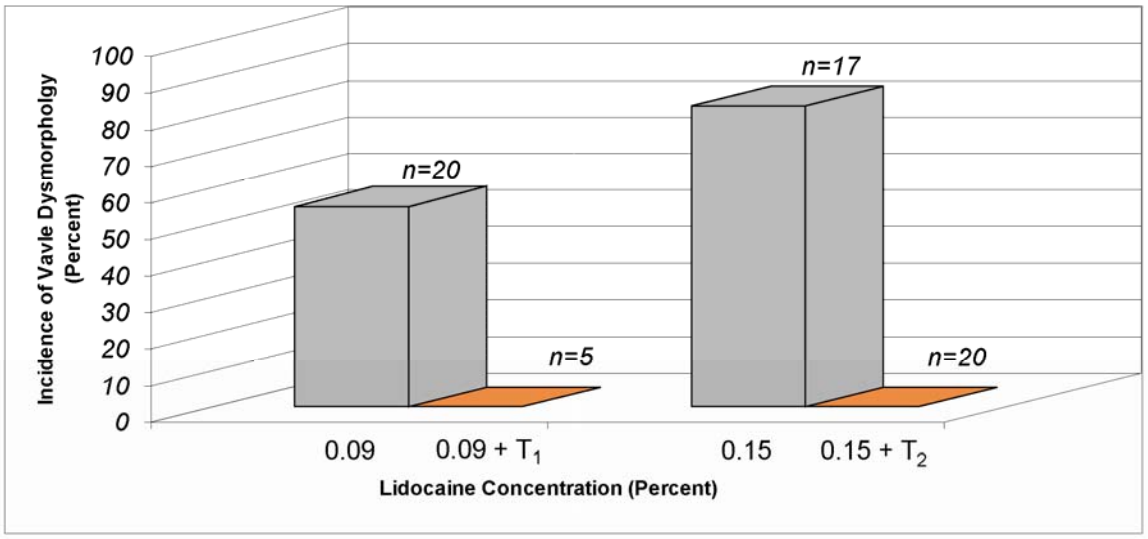

Figure 5.14. Valve dysmorphology rescue with elevated temperatures. Lidocaine treated embryos incubated at elevated temperatures (T1 = 32.5º±0.5ºC, T2 = 34°±0.5ºC) restores the normal heart rate and rescues valve defects.

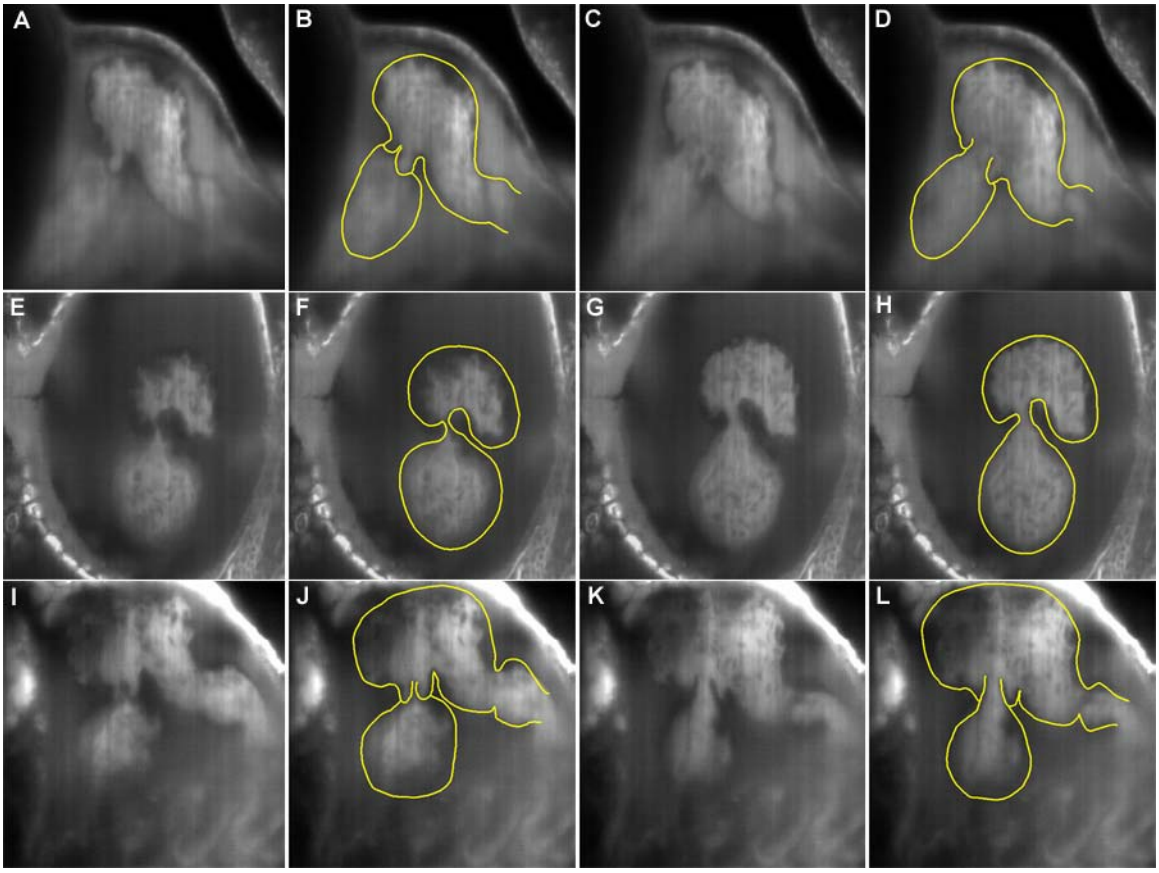

Figure 5.15. Heart valve dysmorphology rescue in embryos treated with 0.15% lidocaine. Heart valve formation in 4 dpf embryos. A pair of images are shown for each fish, the first during systole and the second during diastole. (A-D) AV valve in a wild type embryo. A pair of valve leaflets are present. (E-H) AV valve in embryo treated with 0.15% lidocaine for 24 hours. As a result of less than normal oscillatory flow, valve leaflets do not form. The valve region resembles the cardiac cushions of younger embryos. (I-L) AV valve in embryo treated with 0.15% lidocaine for 24 hours but simultaneously incubated at 34.0º±0.5°C restoring normal oscillatory flow. Heart valve leaflets are present and function normally.

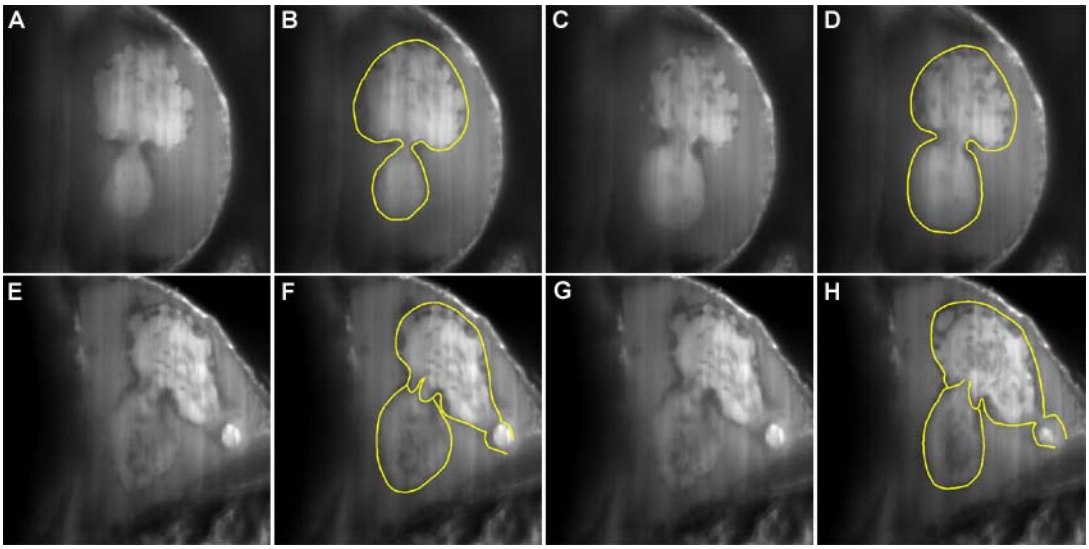

Figure 5.16. Heart valve dysmorphology rescue in embryos treated with 0.09% lidocaine. (A-D) AV valve in embryo treated with 0.09% lidocaine for 24 hours. As a result of less than normal oscillatory flow, valve leaflets do not form. The valve region resembles the cardiac cushions of younger embryos. (E-H) AV valve in embryo treated with 0.15% lidocaine for 24 hours but simultaneously incubated at 32.5º±0.5°C restoring normal oscillatory flow. Heart valve leaflets are present and function normally.

5.8 Discussion and Perspectives

During vertebrate cardiogenesis, the AV canal, as with any constricted cell layer, is exposed to amplified hemodynamic forces and subject to a unique local hemodynamic environment. Consistent with "flow molding" theories, the AV canal is also the site of unique gene regulation and morphological growth, eventually giving way to emerging valve leaflets. When examining flow through this primitive valve region, the amount of

retrograde flow from the ventricle to the atrium during each heartbeat is very curious. It is evident that the valveless heart is an inefficient pump and depends on valves to increase cardiac output. We have presented important preliminary data that supports our hypothesis that oscillatory shear stress is a stimulus for heart valve formation. In addition, we observed retrograde flow in valveless chick hearts (Forouhar and Vermot, preliminary observations), indicating pre-valvular retrograde flow is not only a characteristic of zebrafish hearts. Instead, we speculate that oscillatory flow may stimulate valvulogenesis in higher-order vertebrates (i.e., chicks, mice and humans) as well.

Detailed characterization of oscillatory shear stress still depends on improved flow visualization techniques. In order to derive precise estimates of shear stress, the blood velocity profile near the endocardial wall must be resolved. However, large blood cells (~10 μm) are not the ideal tracer particle to study boundary layer hemodynamics. Recent μPIV studies (Vennemann et al. 2006) have utilized fluorescent liposomes (400 nm) to acquire much higher resolution velocity maps in the embryonic chick heart. These studies should be extended to study oscillatory flow in the zebrafish heart. In addition, improved estimates of blood viscosity are required. Together, they can be used to determine the duration and magnitude of negative near-wall shear stress in order to see if certain hemodynamic parameters are conserved in embryos prior to heart valve formation.

In order to further strengthen the argument that oscillatory flow stimulates heart valve leaflet formation in zebrafish, several additional experiments are necessary, including: (i) exploring the effects of different bradycardia-inducing drugs that act on a variety of pathways and channels: (ii) developing pacing techniques that reliably and

consistently alter contractile frequencies, and thus flow patterns, and (iii) studying valve development and blood flow patterns in mutants with contractile and blood viscosity anomalies (i.e., *sih*, Sehnert et al. 2002; weak atrium, Berdougo et al. 2003; bloodless mutant, Liao et al. 2002, etc.), to see if there is a correlation between minimized negative near-wall shear stress and defective valve growth.

In addition we found that heart rate can modulate the extent of oscillatory flow. Decreased heart rates decrease the duration of oscillatory flow. Our preliminary observations of flow responses to increased heart rate suggest that the duration of near-wall retrograde flow increases with increased heart (n=4). Epinephrine treatments caused heart rate increases in older embryos (~72 hpf) but not in younger embryos (~31 hpf). Anticipating that the relationship between increased heart rate and oscillatory flow holds early in development, we incubated embryos (31-55 hpf) at 32.5º±0.5ºC to see whether valve leaflet formation was accelerated. We found that at 84 hpf all embryos (n=7) had advanced leaflet formation (i.e., resembling 96 hpf embryos, see Fig. 5.3). However, these results need further consideration before any conclusions may be drawn.

Previous studies demonstrating the importance of flow on cardiac development do not appear to have direct therapeutic utility until they offer practical methods to control hemodynamic forces in patients. Our results provide a simple mechanism for manipulating an important characteristic of intracardiac flow through heart rate, a feature of embryos that can be controlled. Perhaps then, monitoring and controlling embryonic heart rates may have therapeutic relevance for rescuing congenital heart valve defects.

5.8 Chapter References

Armstrong EJ, J Bischoff, *Circ Res*. **95**, 459 (2004).

Balser JR, HB Nuss, DW Orias, DC Johns, E Marban, GF Tomaselli, JH Lawrence, *J. Clin. Invest*. **98**, 2874 (1996).

Barrionuevo WR, WW Burggren, *Am J Physiol Regul Integr Comp Phsyiol.* **276**, 505 (1999).

Bartman T, EC Walsh, KK Wen, M McKane, J Ren, J Alexander, PA Rubenstein, DY Stainier, *PLoS Biol*. **2**, E129 (2004).

Beis D, T Bartman, S Jin, IC Scott, LA D'Amico, EA Ober, H Verkade, et al., *Development*. **132,** 4193 (2005).

Berdougo E, H Coleman, DH Lee, DY Stainier, D Yelon, *Development*. **130**, 6121 (2003).

Bernanke DH, RR Markwald, *Dev Biol*. **91**, 235 (1982).

Chang CP, JR Neilson, JH Bayle, JE Gestwicki, A Kuo, K Stankunas, IA Graef, GR Crabtree, *Cell*. **118**, 649 (2004).

Chauvaud S, *J. Cardiovasc. Surg*. **45**, 465 (2004).

Chen BP, YS Li, Y Zhao, KD Chen, S Li, J Lao, S Yuan, JY Shyy, S Chien, *Physiol Genomics*. **7**, 55 (2001).

Chen KD, YS Li, M Kim, S Li, S Yuan, S Chien, JY Shyy, *J Biol Chem*. **274**, 18393 (1999).

Dewey CF, SR Bussolari, MA Gimbrone, PF Davies, *J Biomech Eng* **103**, 177 (1981).

Dor Y, TD Camenisch, A Itin, GI Fishman, JA McDonald, P Carmeliet, E Keshet, *Development*. **128**, 1531 (2001).

Eisenberg LM, RR Markwald, *Circ Res*. 77, 1 (1995).

Fan Z, AL George, JW Kyle, JC Makielski, *J. Physiol*. **496**, 275 (1996).

Gharib M, M Beizaie, *Annals Biomed Eng*, **31**, 678 (2003).

Guyton AC, JE Hall, *Textbook of Medical Physiology.* Saunders, Pennsylvania (2000).

Kambouris NG, HB Nuss, DC Johns, E Marban, GF Tomaselli, JR Balser, *J. Clin. Invest*. **105**, 1133 (2000).

Lee HJ, GY Koh, *Biochem Biophys Res Commun*. **304**, 399 (2003).

Lee YM, JJ Cope, GE Ackermann, K Goishi, EJ Armstrong, BH Paw, J Bischoff, *Dev Dyn*. **235**, 29 (2006).

Liao EC, NS Trede, D Ransom, A Zapata, M Kieran, LI Zon, *Development*. **129**, 649 (2002).

Liebling M, AS Forouhar, R Wolleschensky, B Zimmermann, R Ankerhold, SE Fraser, M Gharib, ME Dickinson, Rapid three-dimensional imaging and analysis of the beating embryonic heart reveals functional changes during development, In preparation.

Motoike T, S Loughna, E Perens, BL Roman, W Liao, TC Chau, CD Richardson, et al., *Genesis*. **28**, 75 (2000).

Osborn EA, A Rabodzey, CF Dewey, JH Hartwig, *Am. J. Phys- Cell Phys*. **290**, 444 (2006).

Passerini AG, A Milsted, SE Rittgers, *J. Vasc. Surg*. **37**, 182 (2003).

Pelster B, W Burggren, *Circ Res*. **79**, 358 (1996).

Schwerte T, S Voigt, B Pelster, *Comp. Biochem. Physiol*. **141**, 200 (2005).

Sehnert AJ, A Huq, BM Weinstein, C Walker, MC Fishman, DY Stainier, *Nat. Genet*. **31**, 106 (2002).

Shay-Salit A, M Shushy, E Wolfovitz, H Yahav, F Breviario, E Dejana, N Resnick, *Proc. Natl. Acad. Sci*. **99**, 9462 (2002).

Sorescu GP, Sykes M, Weiss D, Platt MO, Saha A, Hwang J, Boyd N, Boo YC, Vega JD, Taylor WR, Jo H, *J. Biol. Chem*. **278**, 31128 (2003).

Stainier DY, B Foquet, JN Chen, KS Warren, BM Weinstein, SE Meiler, MA Mohideen, et al., *Development*. **123**, 285 (1996).

Vennemann P, KT Kiger, R Lindken, BCW Groenendijk, S Stekelenburg-de Vos, TLM ten Hagen, NTC Ursem, et al., *J. Biomech*. **39**, 1191 (2006).

Walsh EC, Stainier DY, *Science* **293**, 1670 (2001).

Wang DW, K Yazawa, N Makita, AL George, PB Bennett, *J. Clin. Invest*. **99**, 1714 (1997).

Yamagashi T, Y Nakajima, K Miyazono, H Nakamura, H Bone, *J Cell Physiol*. **180**, 35 (1999).

CHAPTER 6: Conclusions

6.1 Primary Contributions

When this project was originally conceived, our goal was to add the next incremental block of knowledge to the existing body of work studying the role of intracardiac hemodynamics. We initially planned to create plastic molds of the developing heart using structural data from fixed embryos and then pump fluid through the molds to study flow patterns and estimate hemodynamic forces. In our efforts to understand the morphology of the developing heart, we found that with appropriate imaging and visualization techniques, we could directly study flow in vivo. Our results opened numerous avenues to explore the function of intracardiac hemodynamics, and consequently allowed us to study the effects of perturbed intracardiac flow on heart morphogenesis in vivo. Throughout the course of this study, we integrated contemporary biological imaging tools and techniques to describe novel dynamic aspects of vertebrate heart morphogenesis.

The results of our flow occlusion studies published in *Nature* generated a great deal of excitement in the field. For the first time, we showed that hemodynamic forces are critical for proper heart development in vivo. “Researchers in the field had suspected for some time that flowing blood helps the heart develop. Fluid forces can cause cultured cardiac cells to alter gene expression patterns and rearrange their cytoskeleton. But without measurements of the forces, scientists couldn’t prove the connection,” wrote Erica Goldman in a review titled “Growing Hearts Go With the Flow” published in *ScienceNOW* (January 8, 2003). Cardiologist Kent Thornberg of the Oregon Health and

Science University of Portland commented that “this study was groundbreaking because of the novel approach taken by the investigators. Until now, researchers had to rely on theoretical models to study the physical forces that guide the development of the heart.”

After quantifying intracardiac hemodynamics and establishing a critical role for blood flow in heart morphogenesis, we extended our analysis to study the first functional stages of heart development. We found that the embryonic heart tube does not circulate blood through peristalsis, as previously considered. Instead, in results published in *Science*, we showed that the tube acts as a dynamic suction pump, sharing functional characteristics with the adult heart. The pumping mechanism we described is significant since it shows that only a few contractile cells are necessary to initiate mechanical forces that may guide later stages of cardiogenesis. In addition, we speculate that the described heart tube mechanics naturally lead to heart valve formation as a result of the sensitivity between frequency and flow and transition from unidirectional flow to oscillatory flow. Our analysis of in vivo heart tube dynamics provides a protocol for studying cardiac structure and function at a specific developmental stage.

We extended these techniques to study the dynamic relationship between contractile mechanics and flow during the development of heart valves. We provide a method to simultaneously observe transvalvular blood flow patterns, four-dimensional cardiac cell motions, and developing heart valves. Utilizing these methods, we observed oscillatory flow across the developing valve and illustrate cushion and leaflet dynamics during anterograde and retrograde flow phases. We describe a non-invasive, in vivo method to modulate oscillatory flow during valve development and provide evidence that retrograde flow is necessary for leaflet formation.

6.2 Challenges

Building upon the large body of evidence supporting *general* "flow-molding" theories, researchers are now seeking more precise relationships between *specific* flow patterns and developmental processes. The two major challenges in connecting hemodynamic forces with cardiogenesis are (i) quantitatively characterizing relevant intracardiac blood flow patterns, and (ii) non-invasively and acutely manipulating blood flow patterns in vivo. Higher resolution velocity maps and accurate viscosity measurements are still required to reliably extract quantitative in vivo hemodynamic data such as shear stress. Once a comprehensive map of normal blood flow patterns is generated, two protocols may be used to study abnormal flow: (i) apply non-invasive techniques to alter flow in wild-type embryos and screen for changes in gene expression and morphology, or (ii) study mutants with altered flow properties and see how changes in hemodynamics alter expression patterns in otherwise normal genes. Both present fundamental challenges in isolating experimental variables in vivo. Using wild-type embryos, experimental manipulations that only change intracardiac blood flow patterns are still elusive. Thus, it remains a considerable task to differentiate between the primary contributions of hemodynamic forces and the secondary contributions of experimental manipulations. Using genetic mutations, altered contractile mechanics or blood-plasma properties may adjust desirable hemodynamic parameters, but it needs to be confirmed that the mutations do not affect the analyzed developmental processes.

Eventually, when these challenges are appropriately addressed, and informative conclusions are drawn, dynamic imaging should be extended to less accessible embryos.

Ultimately, it is desirable to visualize blood flow, cardiac mechanics, and developmental morphology at sub-micron resolutions in human embryos.

6.3 Future Work

The integration of imaging and four-dimensional analysis tools to study heart morphogenesis provides access to many diagnostic metrics of embryonic cardiac function. A small subset of these include: (i) chamber volume measurements, (ii) cardiac outputs and ejection fractions, (iii) muscle fiber orientations, (iv) excitation-contraction coupling, (v) endocardial cushion, valve plane, and valve leaflet motions, (vi) dynamic properties of the elastic cardiac jelly, (vii) trabeculation, etc. Since many of these parameters will be studied dynamically for the first time, it will be interesting to see how they all come together to shape a more comprehensive description of cardiogenesis.

All of the data provided in this thesis was acquired from zebrafish, but many of the results may be apply to other model systems. The suction pump mechanism of the embryonic zebrafish heart tube should be explored in the mature hearts of lower vertebrates such as Drosophila as well as the embryonic hearts of higher vertebrates such as chick and mouse. This pumping mechanism provides a new paradigm to study other aspects of cardiogenesis (i.e., development of the conduction system, looping, valvulogenesis, etc.). In addition, oscillatory flow across the developing valve may be conserved among vertebrates as well. Consistent with our findings in zebrafish, initial observations of chick hearts prior to valve formation revealed oscillatory flow (Forouhar and Vermot, preliminary observations). Naturally, studies evaluating the effects of

oscillatory flow on valvulogenesis should continue to be explored in zebrafish (both in vivo and in vitro) and should be extended to chick and other vertebrate models.

Specifically in zebrafish, the *sih* mutant appears to provide a unique opportunity to study the role of hemodynamic flow patterns on post-looping cardiogenesis (i.e., cushion formation, valve leaflet formation, trabeculation, etc.). An external pump connected to the inflow and outflow tracts of the intact heart could be used to drive flow (i.e., steady, pulsatile, unidirectional, oscillatory, etc.) through the heart. If it is definitively shown that mutations of cardiac troponin T do not influence the selected aspects of cardiogenesis, then the addition of flow through *sih* mutant hearts may largely determine the role of blood flow on cardiogenesis.

Many researchers in developmental bioengineering ultimately aspire to identify roots of normal and abnormal development in order to design therapies that may rescue congenital defects. The dynamic relationship between structure and function in the heart provides a tremendous opportunity to control pumping mechanics in order to manipulate blood flow patterns. Comprehensive analyses of cardiac contractile mechanics and blood flow can improve our understanding of fluid-structure interactions. Relationships between manageable cardiac parameters (i.e., heart rate, contractility, vasodilation, etc.) should be further explored to design hemodynamic therapies. Therefore, not only should we consider what flow patterns are normal and abnormal, but also how we can manipulate the in vivo system to adhere to normal conditions.

Appendix A:

Intracardiac fluid-forces are an essential epigenetic factor for embryonic cardiogenesis

Published in Nature, 421 172-177 (9 January 2003)

Jay R. Hove[1]*‡, Reinhard W. Köster[2]*‡, **Arian S. Forouhar**[1], Gabriel Acevedo-Bolton[1], Scott E. Fraser[2] & Morteza Gharib[1]

[1]Options of Bioengineering and Aeronautics, Division of Engineering & Applied Science,

[2]Biological Imaging Center, Beckman Institute, and Division of Biology, California Institute of Technology, Pasadena, California 91125, USA

*These authors contributed equally.

‡To whom correspondence should be addressed.

Flow pattern analysis and calculations: e-mail: jhove@caltech.edu

Imaging techniques and embryonic manipulation: e-mail: rkoeste1@gg.caltech.edu

Movies and figures are available at:

http://bicsnap1.caltech.edu/heart/start.htm

User: heartreviewer Password: blood

The pattern of blood flow in the developing heart has long been proposed to play a significant role in cardiac morphogenesis. In response to flow-induced forces, cultured cardiac endothelial cells rearrange their cytoskeletal structure and change their gene expression profile [1,2]. To link such *in vitro* data to the intact heart, we performed quantitative *in vivo* analyses of intracardiac flow-forces in zebrafish embryos. Our *in vivo* imaging reveals the presence of high-shear, vortical flow at two key stages in the developing heart, and predicts flow-induced forces much greater than might have been expected for micro-scale structures at low Reynolds numbers. To test the relevance of these shear forces *in vivo,* flow was occluded at either the cardiac inflow or outflow tracts, resulting in hearts with an abnormal third chamber, diminished looping, and impaired valve formation. The similarity of these defects to those observed in some congenital heart diseases argues for the importance of intracardiac hemodynamics as a key epigenetic factor in embryonic cardiogenesis.

The formation of a functional heart is regulated by the coordinated interplay between a genetic program, fluid mechanical stimuli, and the inter- and intra-cellular processes that link them[3-5]. While the genetics of cardiogenesis are being analyzed intensely[6,7], studies of the influence of epigenetic factors on heart development, such as blood flow, have advanced more slowly due to the difficulty of mapping intracardiac flow *in vivo*. Numerous *in vitro* studies demonstrate that vascular endothelial cells (EC) can both sense and transduce biomechanical stimuli such as wall shear stress and transmural pressure caused by pulsatile blood flow[8]. For example, cultured vascular EC can respond to frictional stresses as low as 0.2 dyne·cm^{-2} [(9)]. The applicability of such *in vitro* data will remain speculative without a quantitative understanding of the flow

conditions within the intact developing vertebrate heart. Small size, optical clarity and external development have made zebrafish (*Danio rerio*) an ideal model for *in vivo* studies of the cellular and molecular events of cardiogenesis[10]. Taking advantage of these properties we quantified the hemodynamics in the developing vertebrate heart. Two different embryonic stages were chosen for detailed analysis: 4.5 days post fertilization (dpf) after key morphogenetic events have generated a heart that is very close to the adult configuration; 37 hours post fertilization (hpf) when the forming heart is not much more than a primitive contractile tube. We defined the gross cardiac dynamics at 4.5dpf using high-speed transmitted light microscopy. Vessels draining the yolk sac via the sinus venosus fill the atrium; atrial contraction forces the blood into a single ventricle from which it is pumped through the bulbus arteriosus, and into the ventral aorta (Fig. A.1A, B; Movie 1). High speed laser-scanning microscopy of the heart in homozygous tie2::GFP transgenic embryos, which express Green Fluorescent Protein (GFP) in the cardiac valves[11], shows that both atrio-ventricular (AV) and ventriculo-bulbal (VB) valves are present and functional at 4.5dpf (Movie 2). Transmitted-light laser scanning microscopy reveals distinct AV- and VB-valve dynamics. The VB-valve appears stiff, opening in a zipper-like manner beginning from the ventricular side during ventricular systole (Fig. A.1C-D) as pressure rises at the onset of ventricular contraction (see Movie 2 and Movie 3). The VB-valve closes at the end of ventricular systole assuring unidirectional blood ejection through the elastic bulbus and into the ventral aorta. In comparison, the AV-valve (and AV-region) appears more flexible, undergoing a 2.8-fold diameter change during the cycle of systole and diastole (Fig. A.1E-F, Movie 4).

To visualize the blood flow patterns inside the heart chambers we utilized a fluorescent dye (Bodipy-Ceramide) to label the blood serum for high-speed fluorescent confocal imaging. The flow patterns of unlabeled blood cells were revealed as dark streaks in the bright fluorescence of the serum. As the time to scan an entire frame

(0.7sec) is in the range of one cardiac cycle, the overall shape of the moving heart is distorted; furthermore, both the speed and the direction of flow will influence the shape and length of the dark streaks. Despite these distortions, the local relationship between neighboring streaks can be assessed in the confocal images because the raster scanning of the laser beam interrogates neighboring regions within microseconds along the line scan direction and within milliseconds in the field scan direction. Individual erythrocytes move rapidly from the atrium to the ventricle during diastole (Fig. A.2A, Movie 5); laminar flow is indicated by the parallel trajectories through the VB-valve (Fig. A.2B). Streak lengths represent the movement of the erythrocytes during the image acquisition period, and therefore are proportional to the speed of the blood cell movement. The lengths and linearity of the streaks suggest high ejection velocities and a jet-like blood flow through the VB-valve.

The enhanced contrast between the blood serum and EC provided by the Bodipy-Ceramide staining permitted us to visualize the blood volume in the beating 4.5dpf zebrafish ventricle. Assuming an ellipsoidal volume for the ventricle[12], we calculated an ejection fraction of ~60%, a value surprisingly close to that of the adult human left ventricle (59±7%)[13]. A large volume ejected rapidly suggests that the blood efflux from the narrow VB-valve creates significant shear forces on the cardiac EC. Combining the ejected volume, apparent ventricular and valve dimensions, and the measured time of contraction yields an estimated intracardiac blood flow of nearly 1 $cm \cdot s^{-1}$.

To more precisely characterize the intracardiac flow and fluid forces, we employed high-speed cine imaging at 440-1000 $frames \cdot s^{-1}$ and digital particle image velocimetry (DPIV)[14]. High framing rates allow the course of small groups of erythrocytes to be followed through the beating heart. DPIV revealed the velocity vector field generated by the fluid motions as vectors indicating the directionality and relative velocity (encoded in different colors) at each instant during the heart cycle. Erythrocytes

moving through the AV-constriction during diastole reached velocities of ~0.5 cm·s^{-1}; similar velocities were measured on either side of the VB-constriction during ventricular systole (Fig. A.2C-D, Movie 6). Superficial tissue masks erythrocyte movement through the V-B valve itself by physically obstructing the optical path and by contributing a non-moving tissue component to the average reported for that DPIV interrogation window. As the latter effect is greatest near chamber walls and in small cross-sectional areas, our estimates of velocity through the V-B valve are conservative. DPIV analysis requires that the captured 3-dimensional erythrocyte movements be projected onto a 2-dimensional plane. This dimensional collapse underestimates distances traveled by a given cell in 3-dimensional space, further suggesting that our calculated intracardiac velocities of ~0.5 cm·s^{-1} should be taken as lower limits of the real velocities. Flow through the micro-scale cardiac structures of zebrafish embryos is highly viscous (Reynolds number (*Re)* much less than one) meaning that high-speed flow produces enormous physiological wall shear stresses (with Re = 0.02, shear >75 dyne·cm^{-2}) in the VB-orifice.

DPIV identifies the circulation patterns of the fluid flow field as a whole (Fig. A.2E-F) and reveals the presence of vortices inside the beating embryonic heart. Although, vorticity is three-dimensional, vortex circulation is the same in 2-D and 3-D flow fields, regardless of the two-dimensional plane sectioned (Kelvin's Law). During the diastolic phase of the heart cycle, vortices are present behind the AV-constriction in the relaxing ventricle (Fig. A.2E). This vortical flow pattern (without flow separation), likely caused by the impulsive influx from the AV-constriction; is in good agreement with the observed curved trajectories at the AV-constriction in Bodipy-Ceramide labeled embryos (compare Fig. A.2A, E). During systole, DPIV reveals a vortex pair just downstream of the VB-orifice, accompanying the blood influx from the ventricle into the bulbus during ventricular contraction (Fig. A.2F). This pronounced vortex formation is

likely to have implications for the shape of the bulbus itself, as the size of the bulbus is just sufficient to contain it. The presence of such complex vortical flow in the living zebrafish suggests that *in vitro* studies should use oscillatory flow regimes rather than simple steady flows to better simulate intracardiac flow conditions *in vivo*.

Such high-shear intracardiac flow during late embryonic stages of cardiac morphogenesis led us to investigate the intracardiac flow patterns in the early embryonic heart (37hpf zebrafish embryo, Fig. A.3A). The dominant morphological feature of the 37hpf heart is the alignment of the atrium and ventricle in a primitive tube, and the absence of a bulbus (Fig. A.3B). Valves will not develop for several hours, consistent with absence of GFP-labeled valve structures in tie2::GFP transgenic embryos; instead, GFP is expressed throughout the endocardium. The 37hpf heart demonstrates a phasic contraction of the ventricle and atrium at little more than half the rate (1.3 Hz at 20°C) of the 4.5 dpf embryo. Using Nomarski optics we were able to visualize two converging blood streams over the yolk sac being drawn into the atrium (Movie 7). Based on individual erythrocyte velocities (~0.5 mm s^{-1}) and the vessel dimensions, these streams should exert shear forces in excess of 1 dyne·cm^{-2}. Despite its lack of valves, the early heart produced a unidirectional flow with little regurgitation, arguing that the chamber dynamics themselves may govern the blood flow direction[15]. To analyze the chamber dynamics of the 37hpf heart in detail we made use of a transgenic strain expressing GFP under control of the *gata1*-enhancer/promoter[16] which exhibits strong GFP-fluorescence in the endocardium, allowing visualization of the heart chamber walls (Fig A.3C-E). A nearly complete collapse of a portion of the chambers during systole (Fig. A.3D-E, see also Movie 8) severely constricts the lumenal cross-section, minimizing backflow. The notion that the early embryonic heart may well act as both a valve and pump is intriguing and current investigations support this hypothesis (JH, GA-B & MG, manuscript in preparation).

To determine the ejection fraction in the 37hpf zebrafish heart, Bodipy-Ceramide serum labeling was used to visualize the diameter changes of the cylindrical ventricle between maximal systolic contraction and diastolic expansion (Fig. A.3F,G) in different transverse planes. The resulting data indicate an ejection fraction of ~60%. The calculated systolic ejection velocity of approximately 1.5 $mm \cdot s^{-1}$ is consistent with the maximum blood velocity measured directly in the AV-tract (0.9 $mm \cdot s^{-1}$); these measures predict shear stresses ranging from 2.5-10 $dyne \cdot cm^{-2}$ in this valve-less heart.

Our *in vivo* data demonstrate that the valved (4.5dpf) embryonic zebrafish heart functions as a high-speed, dynamic pump operating on a size scale (195 μm long x 150 μm wide) comparable to a coarse human hair. Calculations, based upon the observed velocities, predict wall shear stresses ranging from 2.5 $dyne \cdot cm^{-2}$ in the 37hpf heart to 76 $dyne \cdot cm^{-2}$ in the 4.5dpf heart. Shear forces less than 1 $dyne \cdot cm^{-2}$ are detectable by EC *in vitro*, resulting in up- or down-regulation of gene expression[9]. Larger shear forces, on the order of 8 to 15 $dyne \cdot cm^{-2}$, are known to cause cytoskeletal rearrangement[17]. Thus, both the early (37hpf) and the later embryonic hearts (4.5dpf) exhibit shear forces significantly above the threshold of detectability by the cardiac EC deduced from *in vitro* data. This makes it inescapable that shear forces must play some role in the regulation of cardiac morphogenesis during embryogenesis.

To test the possible influences of flow through the embryonic heart on its development, we interfered with blood flow at the primitive heart stage (37hpf) and analyzed the effects on cardiogenesis at the advanced heart stage (4.5dpf). Beads (~50 μm diameter) were implanted into homozygous transgenic tie2::GFP-embryos either in front of the sinus venosus to block blood influx into the atrium (Fig. A.4B); or in the back of the ventricle to block blood efflux from the heart into the aorta (Fig. A.4C). Continuous successful blocking of blood flow (assayed 20 hours after bead implantation) resulted in an accumulation of erythrocytes in front of the atrium (Fig. A.4E arrow) or

inside the heart chambers respectively (Fig. A.4F). In both cases, the embryos showed severe regurgitation of blood inside the heart and reduced blood flows, resulting in dramatically reduced (~ 10 fold) shear forces.

Embryos with impaired cardiac flow demonstrated three dramatic phenotypes. First, their hearts did not form the third chamber, the bulbus. In addition, they lacked heart looping, the normal process resulting in the repositioning of the ventricle and atrium from a cephalo-caudal into a side-by-side arrangement. Finally, the walls of the inflow and outflow tracts collapsed and fused, beginning at 3dpf. This latter phenotype is reminiscent of the zebrafish *jekyll*-mutant, which demonstrates abnormal blood flow due to a missing AV-valve (E. Walsh, D. Stainier, pers. comm.). The similarity of the defects resulting from disrupting either inflow or outflow argues that it was not the changes in transmural pressures in the cardiovascular system that is responsible, as the two different blockades should decrease (blocked inflow) or increase (blocked outflow) the pressure. Instead, the decreased shear forces, the common feature of the two treatments, seems most likely to generate the developmental phenotype.

Control experiments and other considerations support the conclusion that altered shear forces result in the observed cardiac defects. First, control embryos, in which a bead was placed close to the sinus without occluding blood flow through the heart (Fig. A4A, D), showed no obvious change in heart morphology or function at 4.5dpf (Fig. A.4G). Additional control embryos, in which inserted beads were removed after one hour, similarly showed no cardiac abnormalities (n=5, data not shown). Thus, cardiac malformations do not result from either the surgical procedure or the continued presence of a bead. In chick embryos, proper heart looping has been reported after the heart beat and thus hemodynamic forces have been blocked; however, the results were scored after only five hours without a heart beat[18]. In contrast, morphological defects attributable to improper looping could be observed in venous clipping experiments that lasted over

several days[19]. It is unlikely that our observed cardiac abnormalities result from subcritical levels of hypoxia as suggested elsewhere[20]. Zebrafish embryos do not appear sensitive to erythrocyte-mediated oxygen delivery[15], as a mutant specifically lacking erythrocytes for the first five embryonic days displays no vascular defect and can be raised to adulthood[21]. The defects are unlikely to result from reduced transport of nutrients or other biomolecules, as both our operated embryos and mutants lacking blood circulation develop properly over the first several days[22]. For example, *silent heart* embryos establish gut peristalsis and are able to hatch and swim[23]. Swimming is a complicated behavior, initiated at about 5dpf, requiring the orchestration of a functional nervous system with properly organized musculature. Most cardiac zebrafish mutants die around day 7 indicating that proper heart function and nutrient delivery is essential for cardiac morphology only significantly later than 4.5dpf[22]. The normal development of our control embryos, combined with these other findings, suggest that our observed cardiac phenotypes are likely to result from altered intracardiac hemodynamics rather than trauma to the vascular wall and endothelium, hypoxia, or failure of nutrient delivery.

The intracardiac regurgitation of blood observed in our flow-impaired zebrafish embryos points to a failure in valve formation, and the pattern of tie2::GFP-expression confirms abnormal valve formation under conditions of altered hemodynamics. In contrast to normal tie2::GFP embryos, in which the initial GFP expression throughout the endocardium resolves to the forming valves (AV and VB, Fig. A.4J red dashed circles, see Movie 2), specimens with impaired flow showed no signs of forming valves. Both blocked-inflow and blocked-outflow embryos displayed peristaltic heart contraction at 4.5dpf with weak GFP-fluorescence throughout the endocardium (Fig. A.4K, L see also Movie 9 and Movie 10). Thus, direct interference with intracardiac hemodynamics has profound effects on cardiac valve-formation, as well as chamber differentiation and organ morphology during embryogenesis. Approximately forty percent of congenital heart defects involve a valve abnormality as a contributing component (D. Sahn, pers. comm.).

Our defects in hearts with no genetic lesion argue that a critical role is played by blood flow-induced forces during normal heart development and suggests that altered hemodynamics may contribute to the cardiac phenotype in some cardiac mutants and perhaps birth defects.

Through the application of novel flow visualization technologies[24], we have quantified embryonic intracardiac velocities and shear forces directly *in vivo*. Surprisingly, the forces reach levels significantly above cellular sensitivity even in the primitive heart of the early embryo. Interference with these intracardiac flow forces results in severe cardiac malformations. Thus, we conclude that the physiology and development of the embryonic heart is linked by hemodynamics, consistent with recent observations on cardiac pathologies. There is increasing evidence that cardiovascular disease is rooted in processes initiated in the developing embryo and fetus[25]. The results presented here extend this proposal, suggesting that the same responses to shear forces that shape the developing heart may contribute to later abnormalities and disease processes. Our findings underscore the importance of examining the interplay between genetics and epigenetic factors such as fluid forces in analyzing the pathogenesis of embryonic vascular defects and cardiovascular disease[26,27].

Acknowledgements:
We thank S. Lin for providing us with the stable transgenic *gata1*::GFP zebrafish strain, E. Walsh, E. Ober, B. Jungblut and D.Y.R. Stainier for providing us with both the transgenic tie2::GFP strain and their constructive comments on the manuscript, and Magdalena Bak and Ying Gong for fruitful discussions. Supported by the American Heart Association (JRH) and the Human Frontier Science Program (RWK), the NIH (SEF), the Beckman Institute at Caltech, and the SURF program at Caltech.

Methods:

Maintenance of fish

Embryos were raised in 30% Danieau solution. Raising, maintaining and spawning of adult zebrafish were performed as described[28,29]. Adding Phenylthiourea (PTU) in a concentration of 0.15mM to the embryonic raising medium at the 10-somite stage (ca. 14 hpf) blocked pigmentation. Dechorionated embryos were anaesthetized with 0.05% Tricaine, embedded in 1.2% ultra low gelling agarose (Sigma) and mounted on a coverslip.

***In vivo* imaging**

Confocal imaging was performed at 20°C using a Zeiss LSM400 laser-scanning microscope. Imaging at this temperature slowed the beat frequency down to better allow imaging but did not change hemodynamics. For flow pattern and ejection fraction analysis embryos were soaked in 0.001% BodipyFLC5-Ceramide (Molecular Probes) as a contrast agent overnight prior to imaging. Times for continuous high-speed scanning to image flow dynamics were chosen such that individual pictures were out of phase compared to the heart beat cycle to capture subsequent stages of diastole and systole. Thus movies obtained from confocal imaging represent composites. Confocal images were analyzed using LSM software (Zeiss), Object-Image 2.05, Photoshop 5.02 (Adobe) and Freehand 8 (Macromedia).

Images for **DPIV analysis** were acquired at 256x256 pixels in real time using a Dalsa CA-D6-0256 CCD camera, and processed using interrogation windows of 16x16 pixels with an 8x8 pixel overlap (50%). DPIV analysis was performed on images acquired at 20, 25 and 28 °C. The intracardiac blood flow patterns appeared to be temperature invariant across this range although flow velocity did decrease slightly with lower temperature. For this reason the data sets taken at 20 °C were used for final DPIV analysis as they delivered a higher number of frames per heart beat cycle.

Ejection fraction calculation

The volume at the two extremes of the heart cycle was calculated by taking half of the projection through the mid-plane of the heart in two different frames corresponding to the maximum volume and minimum volume. The heart was assumed to be symmetric across this line. For each frame a curve was fit, f(x), to the contour of heart wall in this half section and rotated about the symmetry line. Then the formula for volume of revolution was applied:

$$V = \pi \int_a^b [f(x)]^2 dx$$

Change in volume was calculated by taking the difference in volume between the two frames, ΔV.

Velocity and shear stress calculation:

Without time for a parabolic flow profile to evolve, we assumed a linear velocity profile in the regions of interest, with maximum velocity at the center, and zero velocity at the walls. Velocity was expressed by the equation:

$$u(y) = \frac{U}{a} \times y$$

where *U* was the centerline velocity, *a* was the half width of the region of interest (i.e. radius) and *y* was distance from wall, reaching a maximum value of *a* at the center. Shear stress (τ) was defined as the derivative of velocity multiplied by μ, the dynamic viscosity of the fluid such that:

$$\tau = \mu \times \frac{\partial u(y)}{\partial y}$$

To convert into dynes·cm^{-2} the result was multiplied by a factor of 10. Given the small size of the vessel under examination, μ was assumed to be constant at 5×10^{-3} N·s·m^{-2}, roughly 5 times that of water.

Cardiac occlusion surgery:

Embryos (tie2::GFP; 37hpf) were anaesthetized in 0.05% Tricaine and embedded in low-melting agarose. The epithelium in front of the heart was cut open using micromanipulation needles; beads (BioRad AG1X8 Cl^-) were inserted into the blood stream and positioned with tungsten needles. The size of the bead (~50µm) was chosen to fit into the space between the yolk and the overlying skin close to the sinus venosus. Beads were kept in place by the slight pressure of these two tissues but could be repositioned as necessary.

References and Notes:

1. Topper, J. N. & Gimbrone, M. A. Blood flow and vascular gene expression: fluid shear stress as a modulator of endothelial phenotype. *Molecular Medicine Today* **5**, 40-46 (1999).
2. Davies, P. F. Flow-Mediated Endothelial Mechanotransduction. *Physiological Reviews* **75**, 519-560 (1995).
3. Nerem, R. M., Harrison, D. G., Taylor, W. R. & Alexander, R. W. Hemodynamics and Vascular Endothelial Biology. *Journal of Cardiovascular Pharmacology* **21**, S6-S10 (1993).
4. Takahashi, M., Ishida, T., Traub, O., Corson, M. A. & Berk, B. C. Mechanotransduction in endothelial cells: Temporal signaling events in response to shear stress. *Journal of Vascular Research* **34**, 212-219 (1997).
5. Taber, L. A. Mechanical aspects of cardiac development. *Progress in Biophysics & Molecular Biology* **69**, 237-255 (1998).
6. Chen, J. N. & Fishman, M. C. Genetics of heart development. *Trends in Genetics* **16**, 383-388 (2000).
7. Srivastava, D. & Olson, E. N. A genetic blueprint for cardiac development. *Nature* **407**, 221-226 (2000).
8. Helmlinger, G., Geiger, R. V., Schreck, S. & Nerem, R. M. Effects of Pulsatile Flow on Cultured Vascular Endothelial-Cell Morphology. *Journal of Biomechanical Engineering-Transactions of the Asme* **113**, 123-131 (1991).
9. Olesen, S. P., Clapham, D. E. & Davies, P. F. Hemodynamic Shear-Stress Activates a K^+ Current in Vascular Endothelial-Cells. *Nature* **331**, 168-170 (1988).
10. Stainier, D. Y. R. & Fishman, M. C. The Zebrafish as a Model System to Study Cardiovascular Development. *Trends in Cardiovascular Medicine* **4**, 207-212 (1994).
11. Walsh, E. C. & Stainier, D. Y. R. UDP-glucose dehydrogenase required for cardiac valve formation in zebrafish. *Science* **293**, 1670-1673 (2001).
12. Hou, P-C. L. & Burggren, W. W. Cardiac output and peripheral resistance during larval development in the anuran amphibian *Xenopus laevis*. *American Journal of Physiology - Regulatory Integrative and Comparative Physiology* **38**, R1126-R1132 (1995).
13. Mankad, R. et al. Regional myocardial strain before and after mitral valve repair for severe mitral regurgitation. *Journal of Cardiovascular Magnetic Resonance* **3**, 257-266 (2001).
14. Willert, C.E. and Gharib, M. Digital particle image velocimetry. *Experiments in Fluids* **10**, 181-193 (1991).
15. Pelster, B. & Burggren, W.W. Disruption of hemoglobin oxygen transport does not impact oxygen-dependent physiological processes in developing embryos of zebra fish (*Danio rerio*). *Circulation Research* **79**, 358-362 (1996).

16. Long, Q. M. et al. GATA-1 expression pattern can be recapitulated in living transgenic zebrafish using GFP reporter gene. *Development* **124**, 4105-4111 (1997).

17. Davies, P. F., Remuzzi, A., Gordon, E. J., Dewey, C. F. & Gimbrone, M. A. Turbulent Fluid Shear-Stress Induces Vascular Endothelial-Cell Turnover In vitro. *Proceedings of the National Academy of Sciences of the United States of America* **83**, 2114-2117 (1986).

18. Manasek, F. J. & Monroe, R. G. Early cardiac morphogenesis is independent of function. *Developmental Biology* **27**, 584-588 (1972).

19. Hogers, B., DeRuiter, M. C., GittenbergerdeGroot, A. C. & Poelmam, R. E. Unilateral vitelline vein ligation alters intracardiac blood flow patterns and morphogenesis in the chick embryo. *Circulation Research* **80**, 473-481 (1997).

20. Icardo, J. M. Developmental biology of the vertebrate heart. *Journal of Experimental Zoology* **275**, 144-161 (1996).

21. Liao, E. C. et al. Non-cell autonomous requirement for the *bloodless* gene in primitive hematopoiesis of zebrafish. *Development* **129**, 649-659 (2002).

22. Stainier, D. Y. R. et al. Mutations affecting the formation and function of the cardiovascular system in the zebrafish embryo. *Development* **123**: 285-292 (1996)

23. Sehnert A. J. et al. Cardiac troponin T is essential in sarcomere assembly and cardiac contractility. *Nature Genetics* **31**, 106-110 (2002).

24. Meinhart, C.D., Wereley, S.T., & Santiago, J.G. PIV measurements of a microchannel flow. *Experiments in Fluids* **27**, 414-419 (1999)..

25. O'Brien, S. P. M., Wheeler, T. & Barker, D. J. P. *Fetal programming influences on development and disease in later life* (RCOG Press, London, 1999)

26. Di Stefano, I., Koopmans, D. R. & Langille, B. L. Modulation of arterial growth of the rabbit carotid artery associated with experimental elevation of blood flow. *Journal of Vascular Research* **35**, 1-7 (1998).

27. Langille, B. L. in *Flow-dependent regulation of vascular function* (eds. Bevan, J. A., Kaley, G. & Rubanyi, G.) 277-299 (Oxford Press, New York, 1995).

28. Kimmel, C. B., Ballard, W. W., Kimmel, S. R., Ullmann, B. & Schilling, T. F. Stages of Embryonic-Development of the Zebrafish. *Developmental Dynamics* **203**, 253-310 (1995).

29. Westerfield, M. *The zebrafish book* (University of Oregon Press, Eugene, 1995).

Figures:

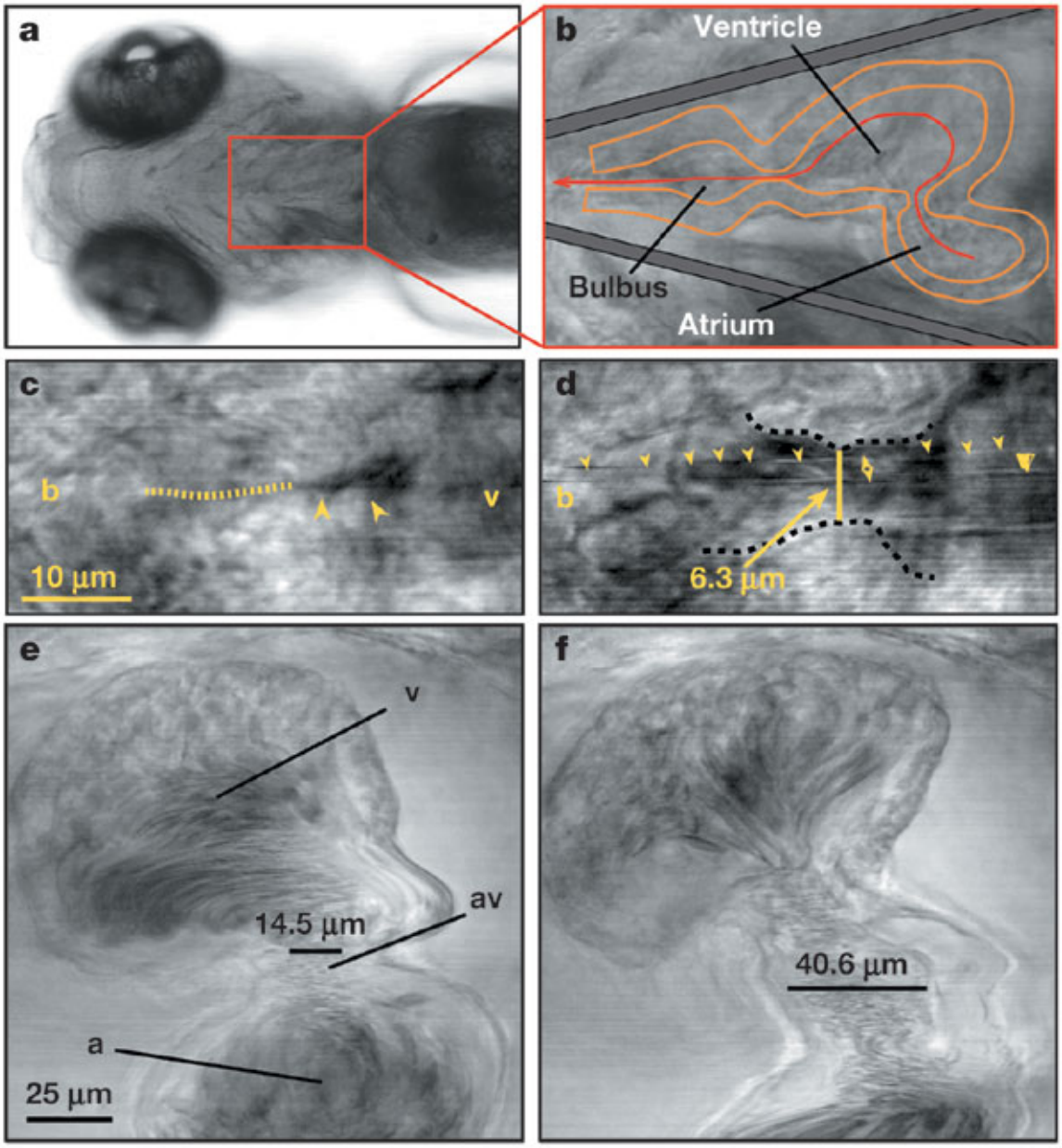

Figure A.1: Cardiac dynamics in the zebrafish embryonic heart at 4.5dpf. Pictures display individual characteristic confocal sections from a time series of the embryonic heart beat cycle. At 20 °C the 4.5dpf zebrafish heart beats at ~2 Hz. **A**, Ventral view of a 4.5dpf embryo with heart contained in red box. **B**, High magnification of heart with overlaid schematic denoting chamber boundaries; for heart beat dynamics see **Movie 1**.

Coronal sections through the ventriculo-bulbal region displaying gating stages of the VB-valve. Opening of the valve starts at the ventricular end (yellow arrowheads and proceeds in a zipper-like fashion (**C,** yellow dashed line indicates seam of VB-valve) at the beginning of ventricular systole due to increasing pressure. **D**, At maximal flow-through gating diameter ranges from 6 to 10 μm. Note streaks (yellow arrowheads) left by blood cells passing through the valve at high speed. To view *in vivo* valve dynamics see **Movie 2** and **Movie 3**. Coronal sections taken during ventricular filling **E**, show the AV-junction is narrow (14.5 μm) and short but enlarges (approximately 2.8-fold) and expands during ventricular systole **F**, 40.6μm, and see **Movie 4** in supplementary material).

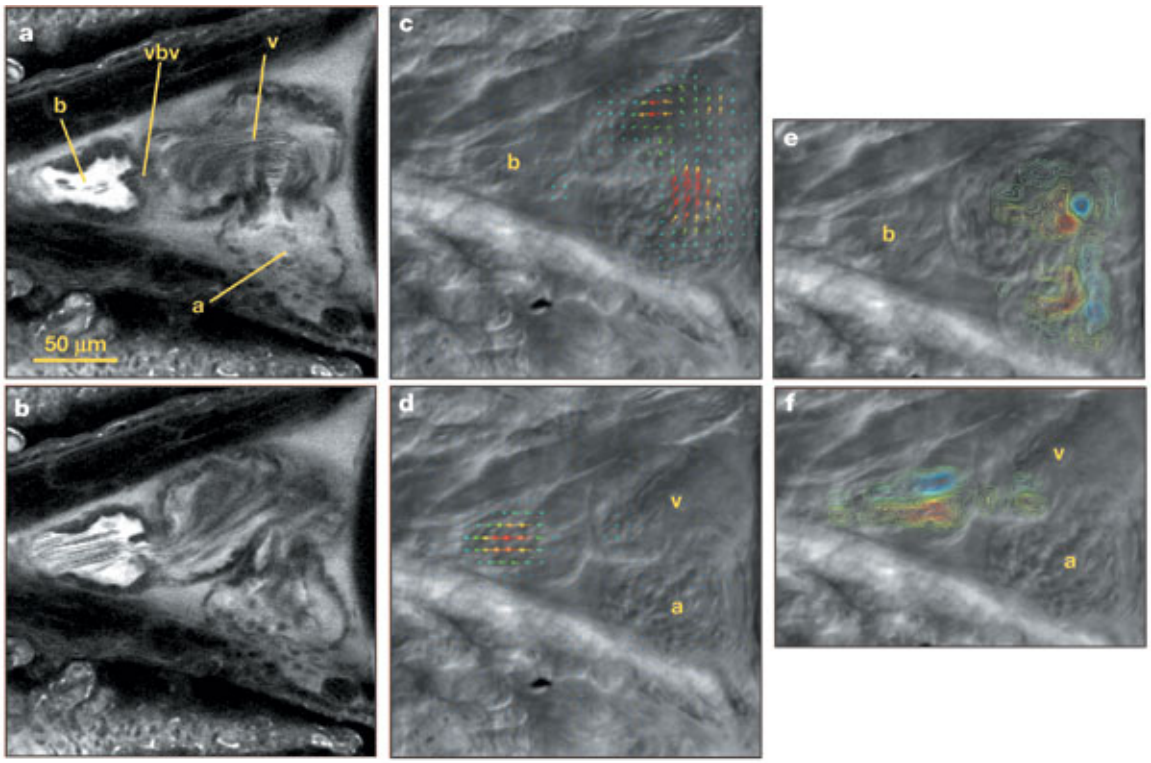

Figure A.2: High-velocity, high-shear conditions generated in the 4.5dpf embryonic zebrafish heart. Pictures display individual characteristic confocal sections from a single time series of Bodipy-Ceramide stained embryos. **A**, Atrial systole and ventricular filling. **B**, Ventricular systole and atrial diastole (leading to the refilling of the atrium).

Note the laminar ejection pattern generated by forceful microjets from the ventricle through the open VB-valve and through the aorta (see also **Movie 5** in supplementary material). **C**, Overlay of DPIV velocity field from real-time, high-speed imaging. Red vectors indicate higher velocity and green vectors represent lower velocity. **D**, DPIV velocity field overlaid on bulbus arteriosus to visualize high-velocity transaortic jet. DPIV analysis quantitatively represents blood flow patterns and vector overlays reveal the fluid jet during **C**, Diastole. **D**, Systole. **E**, **F**, Calculated vorticity field from real-time, high-speed imaging at **E**, ventricular diastole and **F**, ventricular systole. Note the vortical flow behind the AV constriction during ventricular filling **E**, and the significant vortex pair in the bulbus during ventricular systole **F**. Contour colors are indicative of strength and direction of rotation. Inset shows the intra-bulbal vorticity, computed from velocity vector field, defining the jet. See **movie 6** for dynamic changes of intracardiac vorticity field and velocity in the beating embryonic heart *in vivo*. Abbr.: a: atrium, ao: aorta, b: bulbus arteriosus, v: ventricle, vbv: ventriculo-bulbar-valve.

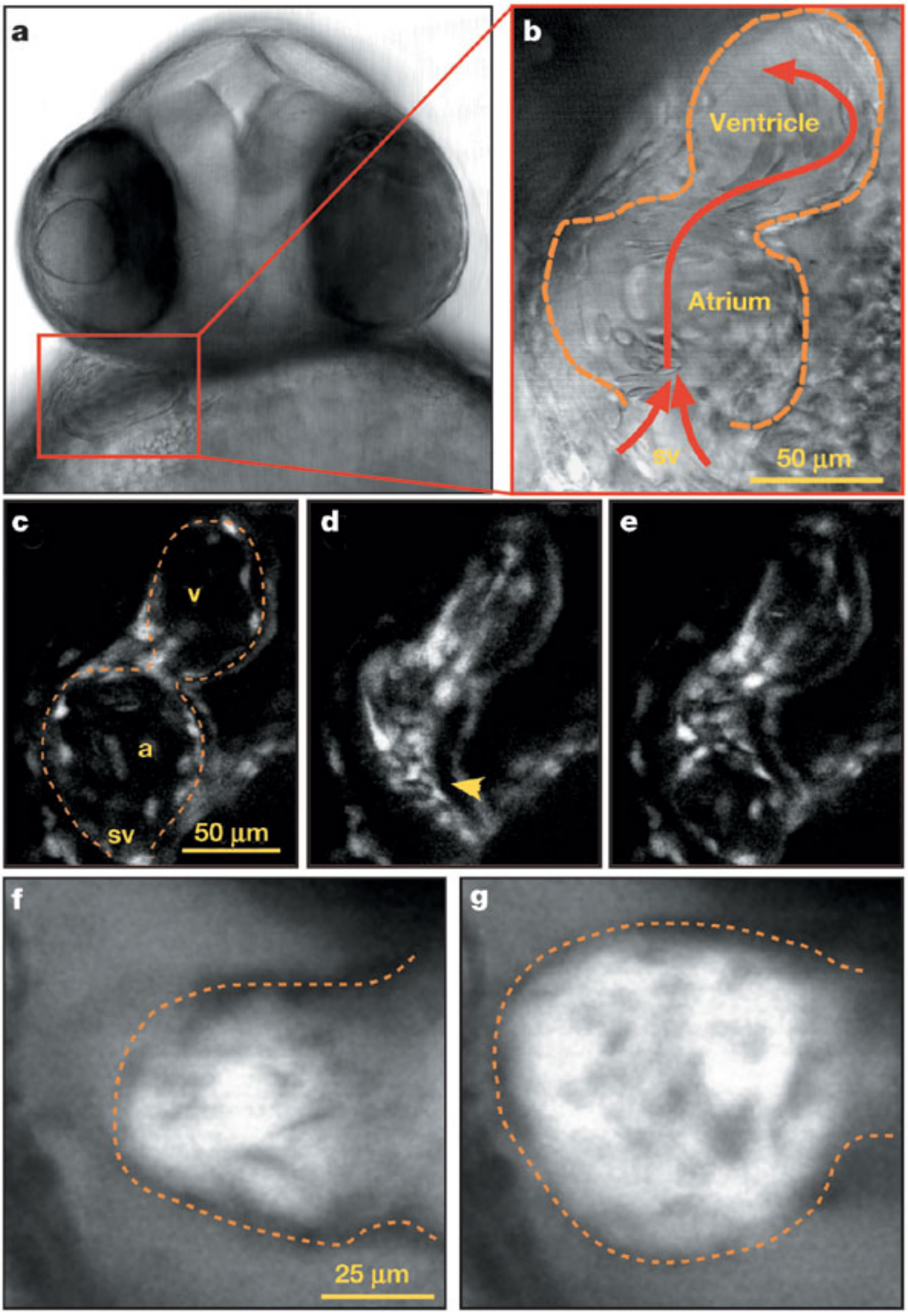

Figure A.3: Dynamics of valve-less atrio-ventricular junction in the 37hpf embryonic zebrafish heart. **A**, Embryo with heart contained in the red box. **B**, High magnification of the heart with overlaid schematic denoting chamber boundaries. Red arrows indicate

mean flow direction. Note streak-like imprints left by moving blood cells during scan indicating their direction and are proportional to their velocity. For influx of blood over the yolk into the atrium through the developing sinus venosus see **Movie 8**. **C-E**, Confocal coronal sections of different stages of a heart beat cycle of a 37hpf homozygous *gata1*::GFP embryo, the endocardium and blood cells are labeled by GFP-fluorescence. **C**, Diastole of atrium and ventricle with chamber outlines indicated by dashed orange lines. **D**, Maximal atrial systole, note the dramatic luminal volume reduction by almost complete collapse of the endocardium (yellow arrowhead), **E**, Beginning atrial diastole and ventricular systole. See supplementary material for **Movie 8**. **F**, Ventricle at systole and **G**. diastole for ejection fraction calculations. To counterstain blood serum for better volume measurements embryos were incubated in Bodipy-Ceramide. Abbr.: a: atrium, sv: sinus venosus, v: ventricle.

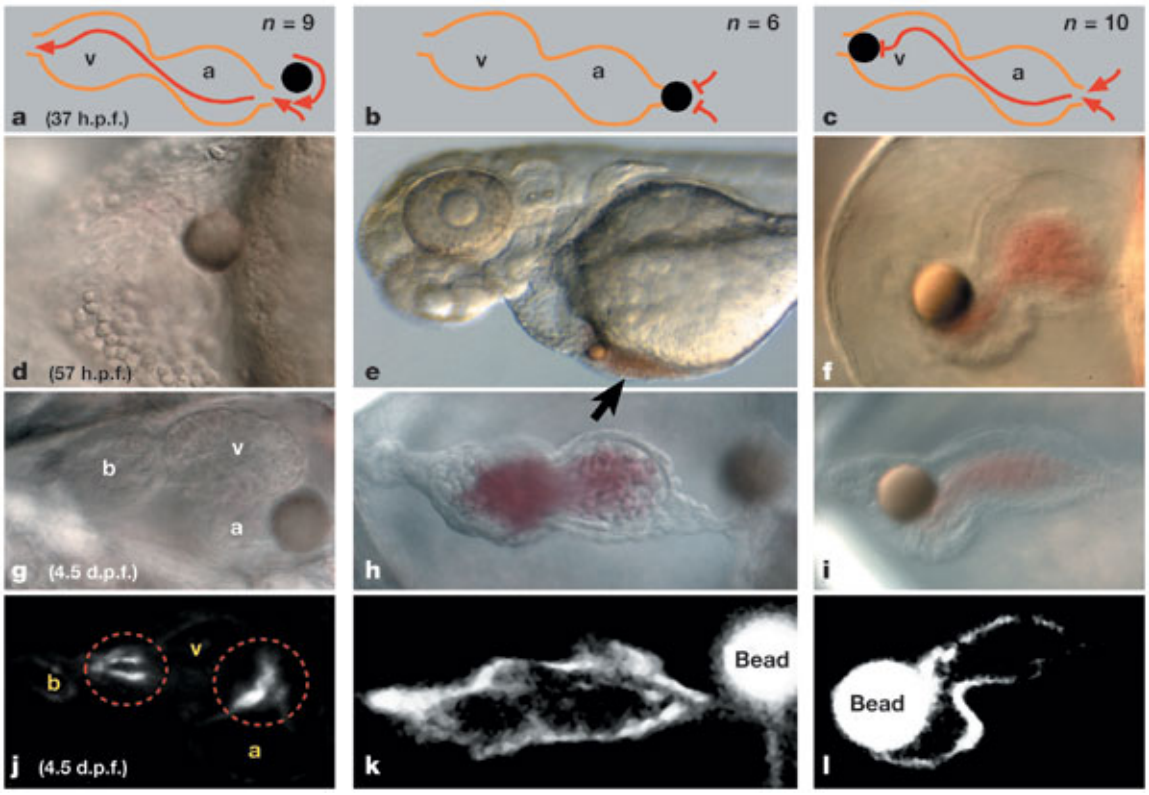

Figure A.4: Impaired blood flow influences cardiogenesis. 50 μm glass beads were inserted into homozygous transgenic tie2::GFP embryos at the primitive heart stage (37hpf) close to the sinus venosus not blocking flow (**A**, n=9), in front of the sinus to block blood influx (**B**, n=6) or into the outflow tract to block blood efflux (**C**, n=10). Successful blockage was checked 20 hours after surgery (**D-F**, note accumulated blood erythrocytes on the yolk in front of the bead while the atrium contains no erythrocytes (**E**, arrowhead). Operated specimens were reexamined at 4.5dpf. **G**, Cardiac chamber development appears unaffected by non-occlusive implantations and both the AV- and VB-valves form properly (**J**, red dashed circles, see also **Movie 2**). In contrast, cardiogenesis in embryos with blocked blood flow is severely disrupted independent of blockage location. Bulbus formation is greatly reduced or fails, heart looping does not occur; and the lateral walls of the sinus and outflow tract collapse and fuse, sealing off the heart (**H, I**). In addition, the AV- and VB-valves do not form, initial endocardial GFP-expression does not concentrate in the forming valves consistent with the peristaltic, primitive-heart like, contraction of the affected hearts (**K**, **L**, see also **Movie 9**, and **Movie 10**). Except for a yolk sac oedema, all other organs and tissues in the operated embryos developed properly and they exhibited normal neurological responses such as escape reflex and eye movements. Abbr.: a: atrium, b: bulbus, v: ventricle.

Appendix B: Viewing Angles for Cardiac Imaging

Rapid cardiac development is clearly an advantage for high experimental throughput, however, it also requires additional consideration for cardiac imaging since the heart is quickly changing shape as well as position in the embryo. Precise imaging angles are required for viewing valve dynamics, and to a lesser extent, chamber dynamics. The following data provides a guide for the optimal viewing angles for four-dimensional cardiac development and dynamics in zebrafish. The major axes we refer to are the anterior-posterior, dorsal-ventral, and left (L) and right (R) lateral planes. Intermediate viewing angles between the ventral and lateral planes are described by an orientation angle (progressive from the ventral surface, 0º-90º) and lateral. For example, midway between the ventral view and the right lateral view would be considered the 45ºR view. At each developmental stage considered, we present a z-stack beginning at the ventral plane of the heart and a left and right lateral progression of the heart with isosurface renderings of the atrium and ventricle. (*note: each z-stack was acquired from a ventral view but is shown from the dorsal view*)

30hpf

At 30 hpf, the heart tube is in transition from the dorsal-ventral axis to the anterior-posterior axis. The heart tube is positioned on the left side of the midline, with the inflow tract posterior and ventral to the outflow tract. During this stage, the head and yolk sac continue to move apart from each other, improving optical access to the heart from the ventral view. The outflow tract, however, remains relatively obscured due to its position near the middle of the dorsal-ventral, and left-right axes. The inflow tract, along with

blood flowing over the yolk sac and into the heart, is optically accessible at this stage. The optimal viewing angle for the heart tube is between 0º-45ºR.

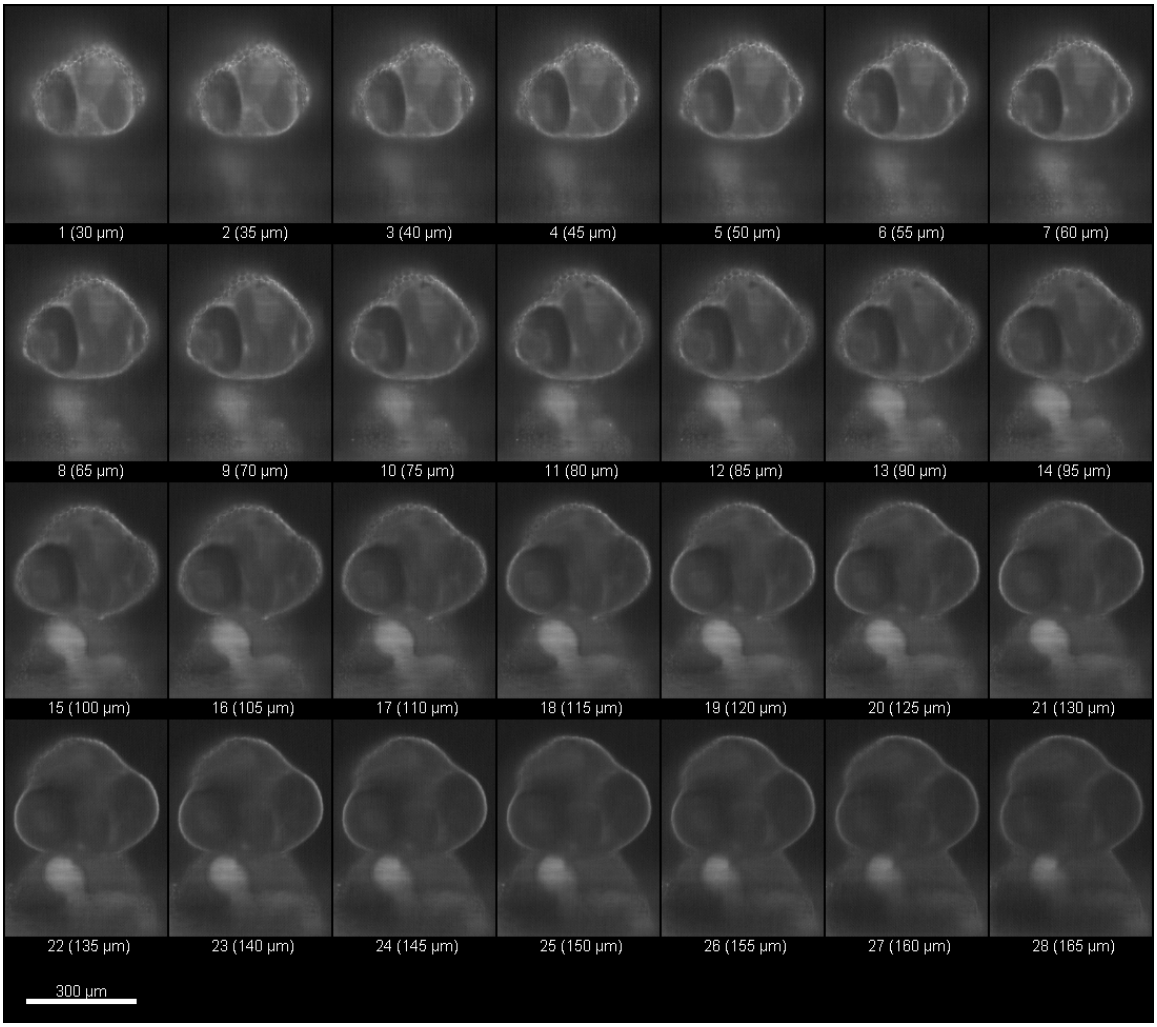

Figure B.1 30 hpf stack.

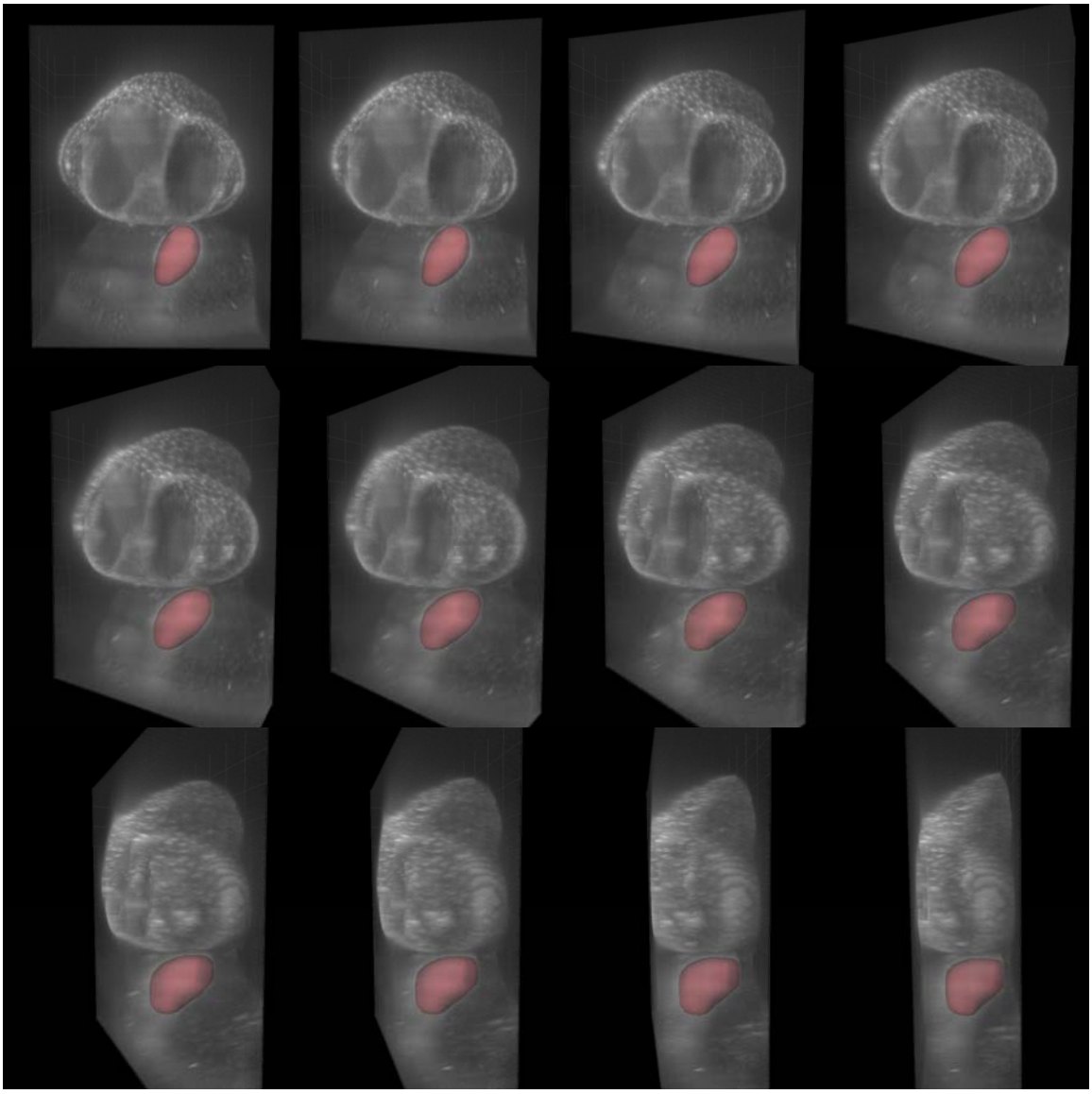

Figure B.2 30 hpf left lateral progression.

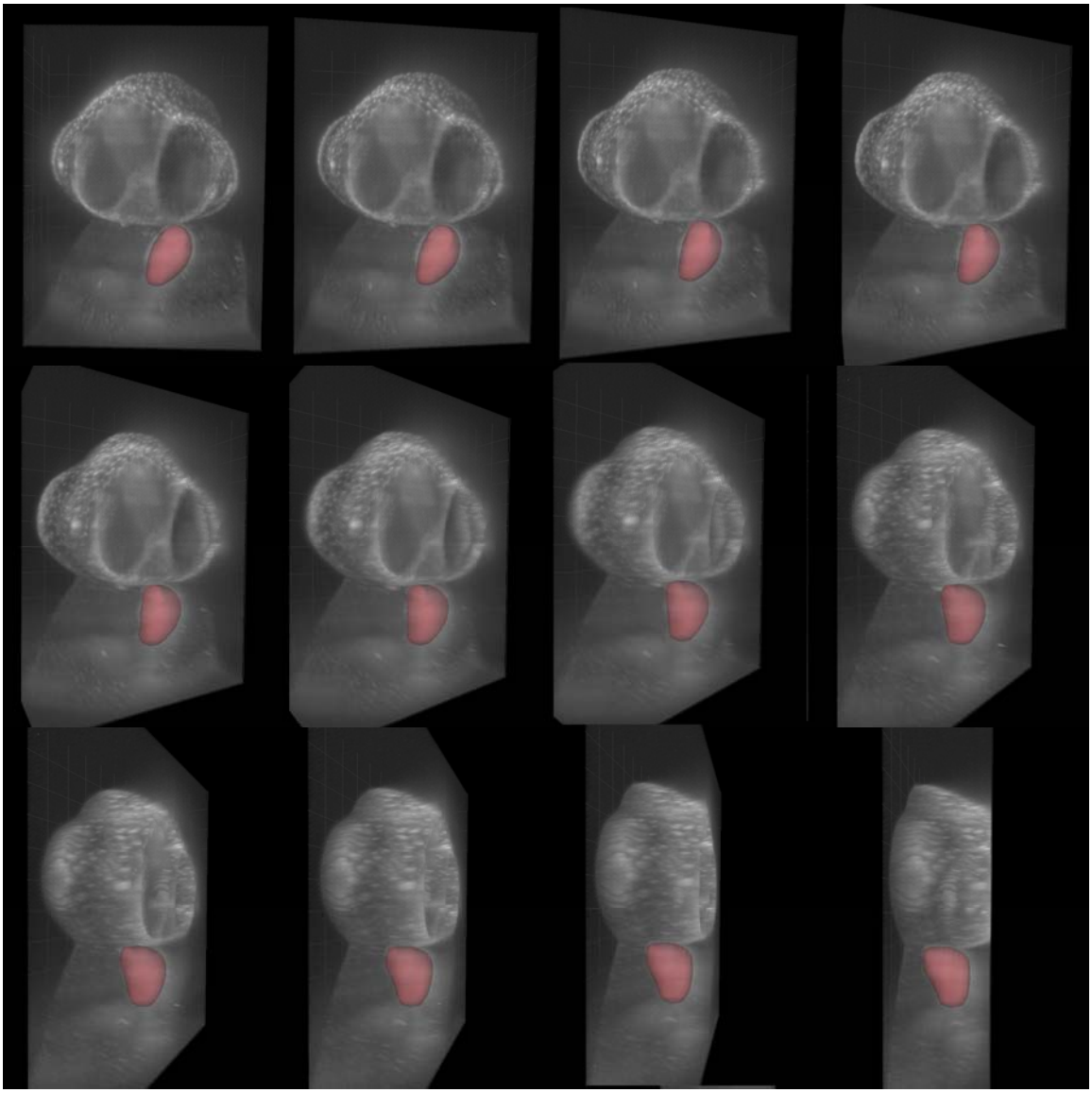

Figure B.3 30 hpf right lateral progression.

48hpf

By 48 hpf, the heart continues repositioning towards the dorsal-ventral axis. The early stages of chamber formation are evident, with the ventricle and atrium comparable in size. The atrium remains posterior and dorsal to the ventricle. The ventricle is positioned near the midline of the embryo and to the right of the atrium. Blood flow into and out of

the heart is optically accessible. The optimal viewing angle to see blood flow into and out of the heart is from the ventral plane. The optimal range to view the atrium and ventricle together is between 45ºL to 45ºR.

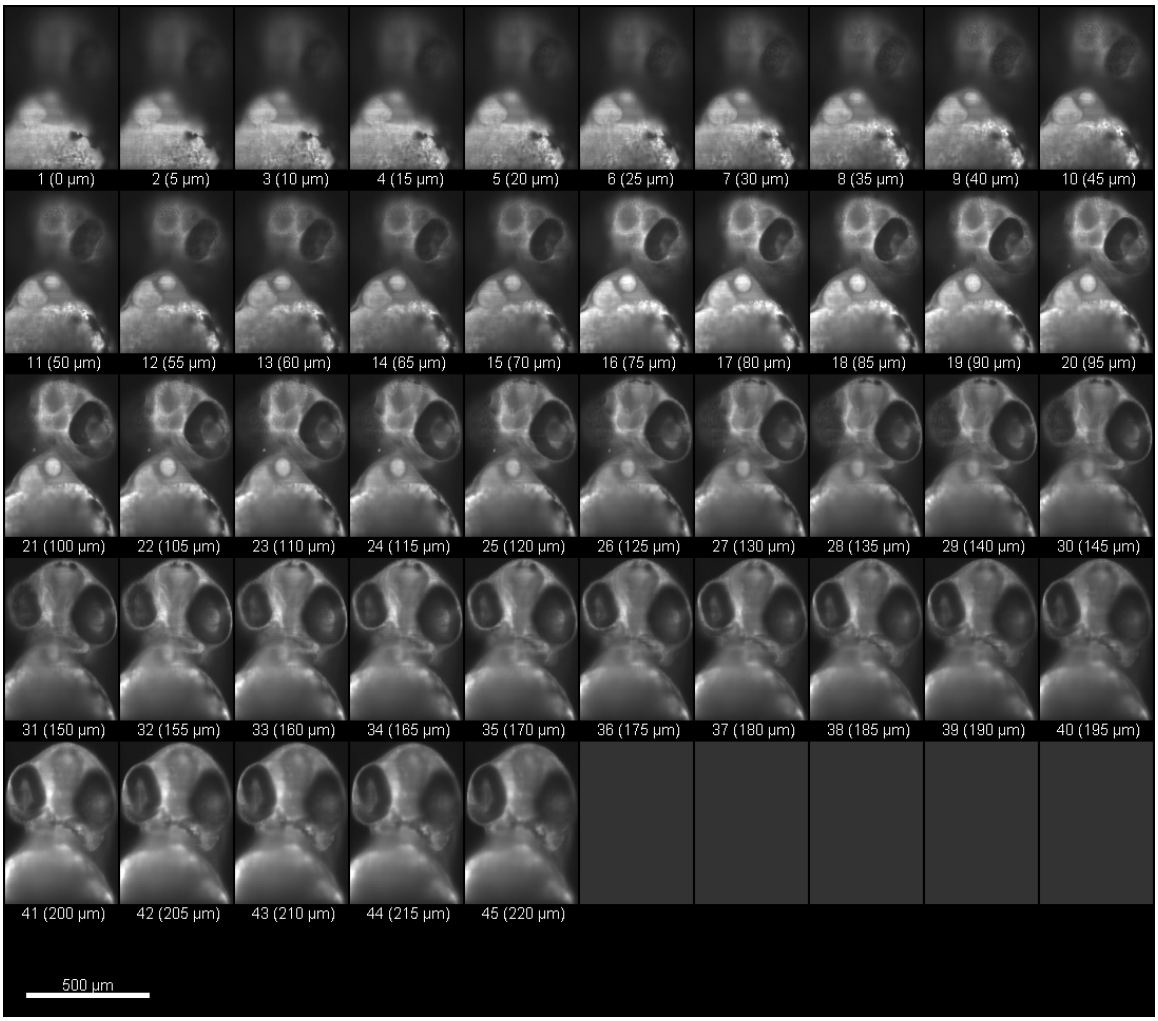

Figure B.4 48 hpf stack.

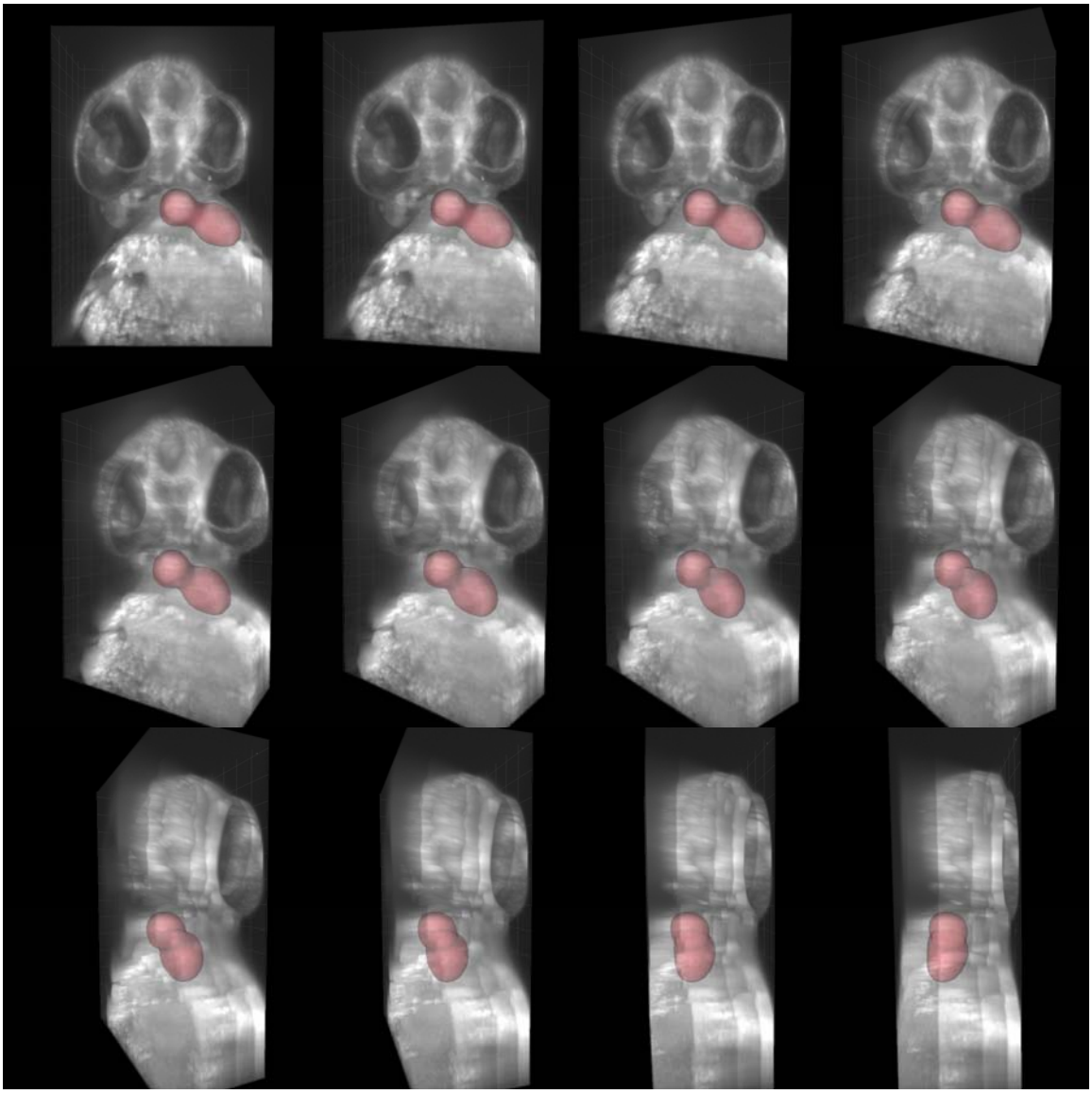

Figure B.5 48 hpf left lateral progression.

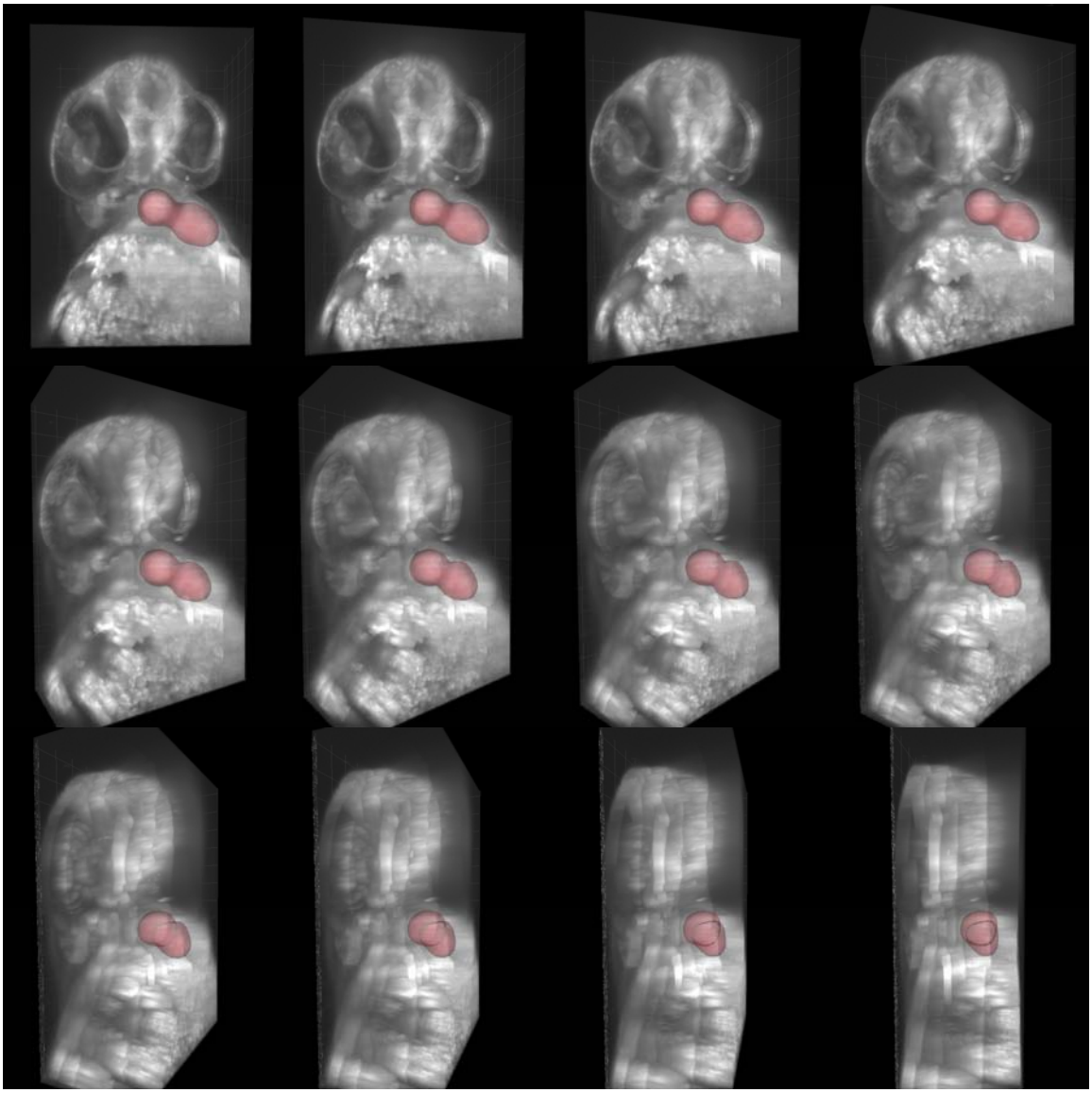

Figure B.6 48 hpf right lateral progression.

72hpf

By 72 hpf, the developing heart is now positioned on the anterior-posterior axis. The sinus venosus is ventral to the bulbus arteriosus, but the atrium and ventricle are nearly on the same dorsal-ventral plane (atrium positioned slightly dorsal to ventricle). The AV canal is positioned near the midline, with the atrium and ventricle on the left and right of

the midline, respectively. The VB canal is positioned to the right of the midline and the outflow tract is centered on midline. The ventral view of the embryo is the optimal angle to image the AV canal. The ventricle can be viewed between 0º-90ºR and the atrium between 0º-90ºL.

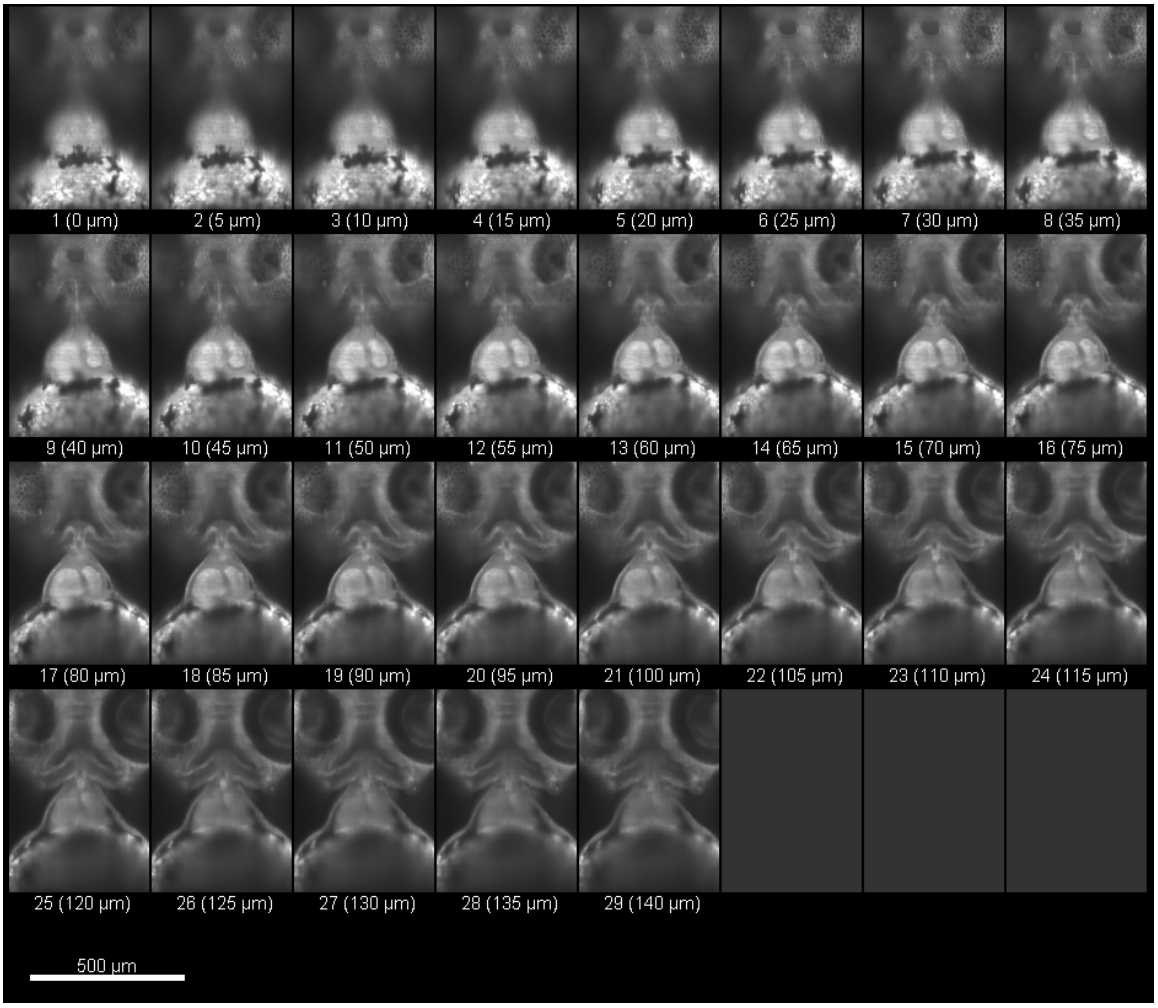

Figure B.7 72 hpf stack.

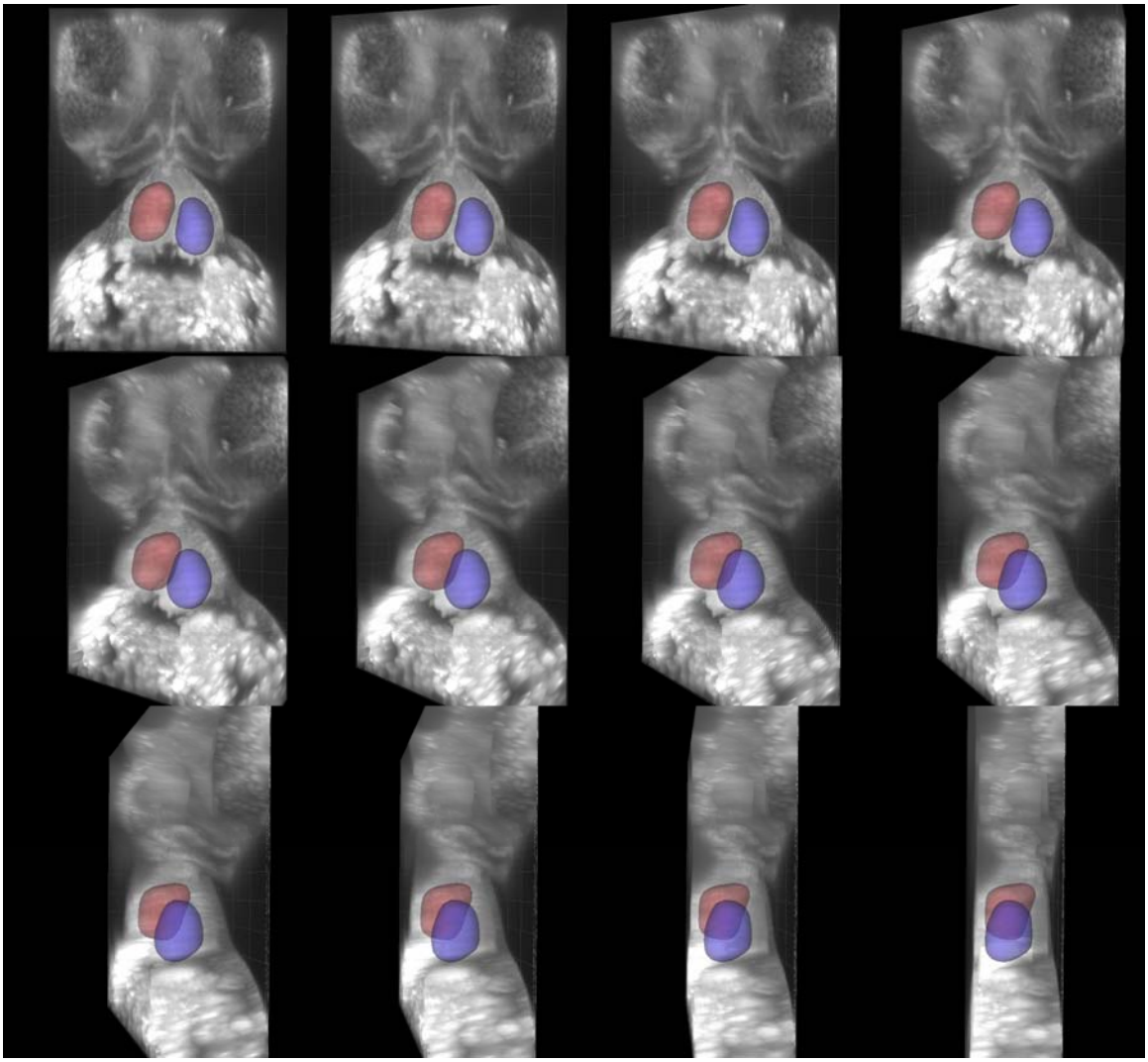

Figure B.8 72 hpf left lateral progression.

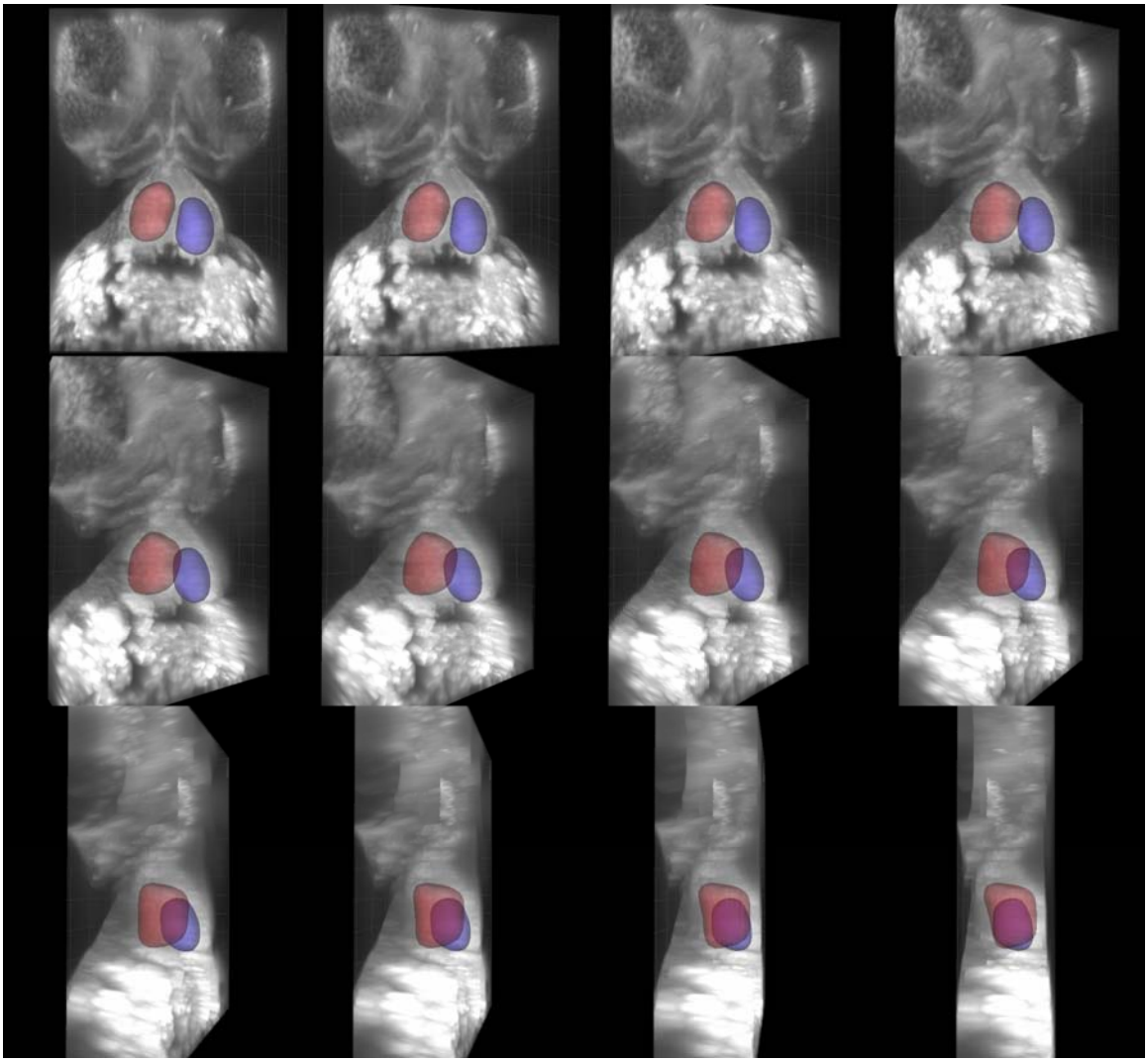

Figure B.9 72 hpf right lateral progression.

96hpf

By 96 hpf, the atrium continues to move relative to the ventricle, now repositioning dorsal to the ventricle. The midline bisects the ventricle, with atrium positioned to the left of the ventricle. The AV valve is positioned ventral to the VB valve. The optimal angles to view AV and VB valve leaflet dynamics is 30ºL and 0º (ventral view), respectively. The best angles to view the ventricle alone are between 0º-90ºR. The best angles to view

the atrium alone are between 0º-90ºL. The two chambers along with the AV valve can viewed together between 0º-60ºL.

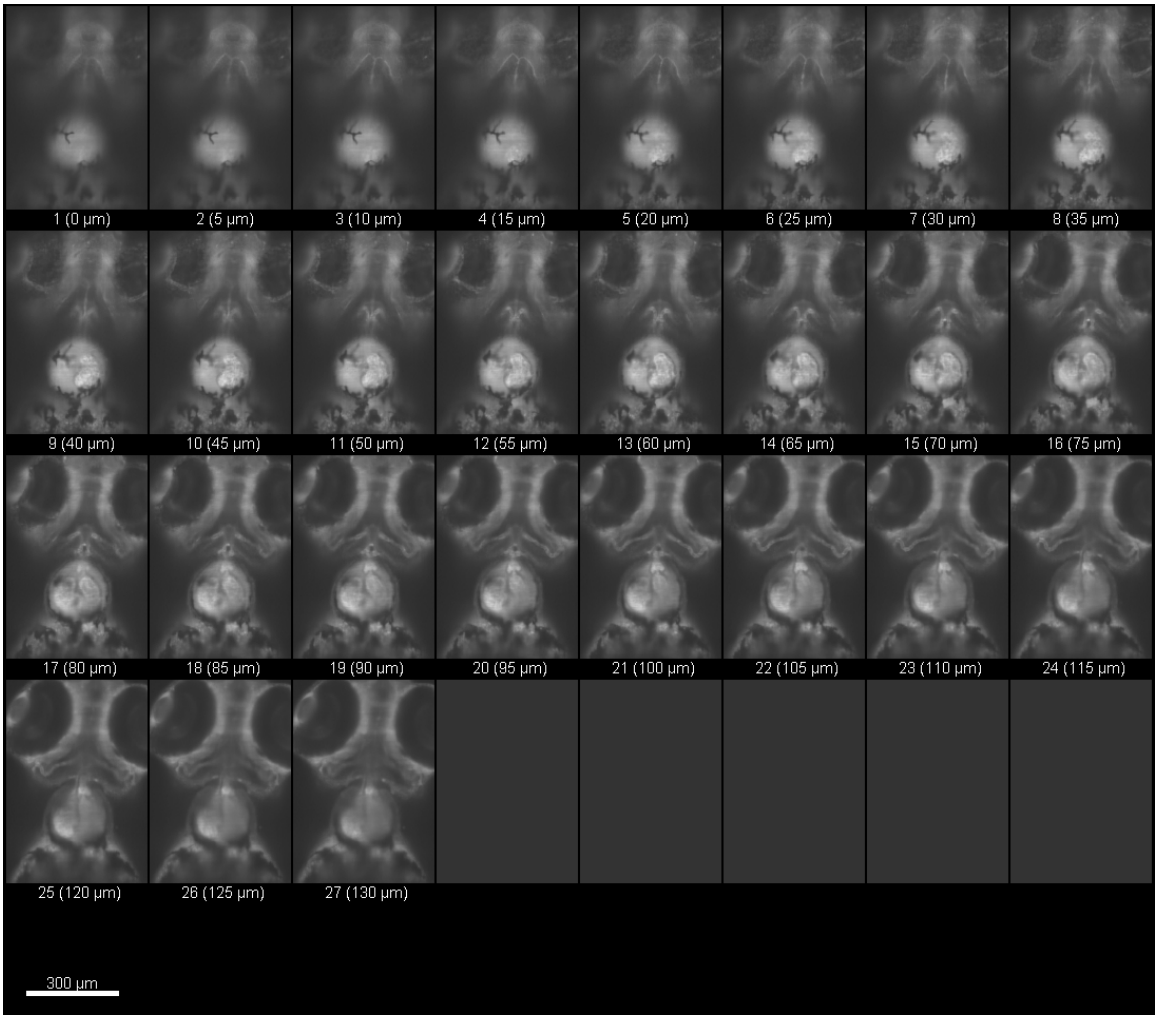

Figure B.10 96 hpf stack.

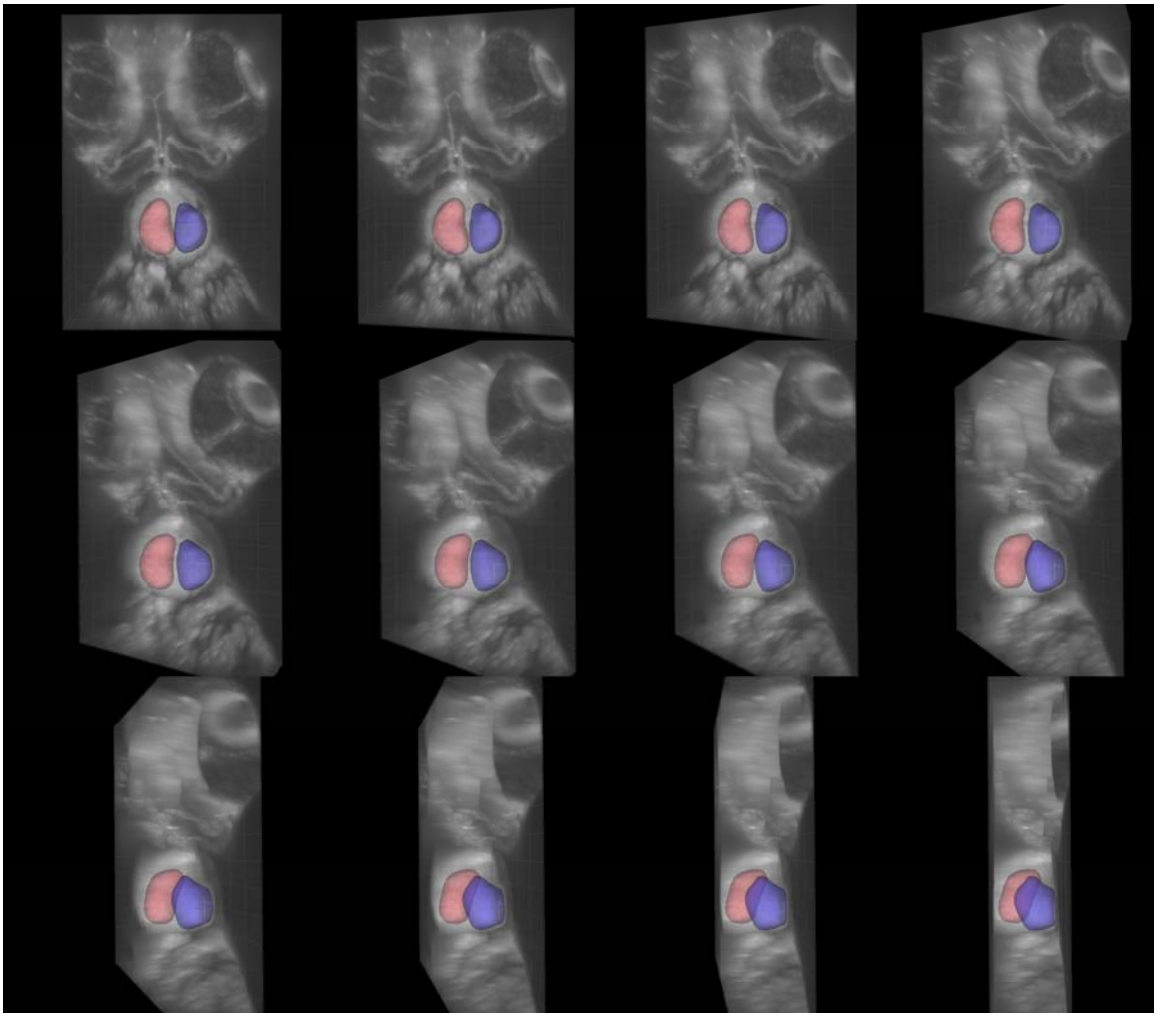

Figure B.11 96 hpf left lateral progression.

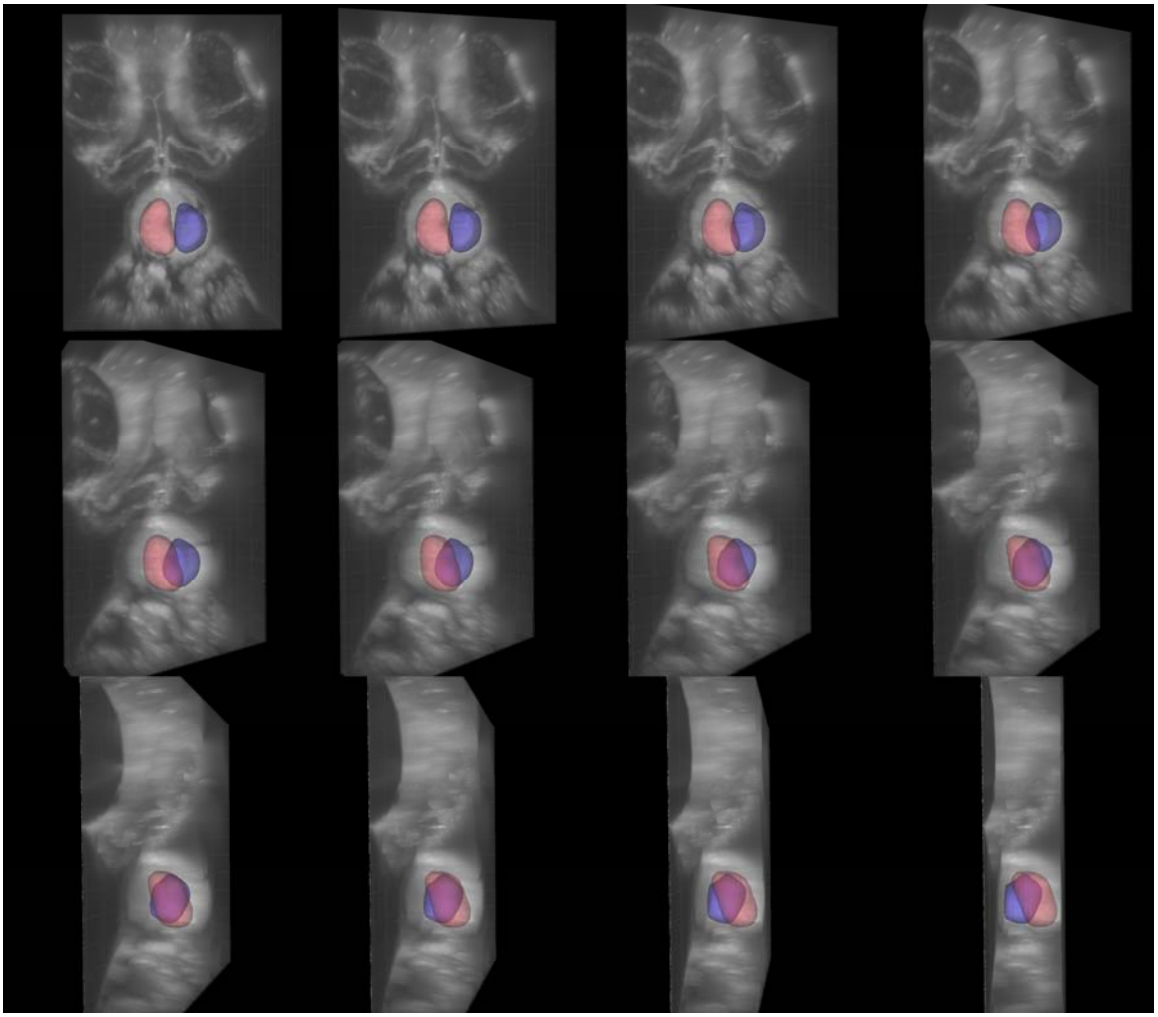

Figure B.12 96 hpf right lateral progression.

144hpf

The atrium has completely repositioned dorsal to the ventricle. The midline still appears to bisect the ventricle and bulbus arteriosus. The atrium lies slightly to the left of the ventricle. The ventral position of the ventricle and bulbus arteriosus makes them accessible from the ventral view of the embryo. Bicuspid VB valve dynamics are also in view from this angle. The ventricle can be viewed between 90ºL to 90ºR, but the atrium and ventricle are in view together only between 0º-90ºL. The dorsal position of the atrium

makes it much more difficult to image in its entirety than the ventricle. The optimal angle to view AV valve leaflet dynamics is 45ºL.

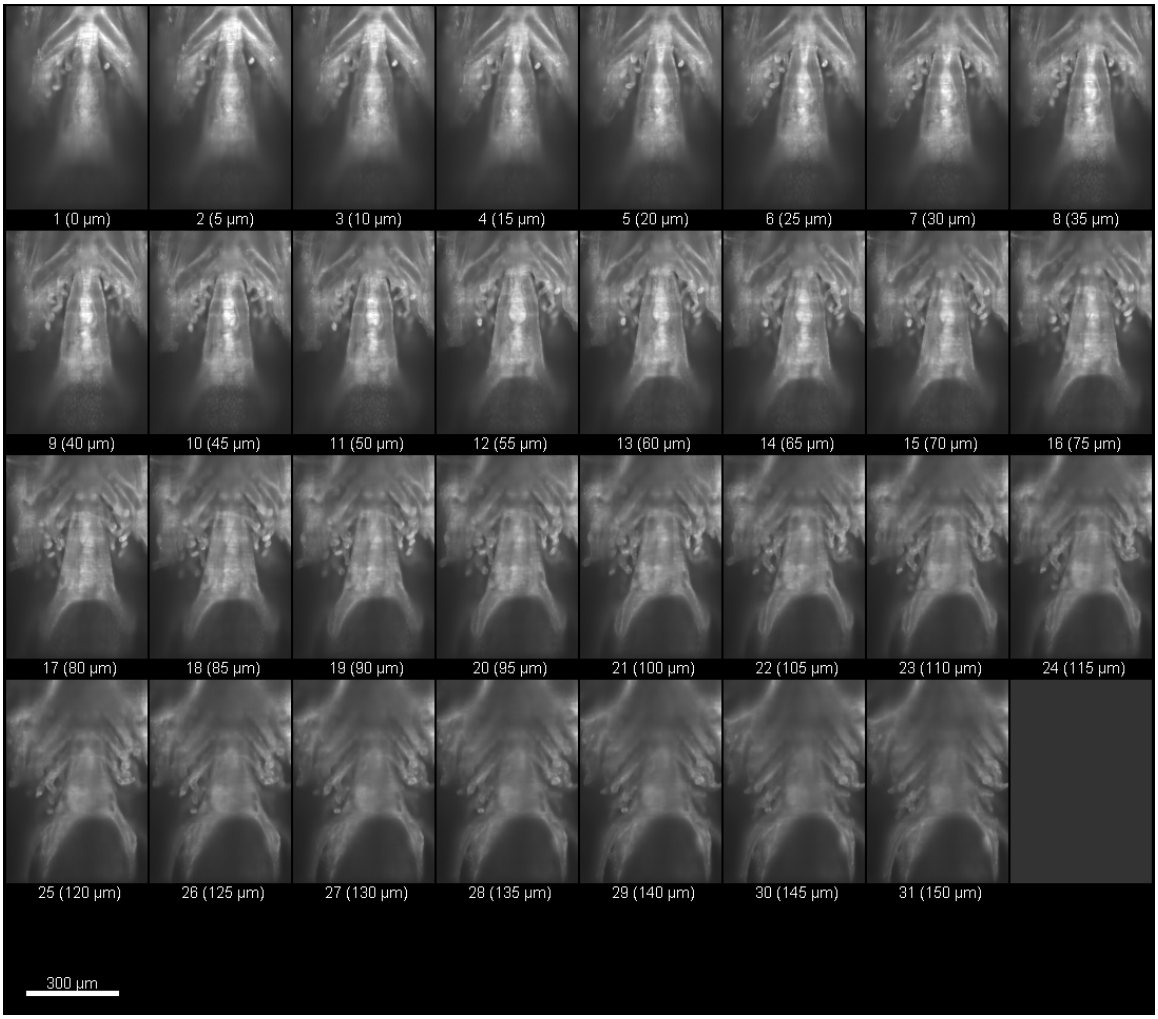

Figure B.13 144 hpf stack.

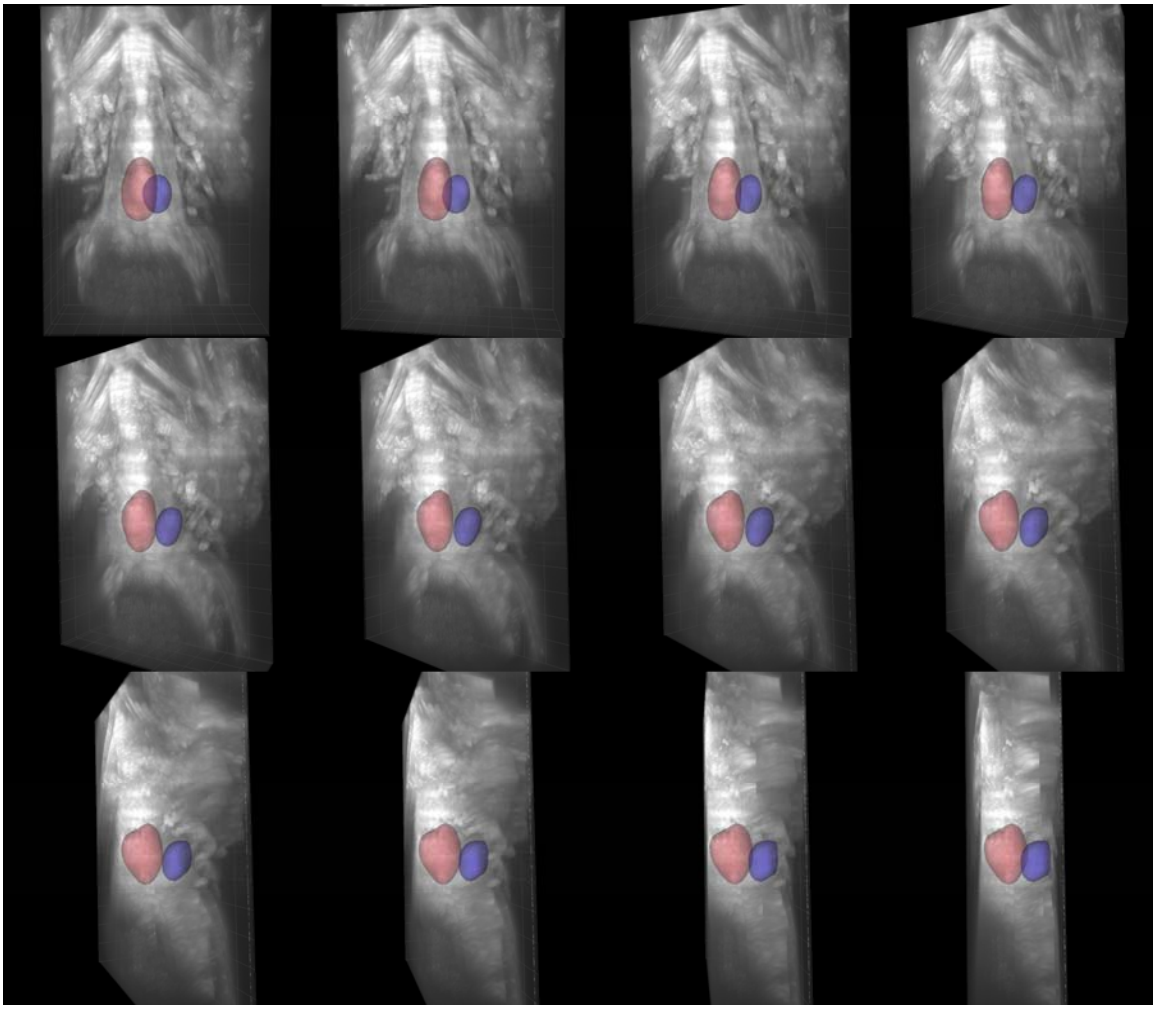

Figure B.14 144 hpf left lateral progression.

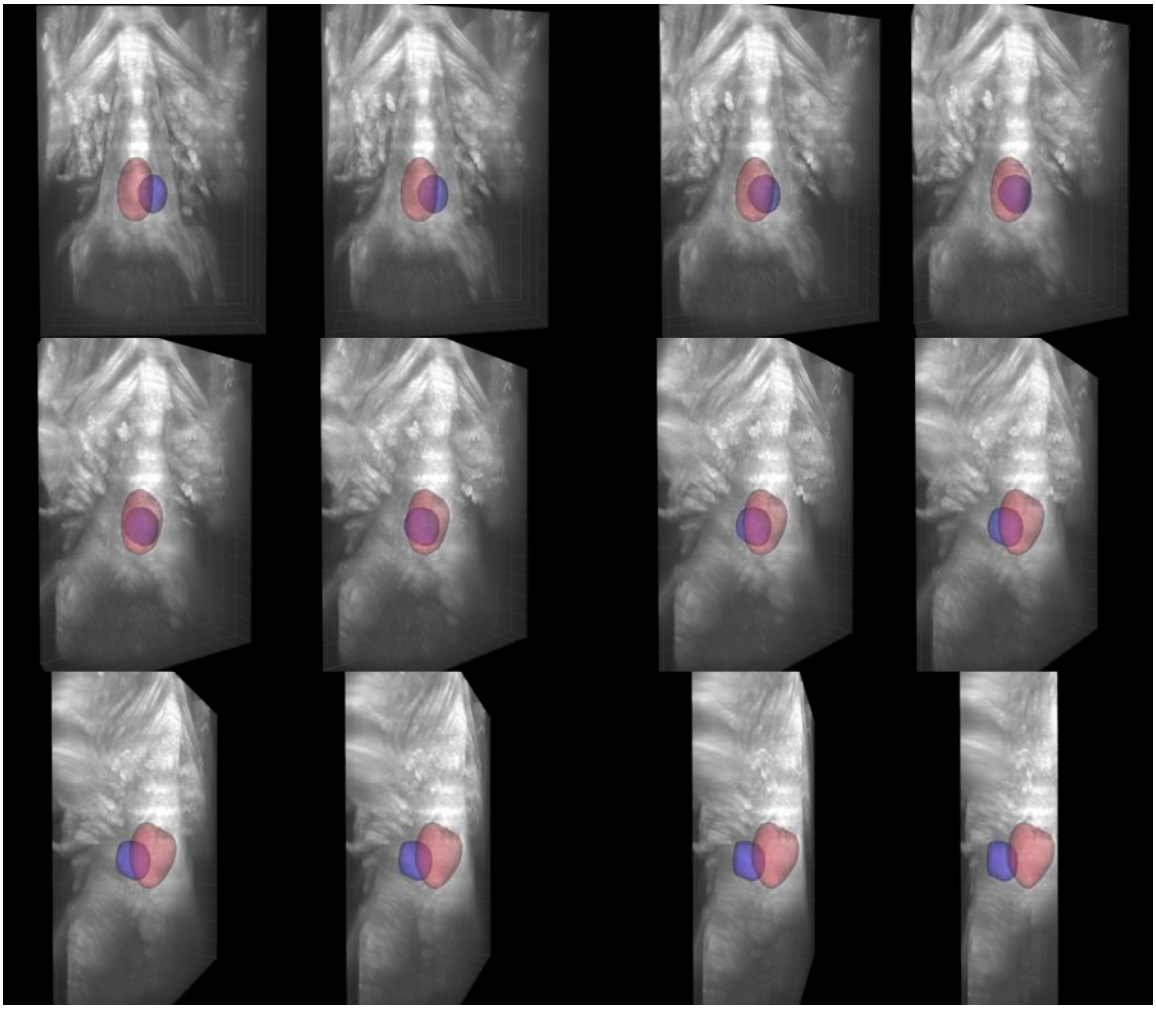

Figure B.15 144 hpf right lateral progression.

Appendix C: Shear Stress Sensitive Genes Involved in Valve Formation

In order to determine the players orchestrating valve formation, a number of in vitro (Bernanke et al. 1982; Eisenberg and Markwald, 1995) and in vivo (reviewed by Armstrong and Bischoff, 2004; Beis et al. 2005) experiments have identified genes and signaling pathways critical to normal valvulogenesis. In a different set of experiments, results have shown that many of the genes involved in valvulogenesis respond to shear stress (Lee and Koh, 2003; Chen et al. 1999; Chen et al. 2001; McCormick et al. 2001; Passerini et al. 2003; Shay-Salit et al. 2002; Sorescu et al. 2003), and a subset of these are specifically regulated by oscillatory shear stress (Sorescu et al. 2003; Passerini et al. 2003). Here, we list a group of shear stress sensitive genes implicated in zebrafish AV valve formation, and regulated during stages of valvulogenesis exhibiting oscillatory flow.

Tie2:

Tyrosine kinase with immunoglobulin and epidermal growth factor homology domain-2 (Tie2), a receptor tyrosine kinase (RTK) (Lee and Koh, 2003), is expressed in endocardial cells in the developing zebrafish. Upregulation of Tie2, as seen in *Tg(tie2:GFP)* embryos (Motoike et al. 2000), in the AV canal at 48 hpf is a common indicator of normal endcardial ring formation (Bartman et al. 2004). Lack of GFP expression in the AV canal *Tg(tie2:GFP)* embryos crossed with mutants has been used to phenotype cardiac valve mutants (Bartman et al. 2004) since they do not form

endocardial cushions. Thus it appears Tie2 is necessary for normal AV valve development in zebrafish. (Lee and Koh, 2003) demonstrated that Tie2 activation, assayed through Tie2 phosphorylation, increased with increasing shear stress (10-30dynes/cm^2).

Flk1:

A second RTK expressed in all endothelial cells in zebrafish is Flk1. In a similar fashion as Tie2, Flk1 is upregulated during endocardial ring formation and has been used as a marker to characterize normal valvulogenesis (Beis et al. 2005). Flk1 phosphorylation is also shear stress dependent. Increases in shear stress (10-30 dynes/cm^2) elevate Flk1 activation (Chen et al. 1999; Lee and Koh, 2003; Shay-Salit et al. 2002).

VEGF-R:

Vascular endothelial growth factor receptor (VEGF-R) is a cell surface receptor involved in heart valve formation. However, its specific role in valvulogenesis has not been clearly defined. Some studies have shown that VEGF expression prevents endocardial cells from differentiating into mesenchyme (Chang et al. 2004; Dor et al. 2001), suggesting a negative role in valvulogenesis, while others have shown VEGF signaling is required for proper valvulogenesis in zebrafish (Lee et al. 2006). Although the role of VEGF has not been specified, it has been shown that retrograde flow (i.e., wall shear stress reversal) decreases VEGF expression (Passerini et al. 2003).

TGF-*β*/BMP:

Signaling pathways involving the TGF-B family of proteins are probably the most commonly studied pathways influencing endocardial cushion formation. These proteins are homodimeric and initiate phosphorylation cascades (Armstrong and Bischoff, 2004) that are critical in EMT (reviewed by Eisenberg and Markwald 1995; Yamagashi et al. 1999). Bone Morphogenic Protein 4 (BMP-4) is member of this family whose expression is restricted to the AV canal during AV boundary specification in zebrafish. BMP-4 expression has been used to phenotype the Jekyll mutant (Walsh and Stainier, 2001), a zebrafish mutant with abnormal AV canal formation. Independent studies using DNA microarray chips found that BMP-4 expression in endothelial cells is upregulated by nearly a factor of two in response to oscillatory shear stress (±5 dynes/cm^2) as compared to static conditions (Sorescu et al. 2003). A number of TGFB members are also regulated by exposure to shear stress (Chen et al. 2001; McCormick et al. 2001; Passerini et al. 2003).

Many of players described here are likely to serve multiple roles in valvulogenesis. In proper valve formation, gene expression must be spatially and temporally regulated. It is not in the scope of this project to determine exactly what signaling pathways controlling valve formation are regulated by oscillatory shear stress in vivo. Instead, we make the case that many of the genes controlling heart valve formation are regulated by shear stress. In some instances, such as BMP-4 expression, upregulation is necessary but overexpression can be detrimental (BMP-4 overexpression leads to thickened valves and hypertension) (Galvin et al. 2000). We speculate that oscillatory shear stress may be involved in several feedback loops that help regulate gene expression.

References

Armstrong EJ, Bischoff J, *Circ Res*. **95**, 459 (2004).

Bartman T, Walsh EC, Wen KK, McKane M, Ren J, Alexander J, Rubenstein PA, Stainier DY, *Plos Biol*. **2**, E129 (2004).

Beis D, Bartman T, Jin S, Scott IC, D'Amico LA, Ober EA, Verkade H, Frantsve J, Field HA, Wehman A, Baier H, Tallafuss A, Bally-Cuif L, Chen JN, Stainier DY, Jungblut B, *Development*. **132,** 4193 (2005).

Bernanke DH, Markwald RR, *Dev Biol*. **91**, 235 (1982).

Chang CP, Neilson JR, Bayle JH, Gestwicki JE, Kuo A, Stankunas K, Graef IA, Crabtree GR, *Cell*. **118**, 649 (2004).

Chen KD, Li YS, Kim M, Li S, Yuan S, Chien S, Shyy JY, *J Biol Chem*. **274**, 18393 (1999).

Dor Y, Camenisch TD, Itin A, Fishman GI, McDonald JA, Carmeliet P, Keshet E, *Development*. **128**, 1531 (2001).

Eisenberg LM, Markwald RR, *Circ Res*. 77, 1 (1995).

Galvin KM, Donovan MJ, Lynch CA, Meyer RI, Paul RJ, Lorenz JN, Fairchild-Huntress V, Dixon KL, Dunmore JH, Gimbrone MA Jr, Falb D, Huszar, *Nat Genet*. **24**, 171 (2000).

Lee HJ, Koh GY, *Biochem Biophys Res Commun*. **304**, 399 (2003).

Lee YM, Cope JJ, Ackermann GE, Goishi K, Armstrong EJ, Paw BH, Bischoff J, *Dev Dyn*. **235**, 29 (2006).

McCormick SM, Eskin SG, McIntire LV, Teng CL, Lu CM, Russell CG, Chittur KK, *Proc. Natl. Acad. Sci. USA*. **98**, 8955 (2001).

Motoike T, Loughna S, Perens E, Roman BL, Liao W, Chau TC, Richardson CD, Kawate T, Kuno J, Weinstein BM, Stainier DY, Sato TN, *Genesis*. **28**, 75 (2000).

Passerini AG, Milsted A, Rittgers SE, *J. Vasc. Surg*. **37**, 182 (2003).

Shay-Salit A, Shushy M, Wolfovitz E, Yahav H, Breviario F, Dejana E, Resnick N, *Proc. Natl. Acad. Sci. USA.* **99**, 9462 (2002).

Sorescu GP, Sykes M, Weiss D, Platt MO, Saha A, Hwang J, Boyd N, Boo YC, Vega JD, Taylor WR, Jo H, *J. Biol. Chem*. **278**, 31128 (2003).

Stainier DY, *PLoS Biol*. **2**, E129 (2004).

Walsh EC, Stainier DY, *Science* **293**, 1670 (2001).

Yamagashi T, Nakajima Y, Miyazono K, Nakamura H. Bone, *J Cell Physiol*. **180**, 35 (1999).